2013-05-03

Examining the effect of anti-tumor lipid drugs on pH homeostasis and membrane structure in Saccharomyces cerevisiae

Czyz, Ola Aleksandra Joanna

UNIVERSITY OF CALGARY

Examining the effect of anti-tumor lipid drugs on pH homeostasis and membrane structure in *Saccharomyces cerevisiae*

by

Ola Aleksandra Joanna Czyz

A THESIS
SUBMITTED TO THE FACULTY OF GRADUATE STUDIES
IN PARTIAL FULFILMENT OF THE REQUIREMENTS FOR THE
DEGREE OF MASTER OF SCIENCE

DEPARTMENT OF BIOLOGICAL SCIENCES

CALGARY, ALBERTA

MAY, 2013

Abstract

The lysophosphatidylcholine analogue, edelfosine is a potent anti-tumor lipid drug that is known to target cellular membranes. The underlying mechanisms leading to cell death remain largely controversial, although previous results obtained using yeast, have indicated that edelfosine associates with lipid rafts at the plasma membrane (PM), resulting in the internalization of essential proton pump, Pma1 and ergosterol. To further elucidate the conditions that enhance or prevent the cytotoxic effect of edelfosine, genome-wide surveys in the model organism *Saccharomyces cerevisiae* were performed. The results of these screens indicated that maintenance of pH homeostasis modulates cell sensitivity to edelfosine. Our studies further demonstrated that edelfosine induces intracellular acidification and alters PM organization by selectively inducing ubiquitination and subsequent endocytosis of PM transporters. We also showed that the second-generation anti-tumor lipids, miltefosine and perifosine, cause PM disorganization in a manner analogous to edelfosine, suggesting a similar mode of action for this drug family.

Acknowledgements

I would like to thank my supervisor Dr. Vanina Zaremberg for accepting me into her lab 3 years ago, and supporting me throughout my entire graduate school experience, both the good and the bad. Her tremendous patience and hours of support helped me reach goals that I didn't know were attainable. I would also like to thank all the past and present members of the Zaremberg lab, but especially Heather Smart, my "useful undergrad" who made this past year and a half a whole lot more entertaining. In addition, I have to extend a thank you to the members of the Ro and Prenner labs who aided in troubleshooting, and in particular Mark Mahadeo, who readily put up with my punctuality. I would also like to thank my supervisory committee, Dr. Elke Lohmeier-Vogel, who first introduced me to Vanina and was always pushing me to achieve more, and Dr. Elmar Prenner, who has always been very supportive of all of my goals. Finally, I would like to extend a big thanks to all of my friends and family who have helped me through everything these past few years.

Table of contents

List of tables

List of figures

List of abbreviations

ADP = adenosine diphosphate
ALP = alkyllysophospholipids
AMP = adenosine monophosphate
APC = alkylphosphocholines
ATL = antitumorlipids
ATP = adenosyl triphosphate
BF = brightfield
CCT= CTP:phosphocholine cytidyl transferase
CDP = cytidine diphosphate
CH_3OH = methanol
$CHCl_3$ = cholorform
CL = cardiolipin
CMC = critical micelle concentration
CPT = cholinephosphotransferase
Cu^{2+} = copper (II)
DAG = diacylglyceride
DAmP = Decreased Abundance by mRNA Perturbation
DIC = differential interference contrast
DISC = death inducing signaling complex
DNA= deoxyribose nucleic acid
DRM = detergent resistant membranes
DUb = deubiquitinase (Ubp7 domain)
EDLF = edelfosine
EDTA = Ethylenediaminetetraacetic acid
EGFR = epidermal growth factor receptors
ER = endoplasmic reticulum
Ergo = ergosterol
ErPC = erucylphospho-N,N,N- trimethylpropylammonium/erucylphosphocholine
ESCRT = endosomal sorting complex required for transport
FADD = Fas-associated death domain-containing protein
Fe^{2+} = Iron (II)
GFP = green fluorescent protein
GO = gene ontology
GPAT= glycerol-3-phosphate acyltransferase
GPI = glycophosphatidylinositol
H+ = proton
HCl= hydrochloric acid
HeNe = helium neon
H_{II} = Hexagonal II shape/micelles
HPLC = high performance liquid chromatography
IC= intracellular
K+ = potassium

kDa = kilodalton
LdMT = *Leishmania donovani* putative miltefosine transporter
LF-YNB = low fluorescence YNB
LiAc = lithium acetate
Lo = liquid ordered phase
LPAAT= lyso-phosphatidic acid acyltransferase
lysoPC = lyso phosphatidylcholine
Lα = liquid crystalline (liquid disordered) phase
Lβ = solid gel phase
M = molarity (moles/liter)
$M(IP)_2C$ = mannose-(inositol-phosphoryl-2)-ceramide
MAPK = Ras-Raf-Mitogen Activating Protein Kinase
MCC = membrane containing Can1p
MCP = membrane containing Pma1p
MIC = minimal inhibitory concentration
mL = milliliter
MLTF = miltefosine
mRNA = messenger ribonucleic acid
MVB = multi vesicular body
MW = molecular weight
NaCl = sodium chloride
NaOH = sodium hydroxide
^{o}C = degrees in celsius
OD = optical density (at 600 nm)
PA = phosphatidic acid
PAF= platelet activating factor
PAP = phosphatidic acid phosphatases
PC = phosphatidylcholine
PCR = polymerase chain reaction
PDME = phosphatidylcholinedimethylethanolamine
PE = phosphatidylethanolamine
PEG = polyethylene glycol
PEMT = phosphatidylethanolamine methyl transferase
PERF = perifosine
PG = phosphatidylglycerol
pHi = intracellular pH
Pi = phosphate
PI = phosphatidylinositol
PI3K/Akt/PKB = phosphatidylinositol 3-kinase/protein kinase B/Akt
PIP = phosphoinositide
PLA1/PLA2/PLB/PLC/PLD = phospholipase A1/A2/B/C/D
PM = plasma membrane
PS = phosphatidylserine
PVDF = polyvinylidene
RFP = red fluorescent protein

SAM = S-adenosylmethionine
SAH = S-adenosylhomocysteine
SAPK/JNK = c-Jun-N-terminal kinase
SD = standard deviation
SD = synthetic defined media
SDS-PAGE = sodium dodecyl sulfate polyacrylamide gel electrophoresis
SGD = *Saccharomyeces* genome database
SM = sphingomyelin
TAG = triacylglyceride
TE = Tris- EDTA
Tm = melting/transition temperature
TNE = Tris-NaCl-EDTA buffer
TXNE = TNE with 0.1% Triton-X 100
UV-VIS = ultraviolet visible
V-ATPase = vacuolar ATPase
WT = wild type
YNB = yeast nitrogen base
YPD = yeast peptone dextrose (rich media)
$\Delta\psi$ = membrane potential
μL = microliter
μM = micromolar (micromole/liter)

Chapter One: Introduction

1.1: Eukaryotic membranes

1.1.1: Model membranes: past to present

Biological membranes are essential aspects of all eukaryotic cells. The plasma membrane (PM) acts as a barrier between the internal and external environment of the cell, and provides structural support. Cells also contain intracellular membranes, which form the boundaries of organelles, such as mitochondria, and the lysosome. This compartmentalization facilitates biochemical processes and allows organelles to maintain conditions that differ from the cytosol, such as low pH or high ionic strengths (1, 2).

The original membrane model proposed in the 1970's, the Fluid Mosaic Model envisioned membranes as structures of homogeneously distributed phospholipids existing to provide a hydrophobic barrier and a matrix for membrane proteins (Figure 1.1). This mosaic structure was proposed to be highly dynamic allowing integral proteins to undergo translational diffusion within the membrane (3). The rate of translation was proposed to depend on the "viscosity" of the membrane. Heterogeneity in this model was mostly considered for proteins although differences in the unsaturation of acyl chains in lipids were discussed. But, if the function of the membrane was simply to be a sea of lipids in order to house proteins, why does such lipid heterogeneity exist within the cell (4, 5)? Why and how do cell types and cellular organelles maintain unique lipid and protein composition in their membranes (4, 6)?

Over the past few decades, new aspects pertaining to cellular membrane organization have been uncovered, giving the pioneer fluid mosaic model a drastic makeover (Figure 1.1) (5). Current models recognize the existence of lipid and protein heterogeneity within membranes and suggest that the biophysical properties of these individual components may provide a mechanistic basis

for understanding membrane functions (4, 7-9). As such, membrane lipid composition is recognized as non-random, but instead the result of highly regulated intracellular trafficking processes, that are not yet fully understood (6).

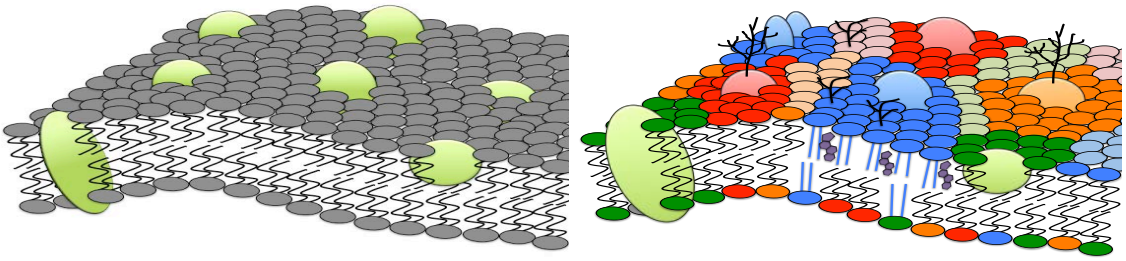

Figure 1.1: Early and current fluid mosaic model (a) Fluid mosaic model as proposed by Singer and Nicholson demonstrates the homogeneous distribution of lipids with embedded proteins **(b)** Current membrane model identifies lipid asymmetry and lateral microdomains enriched in particular lipids and proteins.

1.1.2 Membrane lipid types

In eukaryotes, membrane lipids can be classified into one of three classes, based on their lipid backbone namely, glycerolipids, sphingolipids and sterols (2, 6) (Figure 1.2). **Glycerolipids** contain a glycerol backbone derived from glycerol 3-phosphate and include glycerophospholipids as well as neutral lipids. Glycerophospholipids are amphipathic, with hydrophilic polar headgroups and hydrophobic acyl tails esterified at the *sn-1* and *sn-2* positions of the glycerol backbone.

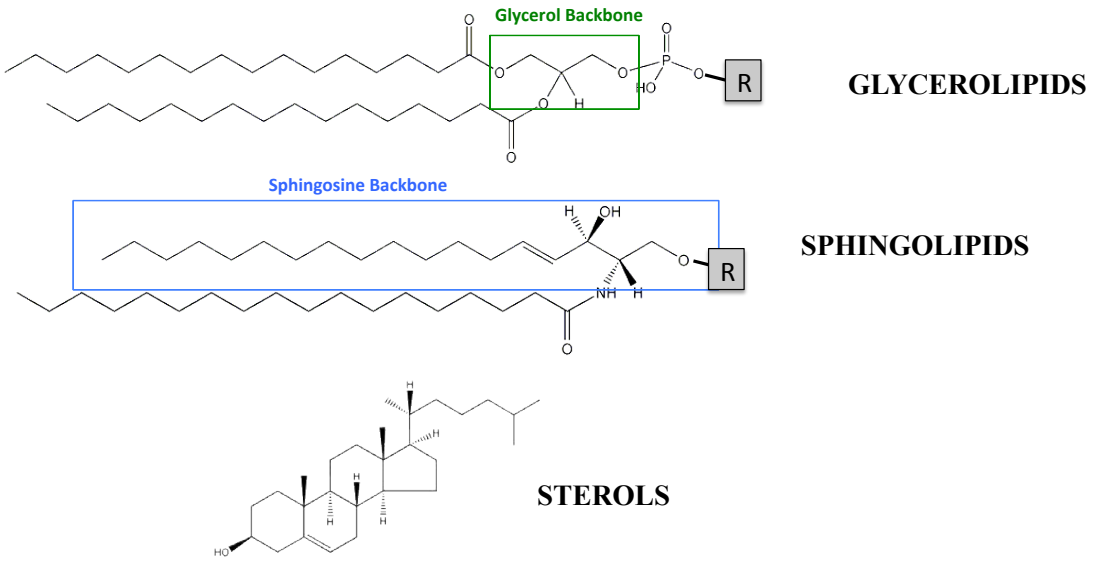

Figure 1.2: Three membrane lipid classes, glycerolipids, sphingolipids and sterols Glycerolipids contain a glycerol backbone (green box), sphingolipids contain a sphingosine backbone (blue box), sterols, contain a four-ring structure. R denotes headgroups.

Phosphatidic acid (PA) is the precursor in the *de novo* synthesis of major glycerophospholipids in eukaryotic cells, phosphatidylcholine (PC), phosphatidylethanolamine (PE), phosphatidylserine (PS), phosphatidylinositol (PI) as well as the mitochondrial lipids phosphatidylglycerol (PG) and cardiolipin (CL) (Figure 1.3). PC is the predominant lipid comprising over 50% of all phospholipids found in eukaryotic membranes (1, 2).

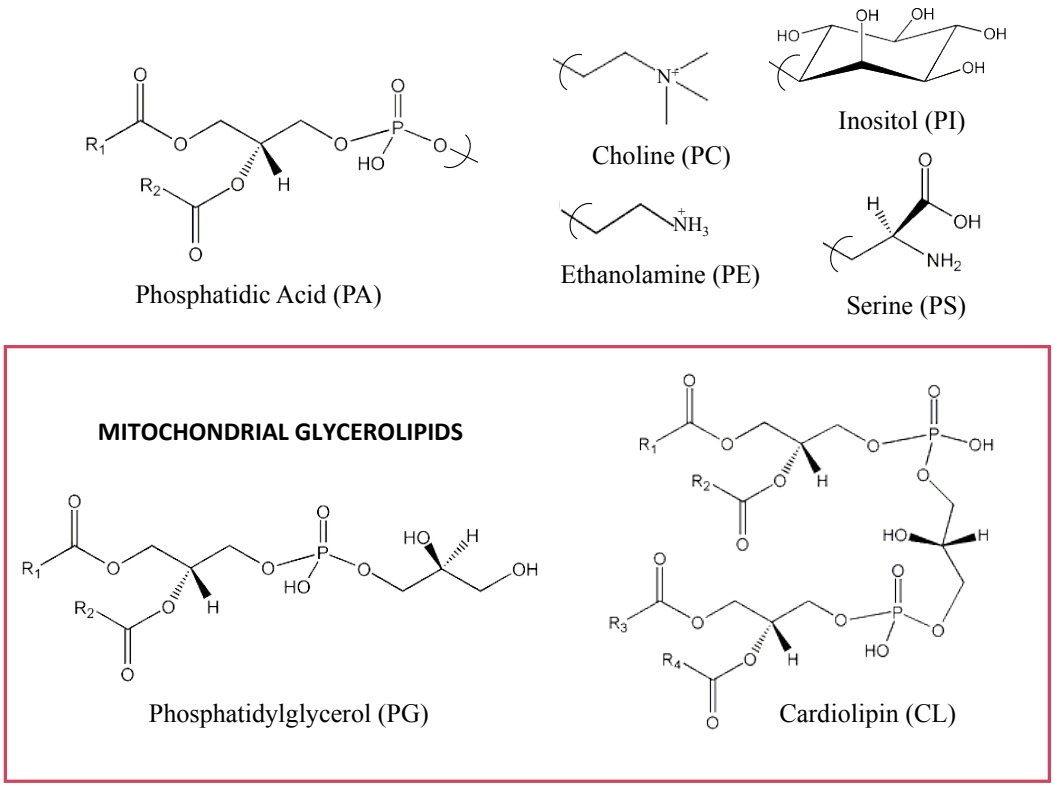

Figure 1.3: Structures of glycerophospholipids Glycerophospholipids are synthesized *de novo* from precursor PA. Headgroups of other glycerophospholipids are shown; choline for PC, inositol for PI, ethanolamine for PE, serine for PS. Mitochondrial localized lipids, PG and CL are highlighted in red box.

Glycerolipids can be remodeled through the Lands cycle, by the sequential action of phospholipases (PLA_1 or PLA_2) and acyltransferases (Figure 1.4). Removal of one acyl chain via a type A phospholipase produces the "lyso" form of the parent phospholipid (10).

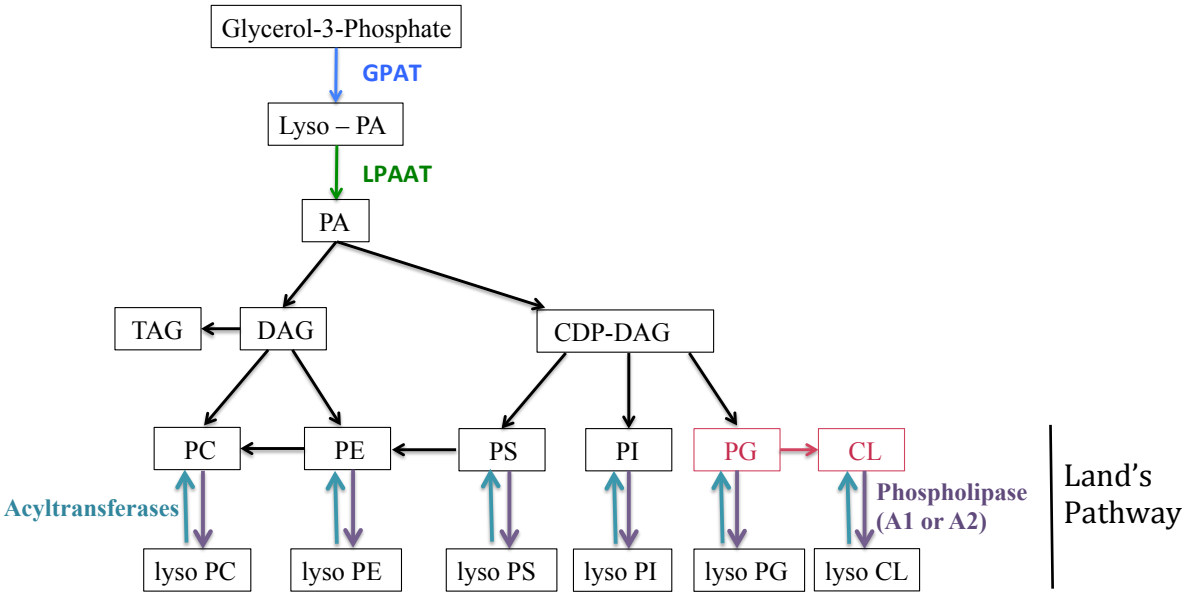

Figure 1.4: Synthesis and remodeling of glycerophospholipids in yeast *De novo* synthesis of glycerophospholipids from glycerol-3-phosphate and lipid turnover (GPAT= glycerol-3-phosphate acyltransferase, LPAAT= lyso-phosphatidic acid acyltransferase, PA= phosphatidic acid, DAG= diacylglyceride, PC= phosphatidylcholine, PE= phosphatidylethanolamine, TAG= triacylglycerides, PI= phosphatidylinositol, CL= cardiolipin, PG= phosphatidylglycerol, PS= phosphatidylserine).

Sphingolipids, contain a sphingoid base, sphingosine in animals, which is the product of the condensation reaction of serine and palmitoyl CoA (2, 6). The addition of a fatty acid to the nitrogen of the amine of sphingosine creates a ceramide (2). Sphingolipids are also amphipathic, as the headgroups are polar and the acyl chains are hydrophobic. Esterification of ceramide with different head groups produces a variety of more complex sphingolipids. A phospho head group produces a phospholipid while addition of sugars gives rise to glycosphingolipids (Figure 1.5). The phospho head group of sphingolipids varies in different species. Phosphorylcholine is the head group of sphingomyelin (SM) in animal cells while phosphorylinositol is found in plant and yeast sphingolipids. In yeast, further mannosylation of inositol generates the most abundant

sphingolipid of this organism, mannose-(inositol-phosphoryl-2)-ceramide ($M(IP)_2C$) (Figure 1.5).

Addition of a single galactose or glucose to ceramide produces the cerebrosides galactosylceramide and glucosylceramide respectively. The addition of a galactose to glucosylceramide makes lactosylceramide, which is the precursor to more complex glycosphingolipids in mammals (Figure 1.5) (2).

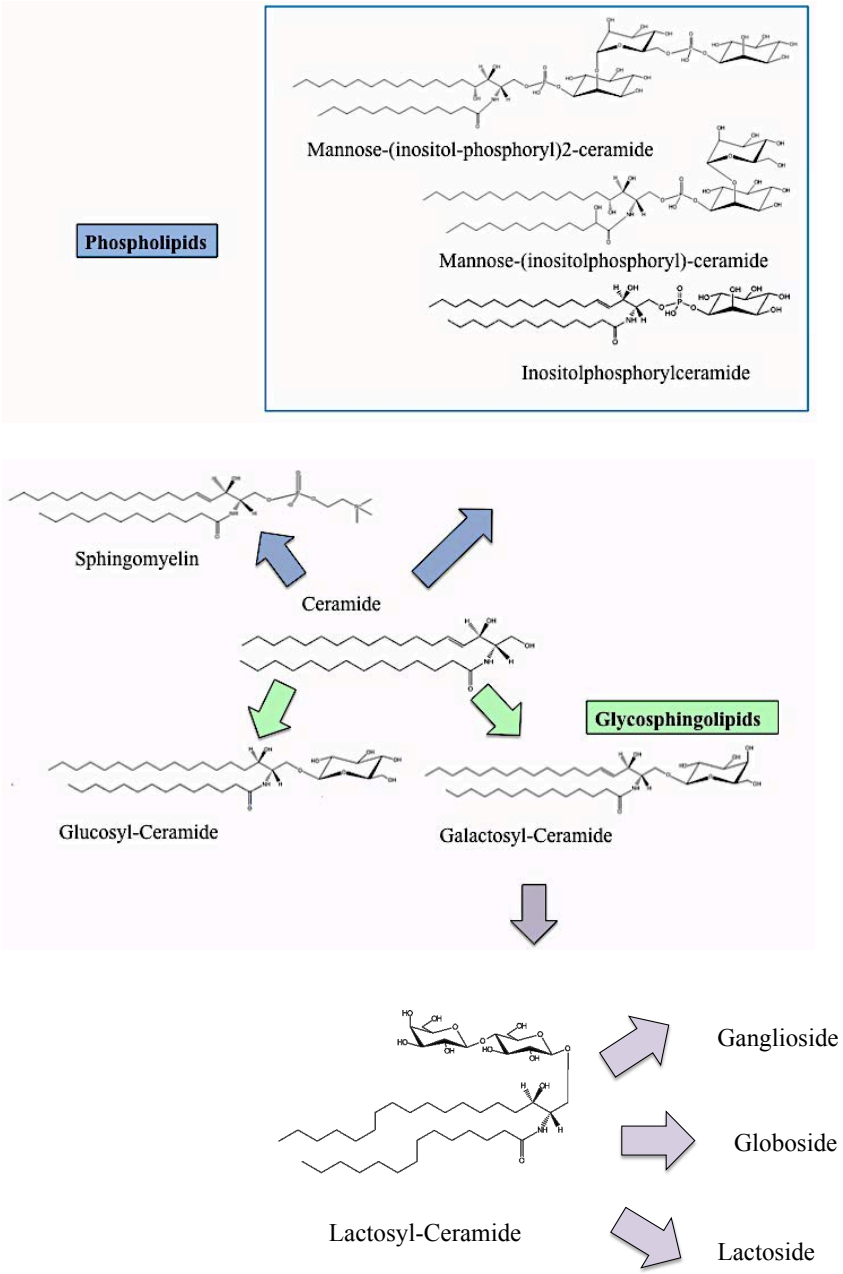

Figure 1.5: Sphingolipid structures Structures of sphingolipids arising from the simplest sphingolipid, ceramide. Phospholipids, sphingomyelin or phosphorylinositol in yeast (blue box). The phosphorylinositol can be mannosylated to mannose-(inositolphosphoryl)-ceramide, or further to mannose-(inositol-phosphoryl-2)ceramide. Glycosphingolipids can be made by addition of sugar moieties, glucose and galactose to form glucosyl- and galactosyl-ceramide. Addition of glucose to galactosyl-ceramide yields lactosyl-ceramide which is a precursor to more complex glycosphingolipids, gangliosides, globosides and lactosides.

The last class of membrane lipids is **sterols**, which contain a four ring planar structure built from isoprenoid units. Synthesis of sterols from acetyl CoA is highly conserved in eukaryotes, with the predominant sterol in mammals being cholesterol, where in yeast it is ergosterol (Figure 1.6) (1, 6, 11). The structural changes include the additional double bonds at carbons 7 and 22 and the additional methyl group at carbon 24 in the side chain of ergosterol (Figure 1.6). The hydroxyl group is ubiquitous in all sterols and is essential for providing amphipathicity to the molecule, although it cannot form bilayers as members of the other two classes of lipids (11). Sterols are known to interact with members of the polyene family of antibiotics, like filipin, which has become a useful tool for studying sterol localization using fluorescence microscopy. It is proposed that filipin forms a 1:1 complex with the un-esterified 3-β hydroxyl group of sterols (12).

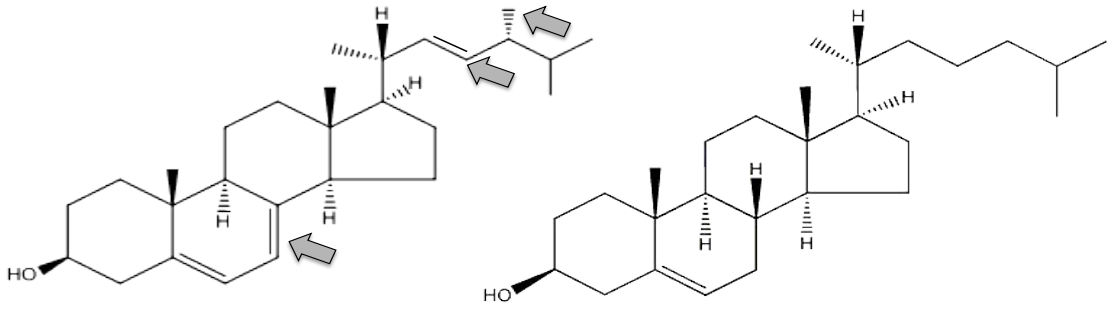

ERGOSTEROL **CHOLESTEROL**

Figure 1.6: Structures of ergosterol and cholesterol Structural differences highlighted between ergosterol (predominant sterol in yeast) and cholesterol (predominant sterol in mammals).

1.1.3. Lipids as structural components: Shape theory, membrane formation, curvature stress

The amphiphillic nature of lipids is essential to the formation of cellular membranes (2, 13). As such, the lipid molecules arrange themselves in a way that allows for the polar hydrophilic headgroups to face the aqueous environment, while shielding the hydrophobic domains. The association of hydrophobic domains is facilitated by the hydrophobic effect, which refers to the repulsion of non-polar molecules for water as a driving force for their interaction in an aqueous environment (13). Polar head groups interact via hydrogen bonding, dipole and electrostatic interactions (2, 13). Since lipid interactions in membranes are non-covalent, membranes tend to be highly dynamic and fluid (14).

The fluidity of a membrane is determined by the mobility of individual lipid components and varies with temperature. In general lipid bilayers can exist in either a solid (gel) (Lβ) or a liquid phase (Lα). The temperature at which a membrane transitions between a solid phase to a liquid phase is known as the transition or melting temperature (Tm) and is dependent on acyl chain length and the degree of unsaturation (15). In addition to these lamellar phases, lipids may also form non-bilayer phases like Hexagonal II (H_{II}) or micelles (Figure 1.7) (2, 14, 15). The phase that a fully hydrated membrane lipid prefers to adopt under a given set of conditions can be rationalized by considering the geometry of the lipid molecule in those conditions and how it would pack in various aggregates.

If we consider different phospholipids that have the same number and type of hydrocarbon chains, the shape will be determined primarily by the differences between cross-sectional areas of the hydrated polar headgroups. When the cross-sectional areas of the head and the tail are

similar the lipid has a cylindrical shape, if the polar head group is smaller then it will adopt a cone shape, but if the polar headgroup is larger it will adopt an inverted cone shape (2, 14, 15). Cylindrical shaped phospholipids like PC, SM, PS, PI, PG, PA, CL form lamellar, bilayer phases (2, 5, 14). Cone shaped lipids such as PE, CL with calcium, PA with calcium, PA at acidic pH, PS at acidic pH, will conform to an inverted micellar structure (Hexagonal II), where the hydrophobic domains are facing outward, surrounding an aqueous core. It is important to note that CL, PA and PS will only conform to cone shape when the negative charges on the headgroups are either masked by a cation, such as calcium or protonated at low pH, as this reduces the size of the headgroup. Conversely, inverted cone shaped lipids, such as lysolipids and detergents will form micellar structures, with hydrophilic headgroups facing outwards, shielding a hydrophobic core (Figure 1.7) (2, 5, 14).

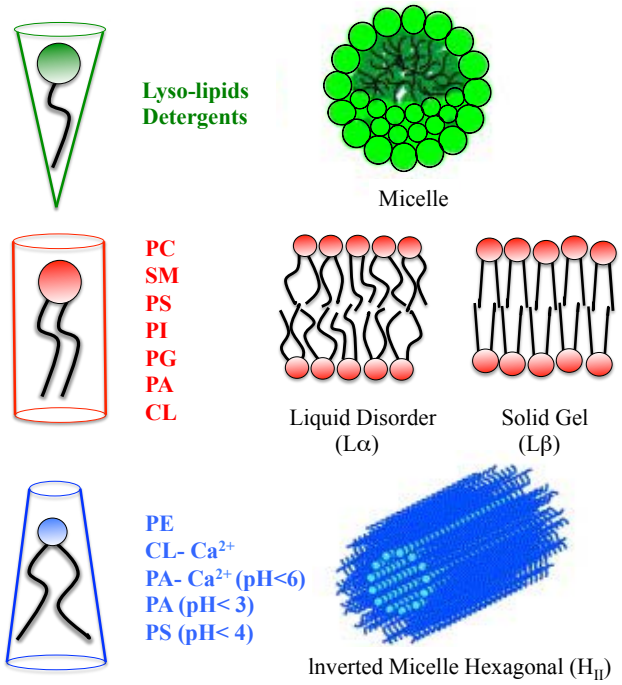

Figure 1.7: Lipid shapes and phases Cone shaped lipids: lysolipids and detergents form micellar structures, Cylindrical shaped lipids: PC, SM, PS, PI, PG, PA, CL will form liquid disordered (Lα) or solid gel (Lβ) phases. Inverted cone shaped lipids: PE, CL- Ca^{2+}, PA - Ca^{2+} at pH <6, PS at pH< 4 (PS) will form inverted micelle/hexagonal structures.

The ability for certain lipids to form micelles is driven by the hydrophobic effect. As the concentration of a lipid monomer within a solution increases, the stability of individual lipids in solution decreases and there is a greater tendency for the lipid molecules to interact with each other forming micellar structures (2, 13). The concentration at which micelles begin to form, the critical micelle concentration (CMC) is a narrow concentration range which is influenced by the size of the hydrophobic moiety in the lipid; the larger the hydrophobic domain, the lower the CMC (2, 13). Lipids in a micellar conformation will have a hydrophobic core, with the head groups facing outward into the aqueous solution (2, 5, 14). It is important to note that under physiological conditions, cells will limit the amount of lysolipids present, and as such, micelles rarely occur. Eukaryotic cell membranes are not single component systems, but in fact complex

lipid mixtures that display phase separation. In other words, lipids forming different phases can coexist within the same membrane. Under physiological conditions, eukaryotic cell membranes form a liquid-crystalline phase. The different lipid phases that exist within this lamellar state, are based on the order (saturation) of the acyl chains, as well as the translational diffusion coefficient, which reflects diffusion rates, based on the tightness of the lipid packing (1). The first phase, the liquid-crystalline (liquid disordered, Lα), is usually observed for unsaturated glycerophospholipids. This phase tends to by highly fluid, with fast rates of diffusion as the double bonds decrease the packing efficiency of the acyl chains. The second phase, solid gel (Lβ), is usually observed in membranes containing sphingolipids, especially SM with saturated acyl chains. This phase tends to have more efficient packing, is therein less fluid and has slower rates of diffusion. The third phase the liquid-ordered (Lo), forms when sterols associate with bilayer-forming lipids. Since sterols are planar and hydrophobic, they tend to interact tightly with the hydrophobic acyl chains of saturated lipids (16). The presence of sterols both increases the membrane thickness, and extends the acyl conformations, creating a tightly packed ordered domain similar to the solid gel phase, while retaining the fast rates of diffusion of the liquid disordered phase (1, 16). The presence of a small amount of non-cylindrical shaped lipids in bilayers will either impose a negative or a positive curvature stress, depending on their shape (14). This type of membrane curvature is essential in transient processes such as budding, fission, fusion, but may also be necessary in order to incorporate certain large or globular shaped proteins in a way that minimizes membrane stress (1, 5).

1.1.4: Lipids are not homogeneously distributed

The same lipid classes exist in all membranes, but their distribution varies among organelles, and even between bilayer leaflets (1, 6, 17, 18). The contributing factors to this non-random segregation depend on the localization of lipid synthesis and intracellular lipid transport mechanisms (1, 6, 17). Within a eukaryotic cell, the endoplasmic reticulum (ER) and the Golgi are the organelles responsible for lipid synthesis. Synthesis of glycerophospholipids, ceramide, sterols and TAG's takes place in the ER, while the Golgi is the site of synthesis for more complex sphingolipids, such as glucosylceramide and SM, as well as PE and PC (1, 6, 17, 18). Lipids are then transported to other organelles, using vesicular and non-vesicular transport mechanisms. This allows for the non-random and preferential transport of membrane lipids to particular organelles, and as such drives membrane heterogeneity (1, 18). For example, the mitochondria is able to synthesize it's own lipids, PE, PG, PA and CL, however it still relies on non-vesicular transport of PC, PS, PI from the ER (17).

The ER contains unsaturated glycerophospholipids but has reduced concentrations of sterols and all together lacks glycosphingolipids, wherein the PM, is enriched in glycosphingolipids, as well as sterols, SM, and PS (1, 6, 17). Since sterols can easily diffuse across membranes, their lowered concentration in the ER may be attributed to the lipids' high affinity for sphingolipids, which are present in the Golgi and enriched in the PM (1, 6, 18). However, the lack of SM and glycosphingolipids in the ER may reflect the absence of a functional need of sphingolipids in the ER (17, 18).

The localization of particular membrane lipids is also non-random and highly dependent on vesicular and non-vesicular lipid transport mechanisms. Lipids are able to laterally diffuse in the plane of the membrane, "flip-flop" between membrane leaflets, but may also be exchanged

between two membranes, in a process known as “monomeric exchange” (6). Lipid “flip-flop” can be spontaneous, albeit for the majority of lipids this is a slow process that may take hours or even days. Therefore when required it can be mediated by translocases called flippases, floppases and scramblases (1, 6). The ER contains adenosine triphosphate (ATP)-independent flippases that help translocate glycerophospholipids, and as a result, allow this organelle to maintain highly symmetric distribution between leaflets. Conversely, the Golgi and the PM have high bilayer asymmetry, due in part to ATP-dependent aminophospholipid translocases that help to move PE and PS onto the cytoplasmic side, leaving glycosphingolipids, SM, PC enriched in the luminal, or extracellular leaflet (1, 6, 17, 18).

1.1.5: Lateral microdomains

The co-existence of different lipid classes and proteins in cellular membranes leads to the formation of lateral segregation of membrane components and the emergence of microdomains known as “lipid rafts” (4, 19). The formation of these patches of heterogeneity is strongly influenced by specific lipid-protein and lipid-lipid interactions, provided by the hydrophobic effect as well as various intra-molecular interactions, such as hydrogen bonding (2, 4, 20). Lipid rafts are enriched in glycosphingolipids, SM, and sterols in the exoplasmic leaflet (Figure 1.8) (19). The ability for sterols to embed in the empty spaces between acyl chains of the sphingolipids, allows for tight packing in order to form a liquid ordered (Lo) phase (2, 9, 21). In addition, membrane soluble globular proteins cluster within these domains, and interact with the present lipids, therein decreasing their lateral movement (2, 22). These micro-domains are impervious to breakdown using non-ionic detergents like Triton-X100 at low temperatures. This

allows for these “detergent resistant membranes” (DRMs) to be purified using density gradient centrifugation (2, 16, 22).

Lipid rafts are more than just nano-scale assemblies of sphingolipids, sterols and proteins, they are also platforms for regulation of cellular signaling pathways (4, 14, 16). The formation of these lipid rafts is essential in compartmentalizing cellular membrane functions (2, 20). To date, lipid rafts have been associated with a variety of signal transduction pathways, as well as endocytotic mechanisms (4, 14, 19, 22). These microdomains can selectively target signaling pathways by confining proteins to specific locations. Moreover, the existence of these rafts may aid in concentrating receptors, leading to faster ligand and effector binding allowing for more effective transduction of intracellular signals, such as those involved in proliferative and pro-apoptotic pathways, which are described in later sections (19, 22).

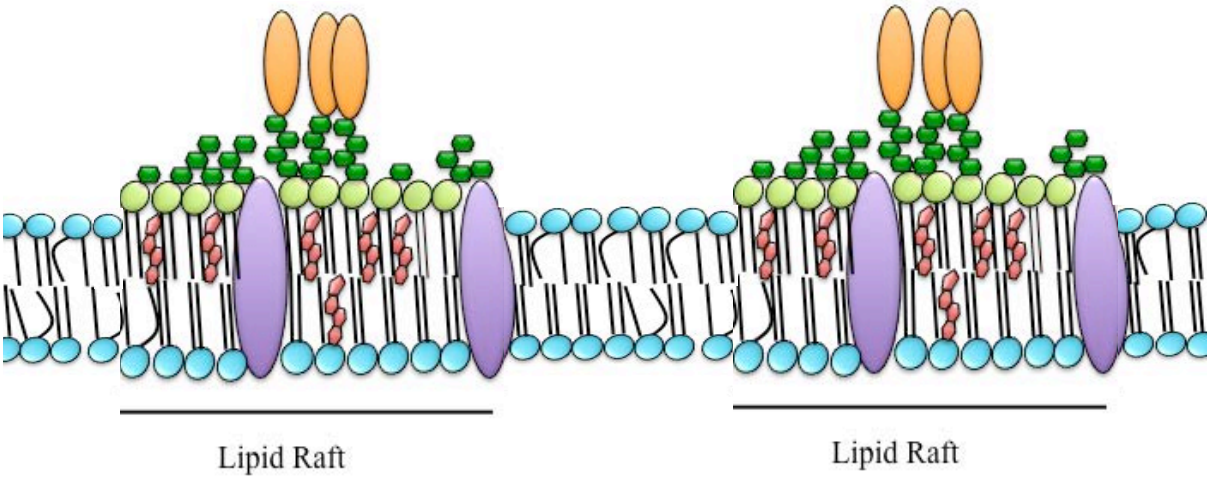

Figure 1.8: Lipid rafts Schematic of lipid microdomains (lipid rafts), containing sterols (red), glycosphingolipids (green) associated with glycophosphatidylinositol (GPI)-anchored proteins (orange) and raft transmembrane proteins (purple) surrounded by glycerophospholipids (blue).

1.2 Anti-tumor lipids: Discovery to present applications

1.2.1 The first generation: Alkyllysophospholipids (ALPs)

Anti-tumor lipids (ATLs) were first synthesized with the purpose of being used in immunomodulating applications. The idea emerged when studies showed that phagocytosis in macrophages was greatly enhanced by the presence of lysophosphatidylcholine (lysolecithin, lysoPC) leading to reason that intracellular accumulation of this lipid may play a significant role in the human immunological response (23-25). It was hypothesized that an increased amount of lysoPC resulting from activation of PLA_2 activity would stimulate the immune system and increase macrophage activity (24-29). Experiments with exogenous lysoPC indeed supported this, however, lysoPC is an intermediary phospholipid with a relatively short intracellular half-life, as it is easily metabolized by lysophospholipase and acyltransferase enzymes to glycerolphosphocholine and PC respectively (23, 24).

Therein, in order to increase the metabolic stability and decrease the turnover rate of lysoPC, Westphal *et al.* synthesized the first generation of lysoPC derivatives, alkyl-lysophospholipids (ALPs) characterized by ether linked aliphatic side chains attached to the glycerol backbone (27, 28, 30, 31). Hydrolysis by PLA_1 and PLA_2 was prevented by converting the ester bond in the *sn1* position of the glycerol backbone to an ether bond, and attachment of an acyl group was blocked by substitution of the hydroxyl group in the *sn2* position with another ether linked molecule (Figure 1.9) (24).

As expected, initial experiments on these synthetic ALPs showed some of them increased immunological responses by increasing macrophage activity, but surprisingly some compounds showed potent antitumor activity both *in vitro* and *in vivo* (24, 32, 33). ALPs, and in particular the prototypic drug of the family, *rac*-1-*O*-octadecyl-2-*O*-methyl-glycero-3-phosphocholine (Et-

18-OCH_3; edelfosine) were determined to be strong anti-neoplastic agents as compared to lysoPC, bearing high selectivity towards tumoral cells, sparing normal healthy cells even at sub-lethal drug concentrations (24, 26, 34-36).

A decade later, a naturally occurring biologically active ether lipid, 1-*O*-alkyl-2-acetyl-*sn*-glycerol-3-phosphocholine (platelet activating factor, PAF) was discovered that bore a structural resemblance to edelfosine (Figure 1.9). While both compounds maintain a phosphocholine headgroup at the *sn3* position, and an ether linked acyl chain at the *sn1* position of the glycerol backbone, PAF has an acetyl group attached via an ester linkage in the *sn2* position. Despite these structural similarities, PAF shows no anti-tumor activity *in vivo* or *in vitro* and edelfosine doesn't show any PAF-like activity *in vivo* (37). Moreover, PAF is recognized by a cell surface receptor, wherein, edelfosine uptake and function is independent of these receptors (37).

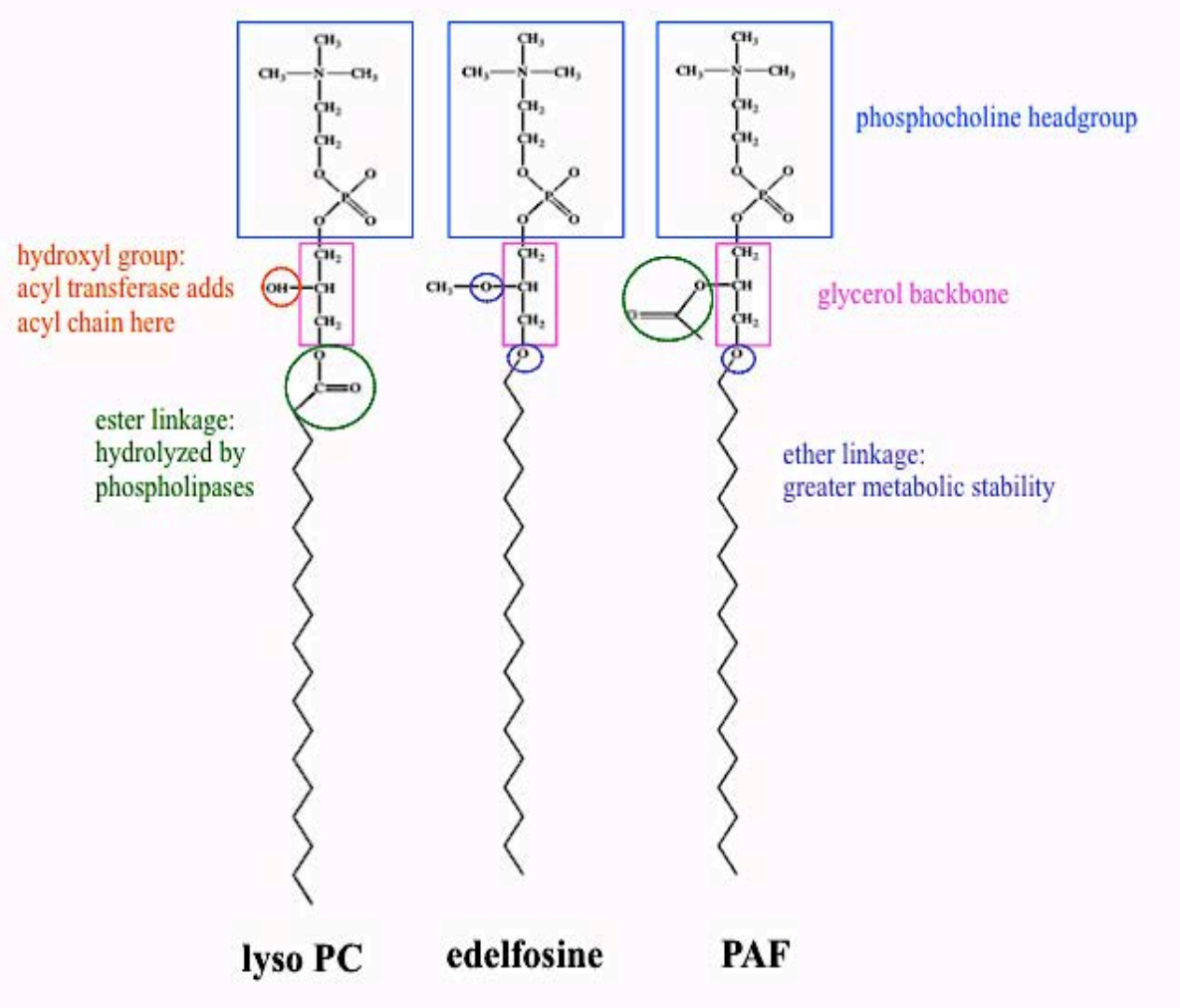

Figure 1.9: Structural comparison of lysoPC, edelfosine, and PAF LysoPC, edelfosine and PAF contain a glycerol backbone (pink box) and a phosphocholine headgroup at the *sn3* position (blue box). LysoPC contains a hydroxyl group at the *sn2* position (orange circle) and an ester linkage at the *sn1* position (green circle) Edelfosine and PAF both contain ether linkages at the *sn3* positions (purple circles). Where edelfosine contains a methyl group at the *sn2* position, PAF has an acetyl group. (LysoPC= lysophosphatidylcholine, PAF= platelet activating factor).

Over the years, edelfosine showed promising *in vitro* anti-tumor activity against cells extracted from malignant sarcoma tumors (35) and ascite tumors of mice (36), and various cell lines, including human leukemic cell lines (38-40), and mouse lymphoma cell lines (41). The results from *in vivo* studies also showed edelfosine exerting an effect on transplanted human ovarian carcinomas in mice (42), mammary carcinomas in rats (43) and leukemia and lymphoma

neoplasias in mice (34). In addition, animal models showed that the effect of edelfosine was independent of the mode of administration, and that at doses cytotoxic to neoplastic cells, there were minimal side effects (34, 42, 43). Gastrointestinal issues, hemolysis and compromised renal function were only seen in a few cases of primates after repeated drug doses (26).

Giving these favorable outcomes in mammalian studies, edelfosine was moved into Phase I clinical studies. The pilot study was performed on 16 patients with a variety of malignant solid tumors. Of these patients, only those with non-small lung cell carcinoma showed a short-term remission, but in the end, edelfosine had no long-term effects and all patients died from disease progression within one year. The side effects in both intravenously and orally treated patients included gastrointestinal effects such as nausea and vomiting, liver and renal toxicity, and erythema, all of which could be reversed after a few days following drug removal, which prompted further clinical studies (44).

Phase II studies were done in patients with non-small-cell lung carcinoma. The major side effects were in compliance with those seen in Phase I studies. Although complete tumor remission was rare, most patients did show a decreased rate of tumor progression, suggesting the drug may have a more cytostatic effect on these cells (45).

Despite these clinical drawbacks, edelfosine still found some applications. Since the ALP had no effect on murine bone marrow cells (35), embryonic human lung fibroblasts or human bone marrow cells (38), it is currently widely used to purge bone marrow in patients suffering from acute leukemia (25, 32, 46).

1.2.2 The second generation: Alkylphosphocholines (APCs)

Further studies demonstrated that the glycerol backbone was not essential for eliciting antitumor activity. The removal of this glycerol moiety, gave rise to hexadecylphosphocholine the prototypic drug of the alkylphosphocholine (APC) family, 2-(N,N,N-trimethylamino)ethyl phosphate (HPC, Miltefosine) (29) (Figure 1.10). In contrast to edelfosine, miltefosine seemed to have little effect on either lymphoma, and lung cells carcinomas (29) and acted as an immunosuppressant by decreasing macrophage phagocytosis (47). Regrettably, Phase I clinical trials using miltefosine in cancer patients showed the drug to have hemolytic properties when administered intravenously (48, 49) and as such, an oral approach was attempted. However, with oral administration, miltefosine targeted the gastrointestinal tract, causing side effects such as abdominal pain, appetite loss, diarrhea, nausea and vomiting (50, 51). From here, miltefosine was developed into a topical formulation and was tested against human breast metastatic cancers, with very promising results (52). Although miltefosine is unable to cure skin metastases, it provides patients with great palliative benefits, with minimal side effects (29, 53). As such, miltefosine, or trade name *Miltex* is currently being used as a treatment for cutaneous lymphoma and cutaneous breast cancers (54, 55).

In an attempt to increase the therapeutic range of APCs, and relieve the unwanted side effects, a few structural changes were made to miltefosine. Since miltefosine can be metabolized into choline and phosphocholine by phospholipases within in the cell, it was proposed that elimination of this head group may alleviate the accumulation of this metabolite, and relieve unwanted side effects.

Of the newly synthesized derivatives, perifosine (octadecyl-(1,1-dimethyl-4-piperidylio)phosphate, D-21266) (Figure 1.10) which had a piperidine moiety in place of the phosphocholine head group, showed the most promising clinical applications (56-58).

Overall, perifosine showed higher anti-tumor activities at lower doses as compared to miltefosine both *in vitro,* in leukemic, lung and prostate mouse cell lines (57), and *in vivo* in mammary carcinomas in rats (56). Despite high activity, perifosine was only able to partially alleviate the gastrointestinal symptoms linked to miltefosine (57, 58). In 2012, perifosine failed Phase III colorectal cancer trials, but is currently in Phase III clinical trials for multiple myeloma (Æterna Zentaris).

The second structural modification, alterations in the length of the alkyl chain had effects on a drugs cytotoxicity, with the most promising candidate, erucylphospho-N,N,N-trimethylpropylammonium (ErPC, erucylphosphocholine) (Figure 1.10) having a 22 carbon length chain with a cis Δ-9 double bond (59). Most notably, erucylphosphocholine showed minimal side effects; the drug showed minimal organ toxicity, did not accumulate in the kidney and was not hemolytic as compared to its predecessor miltefosine (59, 60). As such, erucylphosphocholine became the first of the APCs to be administered intravenously without side effects (59, 60). *In vivo* applications in rats showed that erucylphosphocholine was effective against mammary carcinomas, and that the drug was able to cross the blood brain barrier, and accumulate in the brain, findings that were confirmed using *in vitro* human brain tumor cells (60, 61). As such, erucylphosphocholine has become a promising candidate for human brain tumor treatment, and studies are currently underway (59).

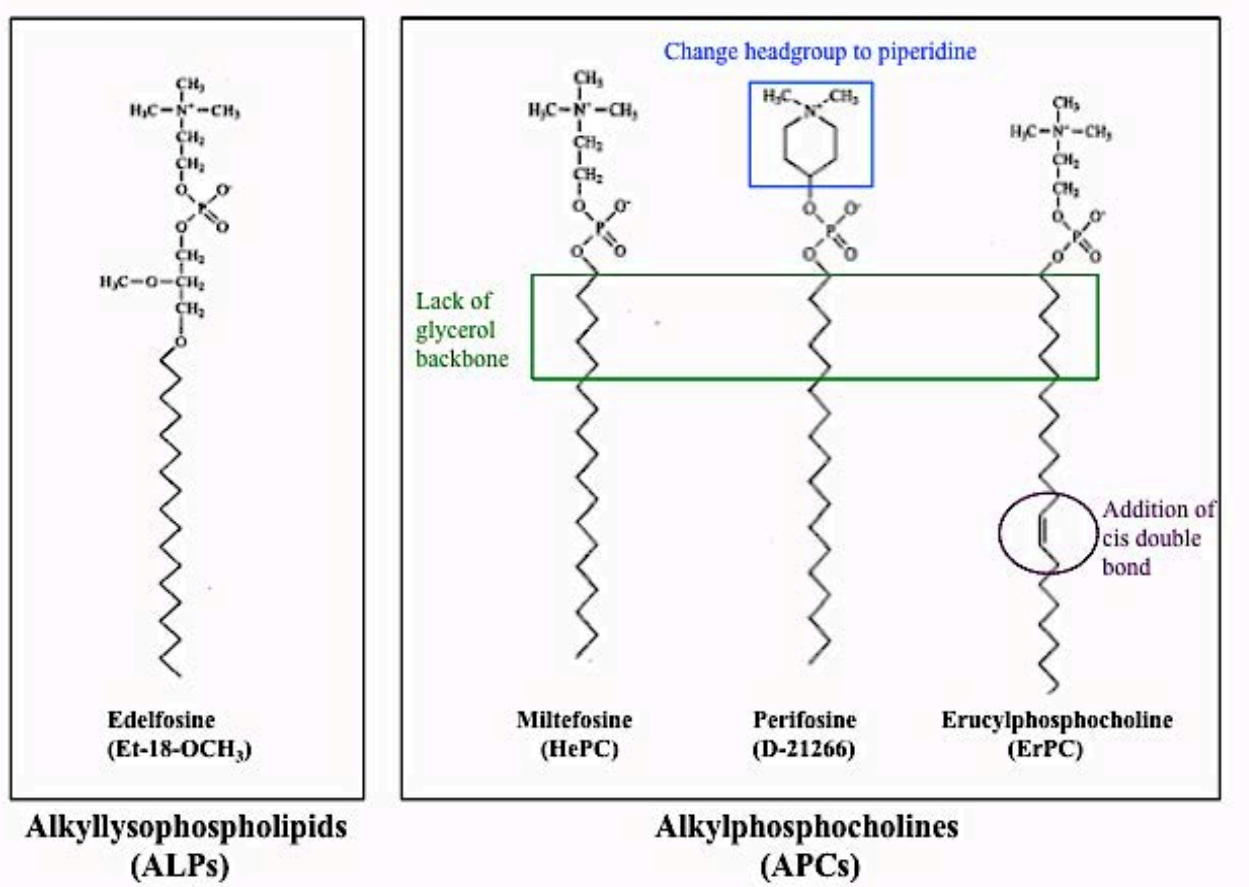

Figure 1.10: Chemical structures of anti-tumor lipids Edelfosine is the prototypic drug of the family and is representative of the ALP's. APC's represent the second generation of ATL's, lacking a glycerol backbone, and acyl chain is esterified to the phosphate. Perifosine substitutes the phosphocholine headgroup for a piperidine moiety. Erucylphosphocholine maintains the phosphocholine headgroup but has introduced a cis-Δ9 double bond in the acyl chain.

1.2.3: Further applications of anti-tumor lipids

In parallel to their anti-tumoral properties, ATLs have other therapeutic functions. For instance, both edelfosine and miltefosine have shown to be important anti-protozoal agents in certain tropical diseases (62). Of importance, both drugs showed a strong cytotoxic effect in all species of Leishmania (62-64). Moreover, their effect was mostly strongly seen in the promastigote stage, (the causative agent of visceral leishmaniasis) in both *Leishmania spp.* and *Trypanosoma cruzi* (62-64). Luckily, the gastrointestinal side effects seen in patients with

leishmaniasis were minimal to mild, as compared to those seen in patients taking miltefosine as a cancer treatment (65). As such, in March 2002, miltefosine became available under the trade name *Impavido* for the oral treatment of visceral Leishmaniasis in India (62, 66).

Following its success as a topical treatment against skin metastases, it was thought that miltefosine may also be used topically in treatment of ulcerating skin lesions caused by *Leishmaniasis spp.* Topical applications of miltefosine were successful in treating infected mice, but had minimal results in human trials, and as such oral administration remains the only effective route for treating all types of Leishmaniasis (51, 67, 68).

Over the last decade, edelfosine has also been patented as treatment for autoimmune diseases, including multiple sclerosis, as an anti-inflammatory, against ulcerative colitis and as an anti-viral agent against herpesvirus and hepatitis B, where miltefosine has also been used for treatment of papilloma induced warts, and psoriasis (66). Clinically, ATLs can be used as biological response modifiers providing a synergistic effect in cancer treatments when combined with other drugs or radiation (69, 70).

1.2.4 The novelty of anti-tumor lipids: Lipid membrane therapy

Despite the lackluster performances this drug family achieved in anti-tumoral clinical trials, there is still a vast amount of research dedicated to understanding how these drugs function and what structural modifications can be done to achieve better clinical results. The driving force behind this continued research is the novel therapeutic approach these drugs bring to the cancer treatment.

General cancer therapies rely on the synergistic effect of chemotherapy and radiation. Where radiation is a localized means of destroying tumoral cells using ionizing radiation; chemotherapy

takes a global approach by targeting all highly proliferative cells including healthy neoplastic cells within the body, causing high toxicity and a plethora of unwanted side effects (4). Conventional chemotherapy targets a specific protein or pathway within the cell, often inducing deoxyribose nucleic acid (DNA) damage, resulting in the inability to proliferate (4, 14). For example, drugs such as cisplatin, bleomycin and doxorubicin target and damage DNA structure directly, where vinblastine and taxol, target the cytoskeleton affecting a cells ability to undergo mitosis (71). These cytotoxic drugs are also both mutagenic and carcinogenic. As such, they may induce permanent damage that not only increases the chance of patients developing secondary cancers, but may also affect fertility, cause an increase in abortions and fetal defects in children of treated patients, and cause residual bone marrow damage (71). Therein, the use of non-mutagenic drugs as alternatives to these cancer treatments would be greatly beneficial to the patient.

In order for cells to proliferate, they need to synthesize more membranes, and as such, tumoral cells are shown to have up-regulated lipid biosynthetic pathways (72). A new therapeutic approach, termed, lipid membrane therapy aims to target membranes as a non-mutagenic strategy to stop proliferation. As most cellular functions and signaling pathways are associated with cellular membranes, or require membrane bound proteins, targeting drugs to alter membrane structure allows for interference with a larger number of cellular pathways, in turn increasing the number of molecular drug targets, while minimizing mutagenesis (14). Expansion of drug targets may increase drug efficiency and make it more difficult for cells to adopt drug resistance. Since ATLs are synthetic phospholipid derivatives, these drugs can easily accumulate in cellular membranes. It is well established that these drugs are highly selective towards tumor cells, while sparing healthy ones, a clear advantage to current chemotherapy. In addition, these drugs are

non-mutagenic as they do not target the DNA. By embedding into cellular membranes, they are able to alter membrane biophysical characteristics that depend on both proteins and lipids. They have also been shown to interfere with metabolic pathways such as phospholipid biosynthesis and re-modeling and lipid based signal transduction pathways (24, 25, 38, 40, 70, 73).

1.2.5: Mode of action of anti-tumor lipids

After four decades of research, lipid membrane therapy has become the new approach to identifying the cellular targets of ATLs. Only recently are ATLs being recognized as non-traditional anticancer agents that target cellular membranes. The following section emphasizes the involvement of membranes in the key cellular signaling pathways affected by ATLs. It is important to note that ATLs are inverted-cone shaped, and can take on detergent-like properties at high concentrations (69, 74). The experiments presented here and conducted in this thesis use clinically relevant, micromolar (μM) concentrations, values that fall below the drug CMCs.

1.2.5.1 Inhibition of phosphatidylcholine synthesis

Edelfosine inhibits the rate limiting, CTP:phosphocholine cytidyl transferase (CCT) step of the Kennedy pathway for *de novo* PC synthesis (75). Since PC is the most abundant phospholipid found in mammalian cellular membranes, the lack of availability may affect a cells ability to make membranes, which are essential for cell proliferation (76). Moreover, PC is an important source for other lipids, as it can be broken down to lipid secondary messengers such as PA and DAG via phospholipase D and C activity respectively and the phosphocholine headgroup of PC may combine with ceramide to produce SM (Figure 12). As such, decreases in PC would

result in decreased levels of SM and mitogenic signaling lipids such as DAG, with increased levels of pro-apoptotic signaling lipids like ceramide (77).

Although it is widely accepted that edelfosine inhibits *de novo* PC synthesis at the CCT step of synthesis in the cytidine di-phosphate (CDP)-choline pathway, cells having alternate means of synthesizing PC, (such as methylation pathways from PE to PC) (Figure 1.11) still show sensitivity to the drug. Therein suggesting that PC inhibition is not the main means by which edelfosine induces cell death (76, 78).

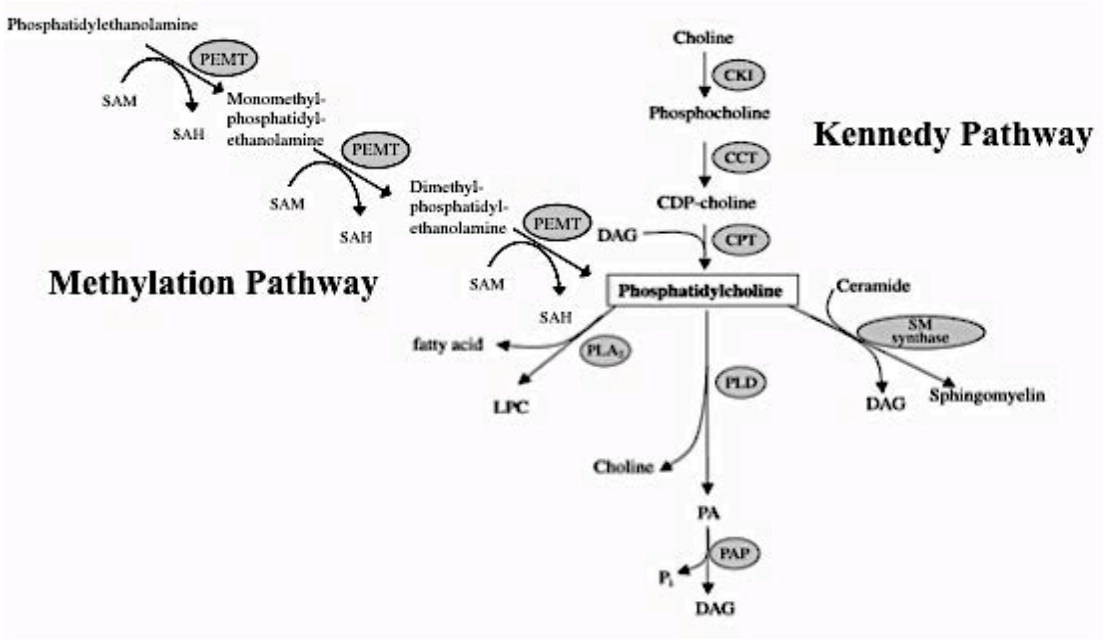

Figure 1.11: Phosphatidylcholine synthesis and turnover pathways implicated in apoptosis *De novo* synthesis of PC through the Kennedy pathway and the methylation pathway (yeast and hepatocytes). The rate-limiting step of PC synthesis is catalysed by CTP:phosphocholine cytidylyltransferase (CCT) in the Kennedy pathway. (DAG= diacylglyceride, CPT=cholinephosphotransferase PLA2= phospholipase A2, PLD= phospholipase D, lysoPC= lysophosphatidylcholine, PA= phosphatidic acid, PAP= phosphatidic acid phosphatases, SM= sphingomyelin, PE= phosphatidylethanolamine, PEMT= phosphatidylethanolamine methyl transferase, SAM= S-adenosylmethionine, SAH= S-adenosylhomocysteine) (Modified from (76)).

1.2.5.2 Inhibition of survival signaling pathways

ATLs have been linked to the inhibition of several survival pathways known to associate with the PM, including the Ras-Raf-Mitogen Activating Protein Kinase (MAPK) and the phosphatidylinositol 3-kinase/protein kinase B/Akt (PI3K/Akt) pathway (69). Edelfosine, miltefosine and perifosine inhibit the MAPK pathway by interfering with the ability of Raf to associate with Ras, resulting in decreased translocation of Raf to the PM (70, 79). Additionally, edelfosine and miltefosine caused the clustering and internalization of epidermal growth factor receptors (EGFR) (80). The lack of EGFR at the PM will inhibit the activation of Ras, which will impede Raf translocation and cause inhibition of subsequent phosphorylation reactions that activate MAPK, therein stopping cell proliferation.

These three ATLs have also been shown to inhibit the PI3K-Akt/PKB survival pathway, upstream of the PI3K (81). The exact mechanism by which ATLs inhibit this pathway is still unknown, but studies with perifosine suggest that the drug interferes with the plextrin homology domain of the Akt/PKB causing a conformational change. As such, the Akt/PKB is unable to bind to the phosphoinositide PIP_3 therefore impairing PM recruitment and activation (82). Supression of Akt/PKB may cause the upregulation of pro-apoptotic proteins such as Bad, Forkhead and caspase-9 (81).

1.2.5.3 Activation of pro-apoptotic pathways

In addition to inhibiting survival pathways, ATLs also stimulate pro-apoptotic pathways, such as the ceramide activated stress activated protein kinase/ c-Jun-N-terminal kinase (SAPK/JNK) signaling cascade and the Fas/CD95 death receptor (69, 81, 83). The SAPK/JNK pathway is activated in response to stimuli such as radiation and ATLs, and through sequential

phosphorylation activates pro-apoptotic mechanisms (80). Wherein the exact mechanisms of activating the SAPK/JNK pathway remain unknown, it has been proposed that the SAPK/JNK and MAPK pathways are inversely related, and as such may function to regulate each other through cross-talk involving secondary messenger lipids, such as ceramide (70, 84).

Normal activation of the Fas/CD95 receptor requires the presence of a Fas ligand, in order to recruit the Fas-associated death domain-containing protein (FADD) and procaspase-8 to form the death inducing signaling complex (DISC).

Treatment with edelfosine has been shown to mimic the role of the Fas ligand, as there is an increase in translocation and capping of the Fas/CD95 proteins into lipid rafts, leading to increased DISC formation and subsequent apoptosis. Furthermore, disruption of lipid rafts by extraction of sterols, using methyl-b-cyclodextrin, inhibits the effect of edelfosine on Fas/CD95 activation (37).

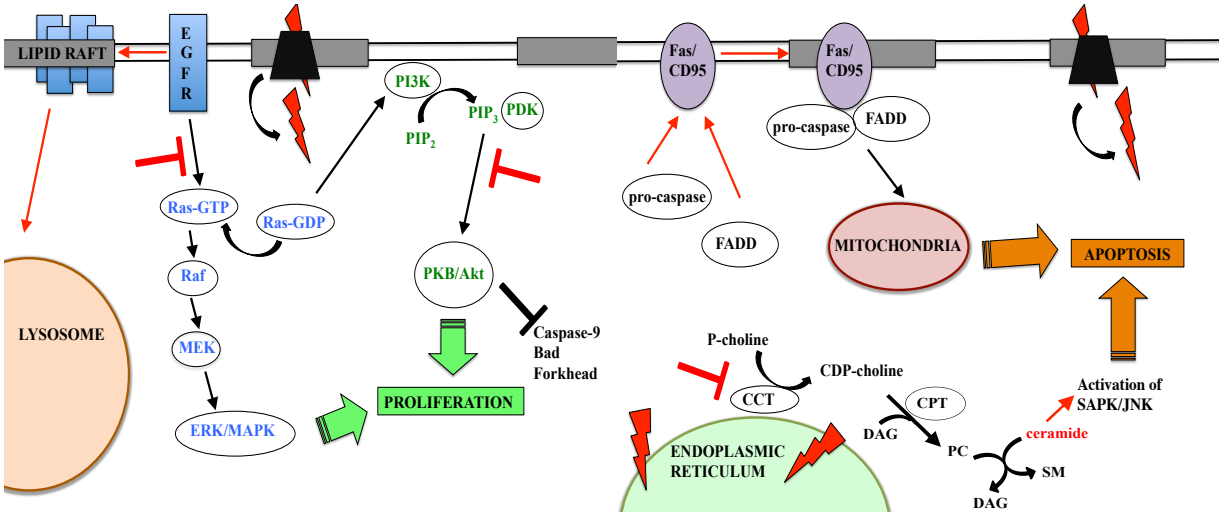

Figure 1.12: Signal transduction pathways affected by anti-tumor lipids Edelfosine (red) is internalized by a flippase associated with lipid rafts (dark grey). Once inside the cell inhibits proliferative pathways: MAPK (green), PKB/Akt (blue) and activates pro-apoptotic pathways, Fas/CD95 (purple). Causes inhibition of PC synthesis at ER; increases ceramide levels that turns on apoptotic pathways, SAPK/JNK.

1.2.5.4 Association with lipid rafts

The effect of ATLs on lipid rafts was simultaneously recognized in studies on mammalian cells as well as in genetic screens performed in yeast, where edelfosine was seen to associate with these microdomains and cause the internalization of lipid raft-proteins and sterols (78). Further studies done in solid tumor and leukemic cells also indicated that edelfosine localized to lipid rafts in the PM, and identified the ER as a secondary drug target membrane (85). Therein, the localization of ATLs to the ER and PM membranes is consistent with the drugs ability to inhibit phospholipid turnover and alter signal transduction pathways respectively (74). Lipid rafts in mammalian and yeast cells, have long been associated with a variety of signal transduction pathways, including all the aforementioned pro/anti-apoptotic pathways affected by ATLs. Both Ras and Raf proteins from the MAPK pathway are associated with lipid rafts, recruitment of Akt to the membrane in the PI3K/Akt/PKB is raft dependent, and the Fas/CD95 receptor is known to cluster in lipid rafts (86). Therefore targeting of lipid rafts by ATLs would explain the large impact these drugs have on a diversity of intracellular signaling pathways.

1.2.5.5 Mechanisms of drug uptake

Much of what is known on edelfosine internalization comes from studies in budding yeast. The uptake of aminophospholipids in yeast is mediated by members of the P-type ATPase family of translocases (flippases) (87). *S. cerevisiae* contains five P4-type ATPases, Drs2, Dnf3 and Neo1 which localize to the Golgi and Dnf1, Dnf2, which are localized to the PM. To aid in proper localization and function, these ATPases require association with a b-subunit composed of members of the Cdc50, Lem3/Ros3, Crf1 family (Table 1.1, Figure 1.13) (87, 88).

Table 1.1: Flippases (α subunits), their corresponding β subunits, and cellular localization

ATPase (α subunit)	β subunit	Subcellular localization
Drs2	Cdc50	Golgi
Dnf1	Lem3/Ros3	PM
Dnf2	Lem3/Ros3	PM
Dnf3	Crf1	Golgi
Neo1	N/A	Golgi

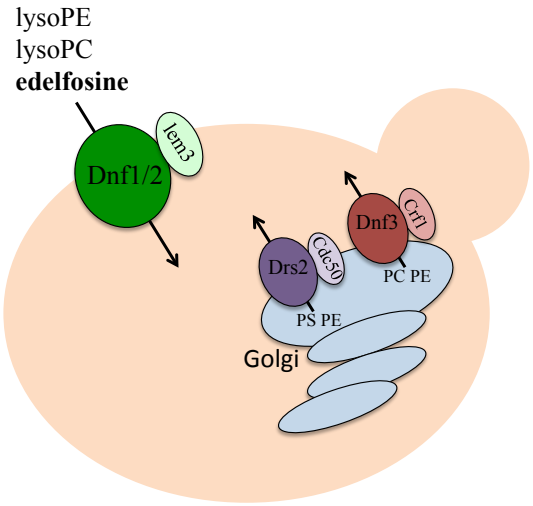

Figure 1.13: Localization and substrate specificity of P4-type ATPases in yeast Dnf1/2 associate with Lem3, localize to the PM and facilitate the transport of lysoPC, lysoPE, edelfosine. Drs2 associates with Cdc50 at the Golgi and transports PS, PE. Dnf3 associates with Crf1 at the Golgi and transports PC, PE. (PC= phosphatidylcholine, PE= phosphatidylethanolamine).

The results from a yeast genetic screen indicated that *lem3* mutants were edelfosine resistant. Further research indicated that edelfosine uptake was actually dependent on the presence of a Lem3 protein (87, 89).

Stemming from these results in yeast, similar uptake mechanisms were seen in *Leishmania donovani,* and carcinoma cells, with the identification of LdMT (*Leishmania donovani* putative

miltefosine transporter) and a P4-ATPase flippase, ATP8B1 respectively (37, 69, 90). ATL uptake was also proposed to be mediated via raft-dependent endocytosis, as seen in leukemic cells (69). Interestingly, yeast Lem3/Ros3 has been found to associate with lipid rafts at the PM (91). Since cells with inhibited uptake mechanisms show ATL resistance, it is suggested that drug internalization is essential to illicit cellular apoptosis, but that these mechanisms may vary depending on the cell type (69, 90).

1.3: Yeast as a model organism

The budding yeast, *Saccharomyces cerevisiae* has proven to be an excellent model organism for the study of eukaryotic processes (92-94). As cellular machinery is highly conserved throughout this domain, approximately, 45% of yeast genes are homologous to mammalian genes, many of which have been associated with human disease (95). Although yeast has simple and inexpensive growth requirements and a short doubling time, its greatest asset remains its molecular and genetic tractability (92-94). Given its relatively small genome, yeast can be used effectively for high throughput genetic screens. These screens are especially advantageous when attempting to define potential drug targets, or genes involved in regulating cellular response to drug treatment (95). While many approaches to drug discovery are reductionist, focusing on previously established drug targets, the use of high throughput genetic screens is an unbiased approach which allows for the identification of novel drug targets that may have otherwise been overlooked (95).

These yeast chemogenomic approaches have been successfully applied to identifying cellular targets of drugs such as cycloheximide and tunicamycin, used to treat bacterial infections, and lovastatin, a drug used to lower cholesterol (95).

1.3.1 Metabolic similarities in yeast and cancer

Cancer results from damage to normal tissues leading to abnormal and unregulated cell growth. Budding yeast is a suitable model organism for cancer cells in particular, as it shares a few key characteristics with tumoral cells. One of the key aspects in the formation of cancer cells from normal ones is the irreversible shift in metabolism from respiration to fermentation (96). This preference for fermentation in cancer cells can be seen even in the presence of oxygen, and is a long-term adaptation known as the "Warburg Effect" or aerobic glycolysis. The purpose of this adaptation remains unknown, but it indicates that cancer cells have the ability to alter their metabolic functions based on environmental conditions. In cancer cells, respiration is highly decreased, and fermentation is used to compensate for the cells' energy demands (96, 97). Interestingly, budding yeast *S.cerevisiae* are also able to shift metabolism under different environmental conditions. In yeast, carbon sources play a role in determining the type of metabolism the cells undertake. When supplemented with glucose, cells will preferentially ferment even in the presence of oxygen ("Warburg effect"), where in non-fermentative carbon sources, like glycerol, ethanol, lactate, and acetate they will be forced to respire (97). In yeast, the type of carbon source is also linked directly to intracellular pH (pHi). When grown on semi or non-fermentative sources, the cells maintain lower pHi of 6.8-7.0 as compared to 7.0 on glucose, therein suggesting that respiration may induce cytosolic acidification (98). As such, the predominant metabolism may be responsible for the slightly lowered acidic pHi range seen in cancer cells ranging from 6.15-7.4 when compared to the pHi of normal cells of 7.0-7.4 (99).

1.3.2. pH homeostasis in yeast

The pHi is tightly regulated in all cell types, as even slight alterations in pH levels may impact cell function. The pHi can influence protonation of amino acids resulting in improper protein folding, or protonation of lipid head-groups, altering lipid shape and inducing membrane stress. Deviations away from normal pHi may disrupt pH dependent gradients across membranes, impeding cellular transport and signaling pathways (98, 100).

Yeast maintains pH homeostasis using two key ATPase proton pumps. The first, Pma1, is a P-type ATPase that functions at the PM to remove excess protons from the cytosol. Auto-phosphorylation of Pma1 induces a conformational change in the protein, and using the energy from ATP hydrolysis drives the export H^+ ions out of the cell. Pma1 is an essential protein that comprises roughly 10-20% of the protein content in the PM and has a half-life of 11-12 hours (101).

The second, vacuolar ATPase (V-ATPase) is a V-type ATPase localized in the vacuolar membrane, and functions to remove excess protons from the cytosol to the vacuole. The V-ATPase is composed of two large subunits, the V1, which includes the ATP binding site, and the Vo, which is the integral membrane subunit. These two subunits assemble independently of one another, but they must come together at the vacuolar membrane in order to form a functional V-ATPase (102). Similar to Pma1, the V-ATPase uses the energy from ATP hydrolysis to drive the movement of protons into the vacuole, a process which is not mediated by autophosphorylation.

Both Pma1 and V-ATPase are electrogenic pumps, and as such create an electrochemical gradient of protons, which forms the membrane potential ($\Delta\psi$) that provides the essential driving force for the functioning of other membrane bound transporters (Figure 1.14). In particular at the

PM, the export of H^+ ions by Pma1 helps to drive the symport transport of other ions and nutrients into the cell (100).

These pumps work together to maintain pHi, and as such respond similarly to external metabolic stimuli. High glucose concentrations will induce the phosphorylation of Pma1, and will acidify the vacuole, indicating that protons are being pumped out of the cytosol. In glucose-deprived conditions, the function of Pma1 is reduced and the V-ATPase is essentially non-functional. Under conditions of low glucose availability, the Vo and V1 subunits of the V-ATPase preferentially disassemble, resulting in cytosolic acidification (100). This disassembly occurs in as little as five minutes post glucose deprivation, but can be just as quickly reversed when glucose is re-introduced into the media. This indicates that the V-ATPase has a means of regulating pHi in direct response to extracellular nutrient conditions (102).

The PM and other organelles have more cation exchangers that are able to contribute to pH homeostasis, but their roles are often secondary. Of these, it is of interest to mention the high and low affinity potassium (K^+) pumps, Trk1 and Trk2 respectively, which are localized at the PM. At low pHi or high external K^+ concentrations, the Trk pumps are activated, causing an influx of K^+ ions into the cytosol (Figure 1.14). This causes the depolarization of the PM, which can stimulate the auto-phosphorylation of Pma1, and help to alkalinize the pHi (100).

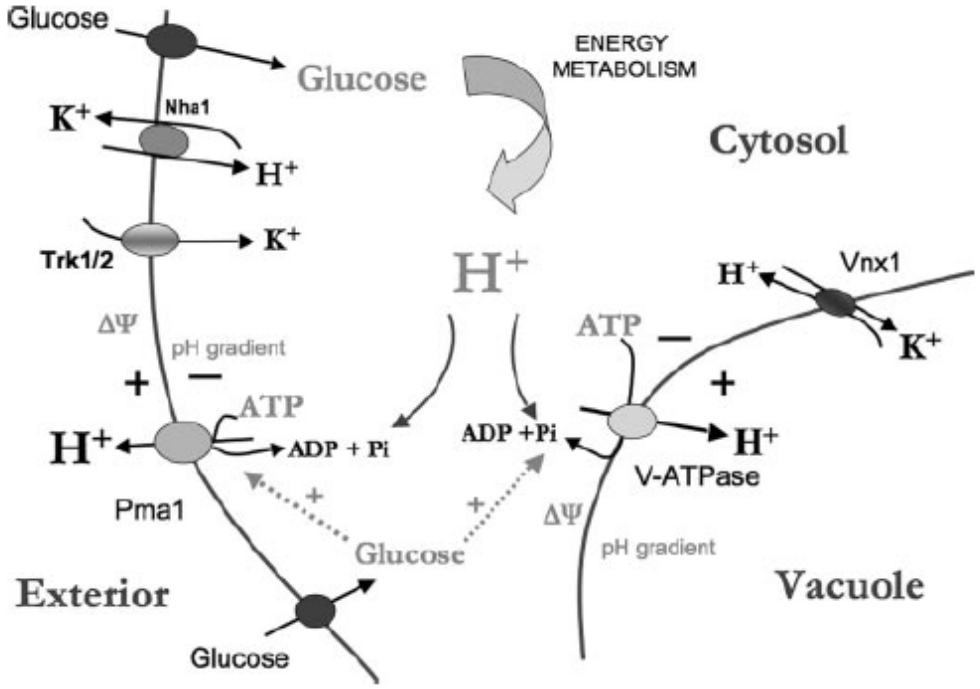

Figure 1.14: pH homeostasis in yeast Model depicts the collaboration of V-ATPase and Pma1 in maintaining intracellular pH homeostasis. Other transporters depicted; potassium antiporters Nhx1 and Vnx1, high and low affinity potassium transporters Trk1/2. Mechanisms driving pH responses to glucose and KCl are also highlighted (arrows). Modified from (100).

1.3.3: Membrane organization in yeast

Similar to other eukaryotic membranes, the yeast PM is also laterally compartmentalized into specific lipid micro-domains (103, 104). In yeast, all the studied PM proteins have been associated with DRMs (refer to section 1.2.3), suggesting that localization of specific proteins to the PM requires their incorporation into lipid rafts (103). Recent studies have shown that proteins may be distributed in the PM into one of three distinct distribution patterns, discrete patches, mesh-shaped compartments (between discrete patches) or homogeneously distributed between both (103, 104).

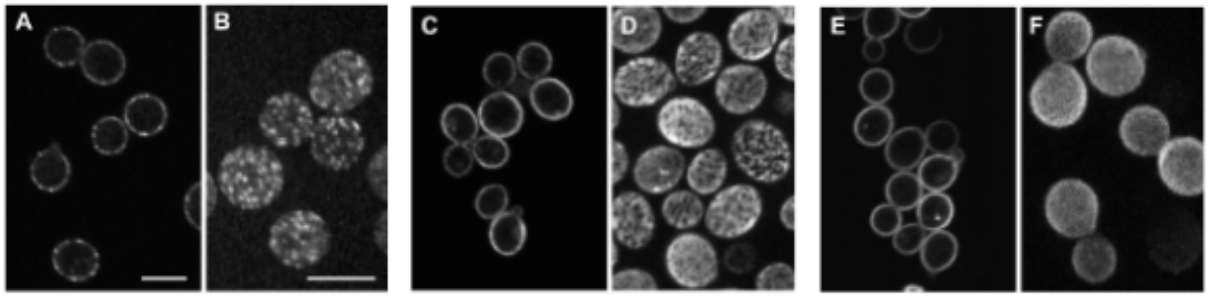

Figure 1.15: Distinct protein distribution patterns in the PM Fluorescence patterns of Can1-GFP (A and B) represents the membrane containing Can1 (MCC) domain, Pma1-GFP (C and D) represents the membrane containing Pma1 (MCP) domain, and Hxt1-GFP (E and F) depicts homogeneously distributed pattern in living *S. cerevisiae* cells. An individual transverse optical section (A, C, and E) and superposition of four consecutive surface optical sections (B, D, and F) are presented for each protein. Bar =5 μm. Modified from (103).

In so far, proteins identified to exhibit homogeneous distribution are Gap1, a general amino acid permease, and Hxt1, a high affinity hexose transporter. Pma1, the essential H^+ATPase has been the only protein shown to segregate into a mesh-shaped compartment, named Membrane Compartment of Pma1 (MCP). Lastly, the discrete patch compartment, the Membrane Compartment of Can1 (MCC) was named after the arginine symporter Can1. Other proteins associated with MCCs include the uracil symporter, Fur4, the, tryptophan symporter, Tat2, and

the eisosome protein, Sur7 (103). Recent work with MCCs has identified another 20 proteins, which either associate or are localized within this compartment (105). The lipid composition of each compartment is variable, with MCC being enriched in ergosterol, but the relevance of these differences remains unclear. Evidence suggests that membrane potential may play a role in this organization, as depolarization results in the exit of ergosterol and H^+ symporters out of these domains (104).

1.3.4: Current model of action of edelfosine in yeast

Edelfosine is able to induce apoptosis in yeast cells at concentrations similar to those used in cancer cells. In order to obtain further insight into the drugs mode of action, unbiased genetic screens were performed in this model organism. The first genetic screen suggested that edelfosine cytotoxicity might be caused in part by biophysical alterations of lipid rafts (78). In our current working model drug uptake is mediated by a membrane bound lysolipid P4-type flippase regulated by the Lem3p subunit (Figure 1.16) (89). Once embedded into the membrane, edelfosine causes the internalization of ergosterol and the essential P-type H+ ATPase, Pma1. The mechanisms of internalization of sterols and subsequent cellular localization are still unknown. On the other hand, Pma1 is internalized through endocytosis, and is then transported and subsequently degraded in the vacuole. Cells with impaired endocytosis combined with suppressed vacuolar protease activity show resistance to edelfosine, however drug uptake is not obstructed (78). This emphasizes that drug uptake is endocytosis-independent, and highlights the importance of Pma1 internalization in mediating the cytotoxic effect of edelfosine (106). Therefore it can be speculated that the loss of Pma1 from the PM should induce intracellular acidification, eventually leading to cell death.

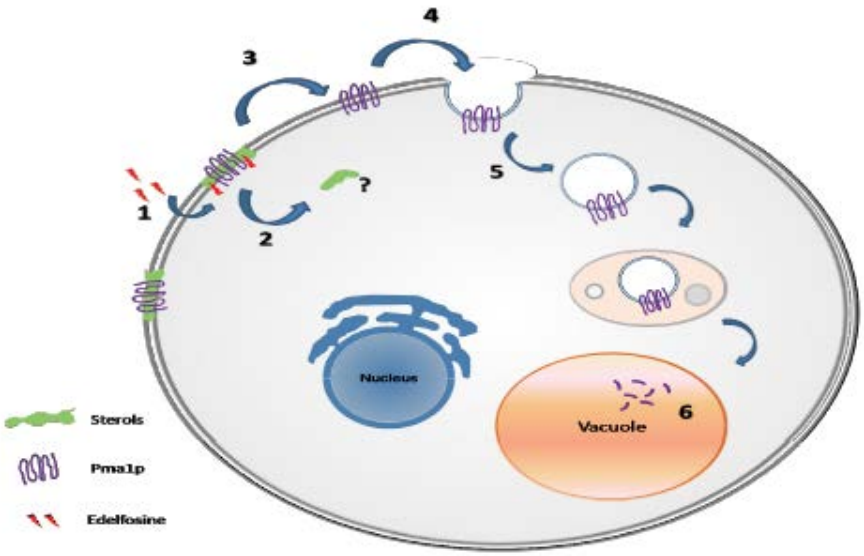

Figure 1.16: Mode of action of edelfosine in yeast (1) Edelfosine (red) inserts into lipid rafts in the PM, and is flipped into the inner leaflet via a flippase that is regulated by Lem3 **(2)** Edelfosine interaction with the PM also causes the internalization of sterols (green) and **(3)** causes displacement of essential proton pump, Pma1 from lipid rafts **(4-5)** Pma1 is endocytosed and degraded in the vacuole.

1.4 Goals and hypothesis

Using this model as starting point, we wanted to further answer the question:

How does altering lipid micro-domain organization impede cellular growth and lead to cellular death?

Taking advantage of the fact that edelfosine is cytotoxic to yeast at similar concentrations as those used to kill cancer cells; unbiased genetic screens in this organism were performed to gain insight into the drug's mode of action. A first screen provided evidence that edelfosine-mediated cytotoxicity is through modification of the biophysical structure of lipid rafts by inducing internalization of sterols and the essential proton pump Pma1 from the PM (78). From here, the genetic screen was expanded to survey the yeast deletion collection for sensitivity and resistance to edelfosine (sensitivity screen was carried out by us while the resistance screen was performed by our collaborator, Dr. Mollinedo from the University of Salamanca, Spain). The investigations outlined in this thesis used the results obtained from these genetic screens as a start point.

The following objectives were identified:

1. To analyze and validate the results of the genetic screens (Chapter 2)
2. To study the role of pH homeostasis in modulating sensitivity to edelfosine (Chapter 3)
3. To investigate the effect of edelfosine on membrane architecture (Chapter 4)
4. To determine if different members of the ATL family share the same mode of action and cellular responses as the prototypic drug edelfosine (Chapter 5)

Chapter Two: Edelfosine chemo-genomic screens

2.1 Introduction

One of our long term goals has been to identify the complete set of molecules that regulate sensitivity and resistance to ATLs, as well as the precise means by which they cause cell death. We have favored the use of genetic screens in budding yeast as a starting point in these studies. The most powerful aspect of carrying out genetic screens is that the approach allows for the identification of pathways that modulate drug sensitivity and resistance that may have otherwise been overlooked. A first genetic screen identified sphingolipid and sterol biosynthetic pathways as regulators of ATL cytotoxicity, which led to investigations directed at analyzing the effect of edelfosine on lipid raft integrity (69, 74). Edelfosine was shown to induce the internalization of sterols and the essential proton pump Pma1, both major components of lipid rafts at the PM. From these experiments, it was not clear whether these events were responsible for the cytotoxic effect of edelfosine in yeast. Therefore, to provide a more comprehensive insight into the mode of action of ATLs, we performed genome-wide screens aimed at identifying proteins that modulate resistance or sensitivity to edelfosine. These screens were performed by Teshager Bitew (a former MSc student from Dr. Zaremberg's lab) and Dr. Zaremberg in collaboration with Dr. Faustino Mollinedo from the University of Salamanca, Spain (106, 107). The following sections present the results obtained from these genetic screens, as they have provided the foundation for the work done for this thesis. After providing a summary of the main findings of the resistance screen (performed in Dr. Mollinedo's lab), we focus on our own cluster analysis and confirmation of the phenotypes of the main hits identified in the sensitivity screen.

2.2 Resistance screen

The haploid yeast strain (BY4741) contains a total of 6200 genes, of which 4672 deletion mutants are viable. The resistance screen was performed by robotically pinning an ordered array of the haploid yeast gene deletion collection into defined liquid medium in the presence or absence of edelfosine. This approach identified 262 genes whose inactivation conferred resistance to edelfosine (Appendix 2). Functional analysis of these genes revealed an enrichment of genes involved in vesicular transport (including endosomal sorting complex required for transport (ESCRT) and retromer complexes), protein biosynthesis, and mitochondrial processes (Figure 2.1a). In addition, this screen also identified novel genes involved in regulation of drug uptake (Figure 2.1b). Table 2.1 lists the most relevant genes involved in edelfosine resistance regarding vesicular traffic and drug uptake.

Drug Uptake

In order to determine whether deficient drug uptake was responsible for edelfosine resistance, [^{3}H]edelfosine was used to measure uptake in 91 of the most resistant mutants. Of those analyzed, only *lem3Δ, agp2Δ* and *doc1Δ* showed deficient drug uptake, showing that resistance (Table 2.1, Figure 2.1b). It has been previously seen that edelfosine uptake is facilitated by a Lem3 regulated flippase (89) thus deficient uptake in strains lacking *LEM3* was expected. These results also identified L-carnitine, polyamine and bleomycin transporter Agp2 (108) and a protein involved in ubiquitination of the anaphase-promoting complex, Doc1, as mediators of edelfosine uptake.

Table 2.1: List of relevant genes identified in the resistance genetic screen

Drug uptake	Vesicular traffic				
	Endocytosis	ESCRT complexes		Retrograde transport	
		Complex 0	Complex III related	Retromer	GARP complex
DRS2	*END3*	*VPS27*	*DID2*	*VPS17*	*VPS52*
DNF2	*MYO5*		*VPS4*	*VPS26/PEP8*	*VPS54*
LEM3	*RHO4*	Complex I		*VPS29*	
AGP2	*LDB17*	*VPS23/STP22*	Associated components	*VPS35*	Others
DOC1		*VPS37/SRN2*	*BRO1*	CORVET	*GYP6*
			DOA4	*VPS3*	*SNX4*
		Complex III	*UBP2*	*VPS8*	*SNX42*
		DID4/VPS2			*CCZ1*
		VPS24			*YPT7*
		VPS20			*TLG2*
					SWF1
					KEX1
					KEX2

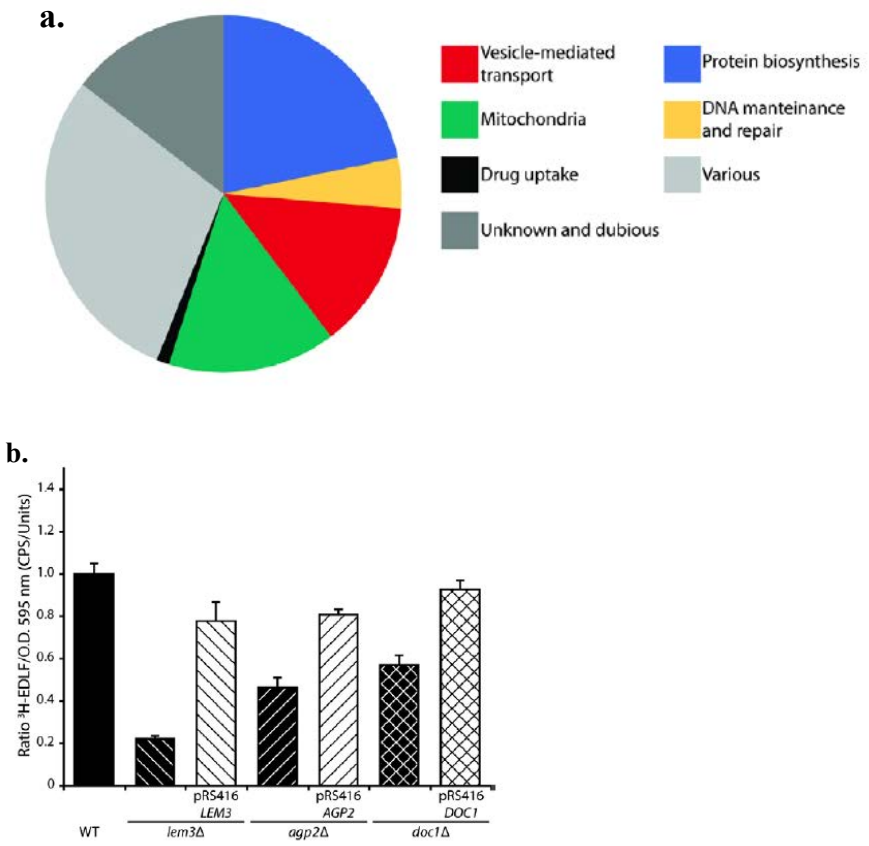

Figure 2.1: High-throughput edelfosine *S.cerevisiae* resistance screen (a) Functional distribution of the 262 genes found to cause resistance to edelfosine when deleted **(b)** Uptake of [^{3}H]edelfosine for the three resistant strains found to have decreased drug incorporation relative to the wild-type (WT, black solid bar). Each pair of bars represents a single-gene deletion mutant (black patterned bar) alongside that mutant complemented by a centromeric plasmid carrying said gene (white patterned bar). Data shown are representative of mean values +/- standard deviation (SD) of at least three independent experiments.

Endocytosis

The second category of enrichment contained endocytosis-related genes, *END3, MYO5, LDB17, RHO4* (Table 2.1, Figure 2.1a). Deletion of *END3* or *END4* is known to lead to defects in endocytosis, and previous studies have shown that a mutant with impaired endocytosis combined with decreased proteolysis in the vacuole (*end4^{ts}pep4Δ*) was resistant to edelfosine (78). Uptake experiments showed that edelfosine was still incorporated into these cells reaching wild type levels, suggesting that drug uptake was endocytosis-independent (106, 109). Therefore it was concluded that the combination of these mutations (*end4^{ts}pep4Δ*) allowed recycling of internalized PM proteins back to the PM, bypassing the cytotoxic effect of edelfosine (Figure 2.2).

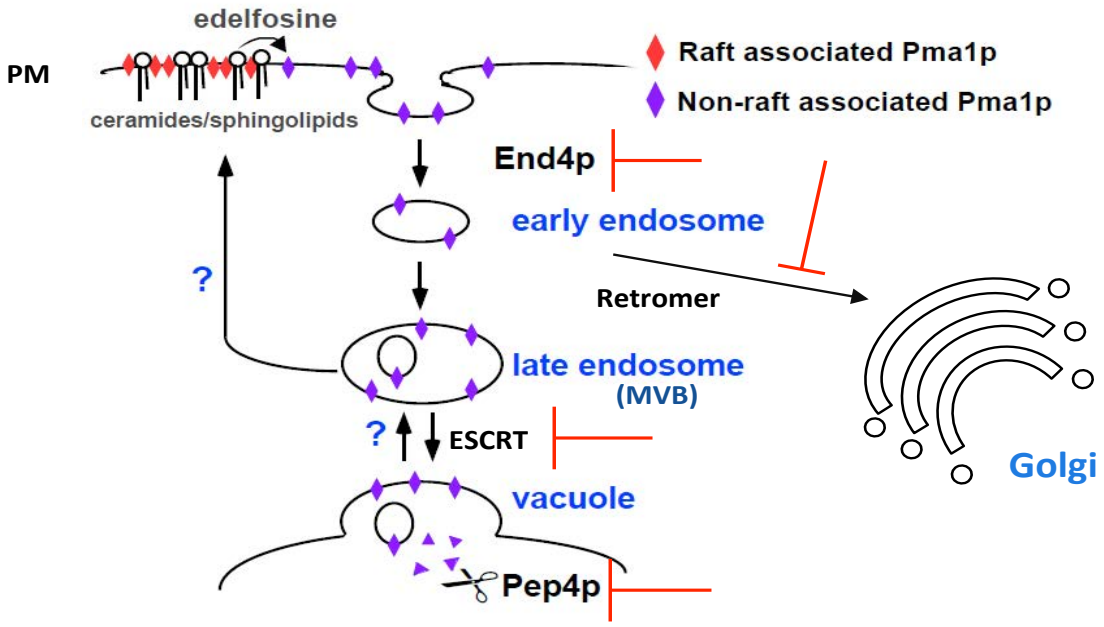

Figure 2.2: Recycling of internalized plasma membrane proteins confers resistance to edelfosine Loss of Pma1 from the plasma membrane as well as other proteins may account for the deleterious effect of edelfosine on cell growth. This effect is bypassed in *end4^{ts} pep4Δ* cells. A fraction of lipid raft associated proteins (like Pma1) is trapped in endocytic intermediates and likely recycled back to the PM in these cells allowing their activities to be sustained despite the presence of the drug. Points of inhibition conferring resistance are indicated in red (PM= plasma membrane; MVB = multivesicular body).

Vesicular Trafficking

Another enrichment category included genes responsible for vesicular trafficking, of which many of these genes are known to be engaged in protein sorting at late endosomes. At the endosome, proteins from the PM (and Golgi) can be transported by ESCRT-mediated multi-vesicular body (MVB) sorting pathway to the vacuole for degradation, or by sorting nexins and retrograde transport into the trans-Golgi network, where they are sorted and sent to various organelles, or recycled back to the PM (Figure 2.2) (110). Results of the resistance screen showed that the deletion of retromer subunits, *VPS35, VPS29, VPS26, VPS17*, sorting nexins responsible for retrograde transport, *SNX4, SNX42* proteases involved in processing cargo proteins, *KEX1, KEX2*, and *YPT7* responsible for retrograde sorting, all conferred resistant to edelfosine (Table 2.1). Further analysis showed that yeast strains defective in retrograde transport did not impact edelfosine uptake. These strains also had greater retention of Pma1 at the PM, indicating that defects in retrograde transport may allow recycling of proteins back to the PM but do not affect drug uptake.

Furthermore, the inactivation of 11 of 18 members of ESCRT complex, and genes associated with ESCRT function, *BRO1, DOA4, UBP2* were also resistant to edelfosine (Table 2.1).

Summary

The resistance genome-wide screen and subsequent experiments performed revealed that vesicular trafficking is a critical process mediating edelfosine resistance, with mutants that result in increased recycling between endosomal compartments and the PM being resistant to edelfosine cytotoxocity (106). This is a highly conserved process and thus this mode of resistance may be extrapolated from yeast to tumor cells.

2.3 Sensitivity screen

2.3.1 Materials and methods

Yeast strains, plasmids and growth conditions

Detailed information on yeast strains and primers used is provided in Table 2.2 and 2.3 respectively. Yeast were grown in yeast complex medium (YPD; 1% yeast extract, 2% bacto-peptone and 2% glucose or in synthetic defined medium (SD; 0.67% yeast nitrogen base without amino acids 2% glucose), with amino acids supplied to complement strain auxotrophies. For plates, 2% agar was added to desired media prior to autoclaving. Growth of cells in liquid media was measured using UV-Vis Spectrophotometer (Shimadzu UV-2450) by optical density at a wavelength of 600nm (OD_{600}).

Edelfosine was a kind gift from Medmark Pharma GmbH. A 10 mg/ml stock solution in ethanol was prepared fresh every time and used within two days. The final ethanol concentration in control (ethanol) and edelfosine containing (edelfosine in ethanol) plates never exceeded 0.2%. Growth on control (with ethanol) plates was indistinguishable from that of control plates lacking ethanol. Edelfosine was added after autoclaving and cooling of the media to at least 60 °C.

Table 2.2 List of yeast strains used in this chapter

	Genotype	**Source**
BY4741	*MATa his3 leu2 met15 ura3*	Euroscarf
YMS084	*MATα can1Δ::MFa1pr-HIS3-MFα1pr-LEU2 his3Δ0 leu2Δ0 ura3Δ0 met1Δ0 lyp1Δ0*	(111)
PMA1-DAmP	YMS084 *YGL008C::3NATB*	(111)
vma1Δ	*MATa his3Δ1 leu2Δ0 met15Δ0 ura3Δ0 YDL185w::kanMX*	Euroscarf
vma2Δ	*MATa his3Δ1 leu2Δ0 met15Δ0 ura3Δ0 YBR127c::kanMX4*	Euroscarf
vma3Δ	*MATa his3Δ1 leu2Δ0 met15Δ0 ura3Δ0 YEL027w::kanMX4*	Euroscarf
vma4Δ	*MATa his3Δ1 leu2Δ0 met15Δ0 ura3Δ0 YOR332w::kanMX4*	Euroscarf
vma5Δ	*MATa his3Δ1 leu2Δ0 met15Δ0 ura3Δ0 YKL080w::kanMX4*	Euroscarf
vma6Δ	*MATa his3Δ1 leu2Δ0 met15Δ0 ura3Δ0 YLR447c::kanMX4*	Euroscarf
vma7Δ	*MATa his3Δ1 leu2Δ0 met15Δ0 ura3Δ0 YGR020c::kanMX4*	Euroscarf
vma8Δ	*MATa his3Δ1 leu2Δ0 met15Δ0 ura3Δ0 YEL051w::kanMX*	Euroscarf
vma9Δ	*MATa his3Δ1 leu2Δ0 met15Δ0 ura3Δ0 YCL005w::kanMX4*	Euroscarf
vma10Δ	*MATa his3Δ1 leu2Δ0 met15Δ0 ura3Δ0 YHR039c::kanMX4*	Euroscarf
vma11Δ	*MATa his3Δ1 leu2Δ0 met15Δ0 ura3Δ0 YPL234c::kanMX4*	Euroscarf
vma12Δ	*MATa his3Δ1 leu2Δ0 met15Δ0 ura3Δ0 YKL119c::kanMX4*	Euroscarf
vma13Δ	*MATa his3Δ1 leu2Δ0 met15Δ0 ura3Δ0 YPR036w::kanMX4*	Euroscarf
vma16Δ	*MATa his3Δ1 leu2Δ0 met15Δ0 ura3Δ0 YHR026w::kanMX4*	Euroscarf
vma21Δ	*MATa his3Δ1 leu2Δ0 met15Δ0 ura3Δ0 YGR105w::kanMX4*	Euroscarf
vma22Δ	*MATa his3Δ1 leu2Δ0 met15Δ0 ura3Δ0 YHR060w::kanMX4*	Euroscarf
snf1Δ	*MATa his3Δ1 leu2Δ0 met15Δ0 ura3Δ0 YDR477w::kanMX4*	Euroscarf
snf4Δ	*MATa his3Δ1 leu2Δ0 met15Δ0 ura3Δ0 YGL115w::kanMX4*	Euroscarf
trk1Δ	*MATa his3Δ1 leu2Δ0 met15Δ0 ura3Δ0 YJL129c::kanMX4*	Euroscarf
vps35Δ	*MATa his3Δ1 leu2Δ0 met15Δ0 ura3Δ0 YJL154c::kanMX4*	Euroscarf
lem3Δ	*MATa his3Δ1 leu2Δ0 met15Δ0 ura3Δ0 YNL323w::kanMX4*	Euroscarf

Table 2.3 List of primers used in this chapter

Plasmid	**Description**
VMA2	VMA2-F GAGAGTCGACGGTACGTGGTAGGCTAGAGTG VMA2-R GAGAGCGGCCGCCGCTTGATGTGCCCAGGGTGA
TRK1	TRK1-F GAGAGTCGACGGGCACGAATTATGACAGAGTA TRK1-R GAGAGCGGCCGCACTAATGGCGTTGACGATGACG
SNF1	SNF1-F GAGAGTCGACGCAGGCTATGATGTCCCATATG SNF1-R GAGAGCGGCCGCTTCTGCCTGGTCTTTATTCAT

Cloning

The *VMA2, SNF1 and TRK1* genes including their own promoter and termination sequences were PCR amplified from genomic DNA obtained from the wild type strain, BY4741. *SalI* and *NotI* sites were engineered in the forward and reverse primer respectively, to allow directional cloning into the centromeric plasmid pRS315 (*LEU2*). The specific primers used are listed in Table 2.3.

Identification of edelfosine hypersensitive mutants in *S. cerevisiae*

A total of 4672 different yeast deletion mutants, generated by the international deletion consortium were obtained from Euroscarf (112, 113). This collection of deletion mutants represents the total number of viable single mutants from a total of approximately 6,200 potential genes. All strains are derivatives of BY4741. The specific genes were disrupted with a kanamycin-resistant (kan^R) cassette. Strains from the deletion collection were screened for hypersensitivity to edelfosine in solid medium. For this purpose strains were arrayed individually on a series of rectangular OmniTray agar plates (Nalgene Nunc International) at 384 strains per plate and manipulated robotically using a Virtek Colony Arrayer (Bio-Rad). Edelfosine was added to SD media containing 2% agar after autoclaving and cooling of the media to at least 60 °C. We and others have observed that the effect of lipids on cell growth in solid media can be affected by cell density (78, 114). The robot pins a large number of cells in one spot so the concentration of edelfosine had to be increased from those normally used in serial dilution assays. For the chemical-genetic screen a final concentration of 190 μM edelfosine was used. This concentration did not affect growth of wild type (BY4741) colonies while it inhibited growth of a sensitive strain lacking Spo14 (78). Plates were incubated for 2 days at 30°C and

imaged using a Versa Doc (Bio-Rad) apparatus. Colony size comparison on yeast array plates was determined visually using a scoring system. Briefly, images of plates were obtained and using Photoshop, colonies were false colored to be green (control) and red (edelfosine). Images were overlaid and colonies that appeared green with faint yellow dot in the middle were evaluated as hypersensitive to edelfosine (115). The screen was run four independent times. Genes identified at least three times out of the four runs are reported herein (Table 2.4).

Serial dilutions

Yeast cells were grown to mid-log phase (OD_{600}= 0.4-0.6) in YPD or SD media and concentrated in order to obtain OD_{600} =1. Three subsequent 1/10 dilutions were carried out to obtain, OD_{600} = 0.1, 0.01 and 0.001. Five µl of each dilution was spotted onto desired solid media plates in the absence or presence of the indicated concentrations of edelfosine. Each plate growth assay experiments was done in triplicate and repeated two times. Plates were incubated at 30 °C for the indicated periods of time and imaged using a GelDoc system (BioRad).

Data analysis and functional group classification

Enrichment of data sets for Gene Ontology (GO) terms was performed using the Gene Ontology Term Finder at the *Saccharomyces* Genome Database (SGD, http://db.yeastgenome.org/cgi-bin/GO/goTermFinder.pl) and the MIPS database (http://mips.helmholtz-muenchen.de/genre/proj/yeast). Interaction networks were visualized with Osprey using data from several databases (116).

Funspec (117) was used to identify functional clusters of genes and statistical evaluation. Gene classification was done subjectively, supported by SGD, MIPS as well as the literature.

2.3.2 Results

A high-throughput edelfosine sensitivity screen was performed by robotically pinning an ordered array of 4672 haploid yeast gene deletion mutants onto solid defined medium in the absence or presence of edelfosine (Figure 2.3). Fifty-four genes whose inactivation reproducibly resulted in increased sensitivity to edelfosine compared to wild-type were identified. This data set was enriched in genes known to participate in pH homeostasis, regulation of transcription and lipid biosynthesis (Figure 2.3, 2.4, Table 2.4).

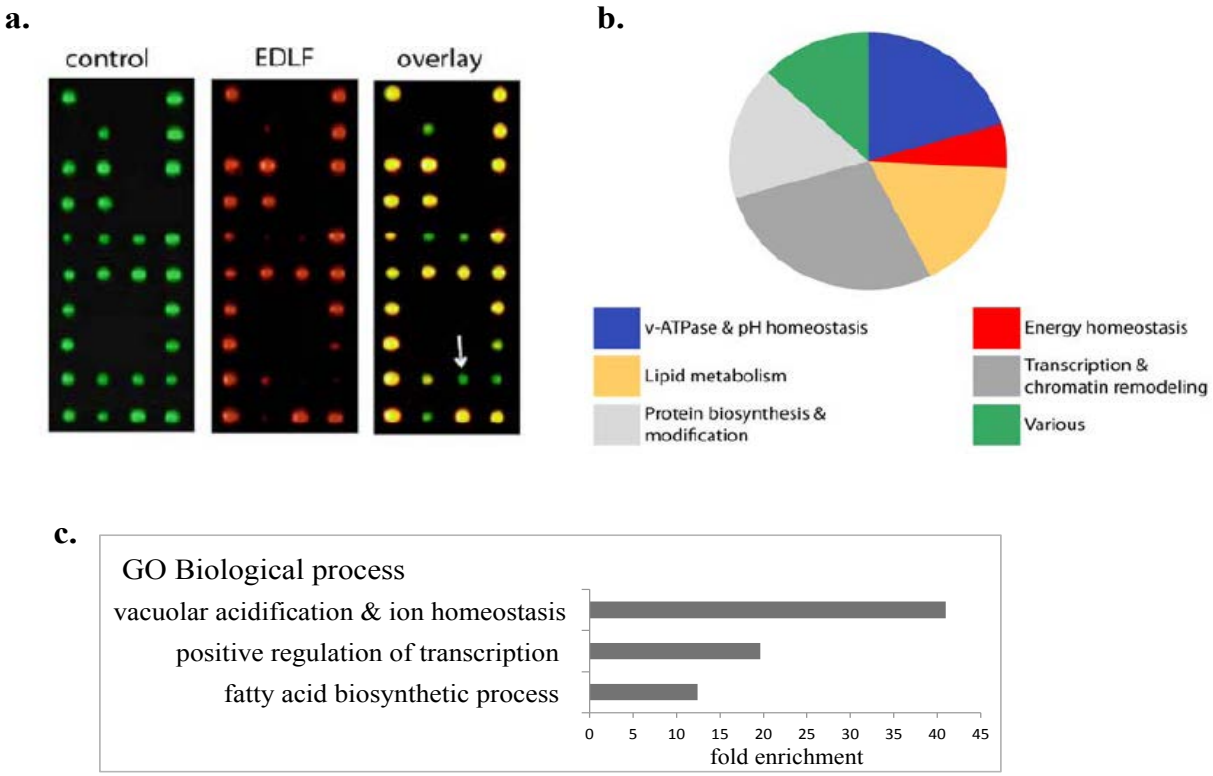

Figure 2.3: High-throughput edelfosine *S.cerevisiae* sensitive screen (a) The complete set of haploid *S.cerevisiae* yeast deletion mutants (4872 strains) was arrayed onto 20 plates and robotically pinned onto SD media (computerized green colonies) or SD+edelfosine (computerized red colonies). Putative edelfosine-sensitive mutants lead to the formation of smaller colonies (or no colony) when grown on edelfosine containing media (green after overlay, arrow) **(b)** Functional distribution of the 54 genes found to cause sensitivity to edelfosine when deleted. The functional categories corresponding to vacuolar acidification and ion transport, grouped as V-ATPase & pH homeostasis in the figure, had the lowest p-values (2.784e-12 and 3.099e-08 respectively, Funspec analysis) indicative of a significant enrichment **(c)** Enrichment of genes in the dataset clustering according to gene ontology (GO). Enrichment is calculated relative to the frequency of that cluster in the whole genome (EDFL= edelfosine).

Table 2.4: Complete list of genes identified in sensitive genetic screen

Sensitivity	Gene	Cellular role	Localization
+++	AFG3	Protein phosphorylation	mitochondria
+++	BEM1	Cell organization and biogenesis	bud tip-bud neck-cell periphery
+++	DBF2	Protein phosphorylation	bud neck-cytoplasm
+++	ERG3	Lipid metabolism	ER
+++	GAL11	Transcription	nucleus
+++	HTA3 (HTZ1)	Chromatin remodeling	nucleus
+++	PGD1	Transcription	nucleus
+++	REI1	Translation	cytoplasm-ribosome
+++	SIN3	Chromatin remodeling	mitochondria-nucleus
+++	SIP3	Energy homeostasis	nucleus
+++	**SNF1**	Energy homeostasis	nucleus-mitochondria-vacuole-cytoplasm
+++	SNF2	Chromatin remodeling	nucleus
+++	SNF6	Chromatin remodeling	nucleus
+++	SPT7	Transcription	nucleus-mitochondria
+++	**VMA16 (PPA1)**	Vacuolar ATPase	vacuole
+++	**VMA2**	Vacuolar ATPase	vacuole
+++	**VMA4**	Vacuolar ATPase	vacuole
+++	**VMA5**	Vacuolar ATPase	vacuole
+++	**VMA9**	Vacuolar ATPase	vacuole
+++	**VPH2 (VMA12)**	Vacuolar ATPase assembly	ER
+++	YJL175W	Chromatin remodeling	probably SWI3 (nucleus)
++	AKR1	Protein pamitoylation	golgi
++	ASC1	Translation	cytosol-ribosome
++	BIM1	Cell organization and biogenesis	microtubule
++	COX17	Cytochrome C assembly	mitochondria-nucleus?
++	CYC2	Cytochrome C regulation	mitochondria
++	DEF1	Protein degradation	nucleus-cytoplasm
++	ELO2	Lipid metabolism	ER
++	ETR1	Lipid metabolism	mitochondria-nucleus
++	LIP5	Lipid metabolism	mitochondria
++	NAP1	Chromatin remodeling	nucleus-cytoplasm
++	PAA1	Chromatin remodeling	cytoplasm
++	PDA1	Acetyl-CoA production (impact on lipid metabolism)	mitochondria
++	RPB4	Transcription	nucleus
++	SEC22	Vesicular transport	golgi-ER
++	SER1	Serine metabolism- (impact on lipid metabolism)	cytoplasm
++	SHY1	Cytochrome C assembly	mitochondria
++	**SNF4**	Energy homeostasis	nucleus-PM-cytoplasm
++	SNF5	Chromatin remodeling	nucleus
++	SPF1	Ion transport (P-type ATPase)	ER-mitochondria
++	SPO14	Lipid metabolism	endosomes?
++	SRB2	Transcription	nucleus-cytoplasm
++	SUR4	Lipid metabolism	ER
++	SWI6	Transcription	nucleus-cytoplasm
++	TRK1	pH homeostasis and K^+ transport	PM
++	UBP6	Protein degradation	nucleus-cytoplasm
++	**VMA10**	Vacuolar ATPase	vacuole
++	**VMA11 (TFP3)**	Vacuolar ATPase	vacuole-ER
++	**VMA21**	Vacuolar ATPase assembly	vacuole
++	**VMA7**	Vacuolar ATPase	vacuole
++	YBR178W	Lipid metabolism	probably EHT1 (mitochondria-lipid particle
++	YDR521W	Transcription	probably YDR520C (nucleus)
+	PDX3	Lipid metabolism	?
+	**VMA6**	Vacuolar ATPase	vacuole

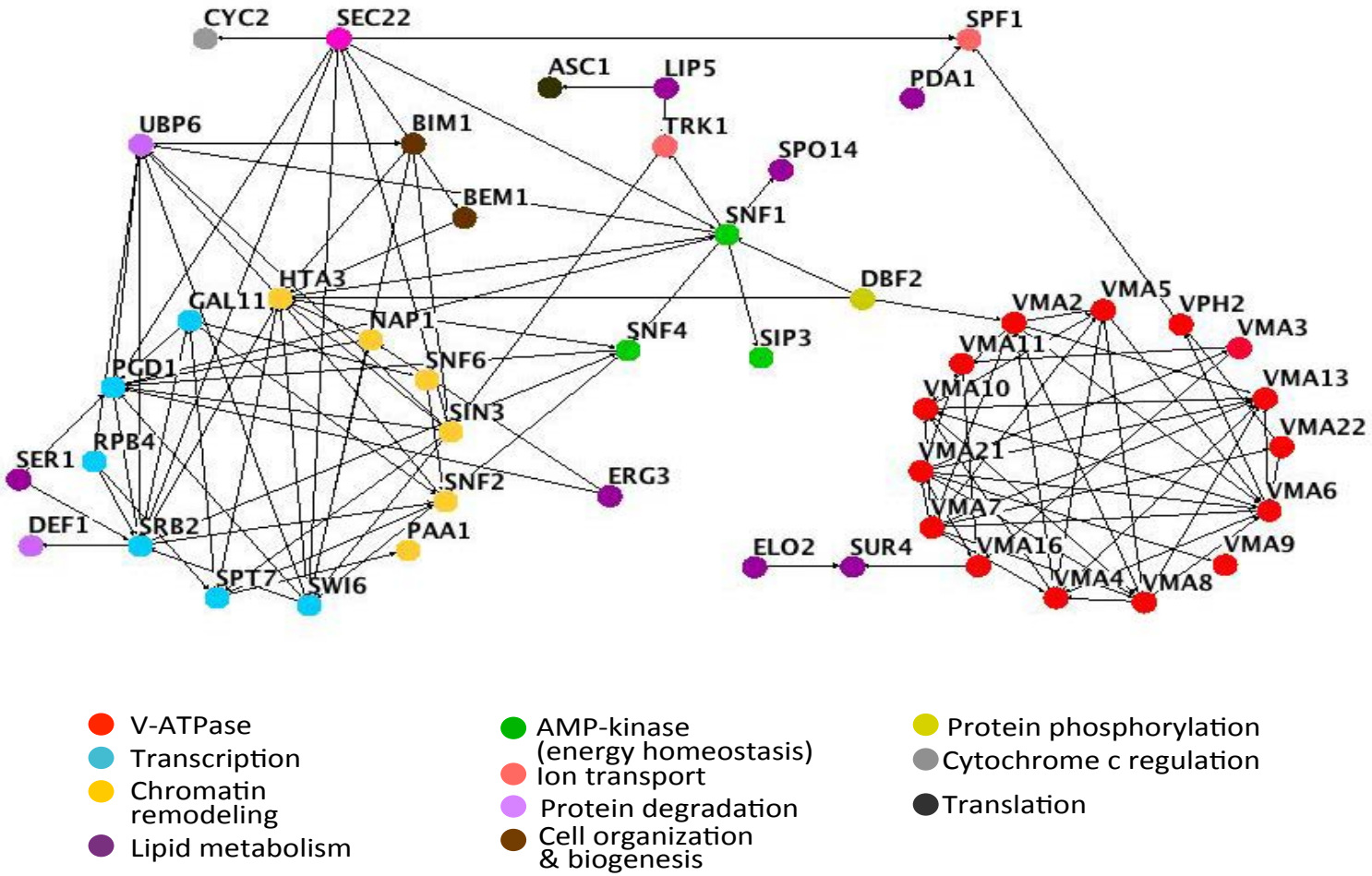

Figure 2.4: Interactome map of genes identified in edelfosine sensitive screen Nodes represent genes identified as hypersensitive to edelfosine from the screen. Genes belonging to the same pathway or complex are colored according to the categories shown at the bottom of the figure. Edges indicate experimentally determined genetic or physical interactions. Nodes with a minimum of one connection are shown.

pH homeostasis

A cluster comprising genes coding for 9 of the 14 subunits of the vacuolar proton-translocating ATPase (V-ATPase), as well as *VPH2* and *VMA21* encoding proteins that participate in V-ATPase assembly in the ER (118), were identified (Table 2.4). Serial dilution analysis expanded this result to include 12 V-ATPase subunits and one other gene coding for an assembly protein (*VMA22*) (Table 2.4, Figure 2.5). In addition, *TRK1*, coding for the high affinity potassium transporter of the PM was among the genes identified (Table 2.4, Figure 2.5). It is well documented that V-ATPase in the vacuole collaborates with Pma1 at the PM to maintain pH homeostasis in yeast (100). Trk1 also participates in regulation of intracellular pH by positively regulating Pma1 activity (100, 119, 120).

The second largest category of enrichment in our screen contained genes that positively regulate transcription. Genes coding for the yeast adenosine mono-phosphate (AMP) dependent kinase (AMPK) *SNF1* and its γ subunit *SNF4* were among these genes (Table 2.4, Figure 2.4, 2.5). AMPK/Snf1p plays a central role in controlling energy homeostasis in eukaryotes (121). Snf1 responds to glucose depletion and is a modulator of Trk1 activity (122, 123). Furthermore, cells deleted for *SNF1* or *SNF4* display pH-dependent phenotypes (120, 124). Deletion mutants *vma2*, *trk1* and *snf1* transformed with the corresponding wild type genes displayed wild type sensitivity to edelfosine (Figure 2.6). Therefore the hypersensitive phenotype is not due to secondary mutations present in these strains.

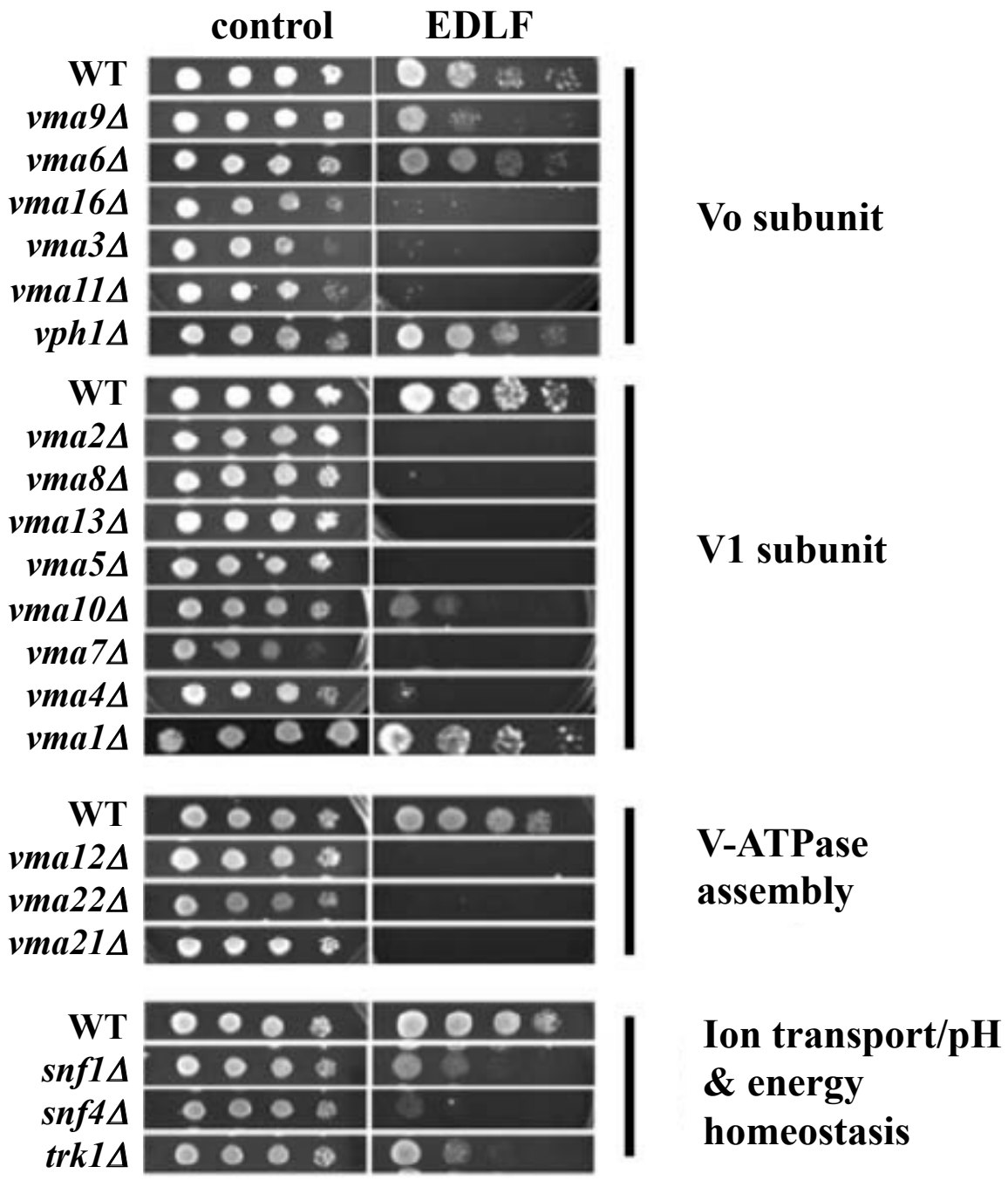

Figure 2.5: Mutants with compromised pH homeostasis are hypersensitive to edelfosine Strains scored as sensitive at least three times (from four screens completed) were verified by spotting serial dilutions of the cells onto media containing 19 μM edelfosine. Thus, a total of 54 deletion strains were confirmed to be edelfosine sensitive. (a) The analysis was extended to all known V-ATPase-related genes by spotting serial dilutions of their corresponding deletion strains onto rich (YPD) medium control or plates containing 19 μM edelfosine (EDLF). Plates were incubated at 30°C for 3 days. Data shown are representative of three independent experiments.

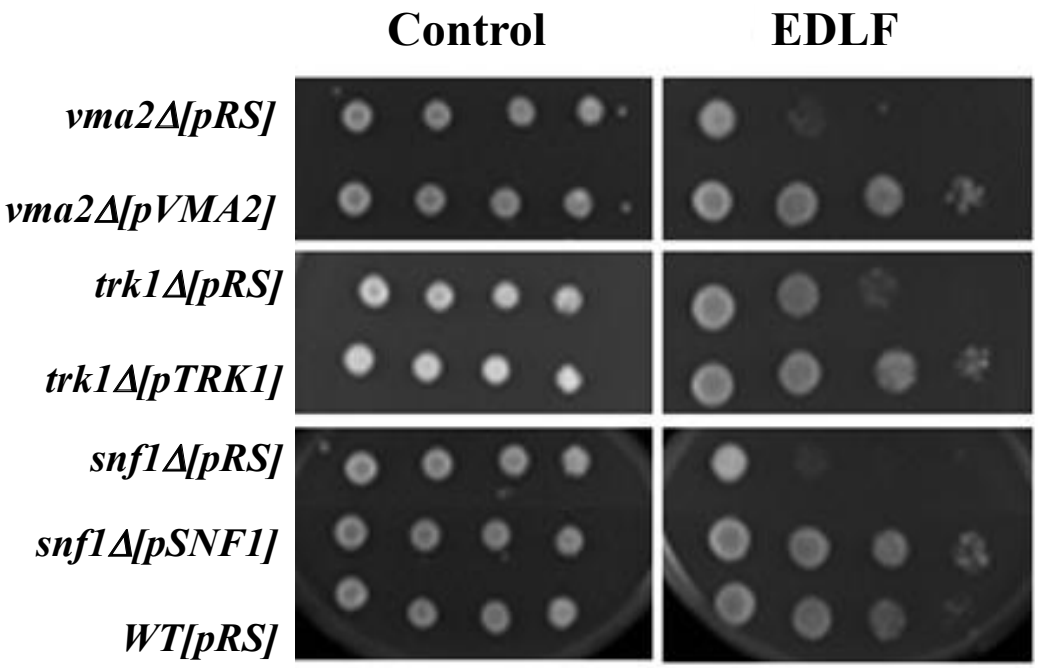

Figure 2.6: Reversion of edelfosine sensitivity Deletion strains *vma2*, *trk1* and *snf1*were transformed with empty pRS315 (CEN) plasmids or same plasmids containing the corresponding wild type gene under their own promoters. Strains were grown in presence of absence of edelfosine (19 μM) for 3 days (EDLF = edelfosine).

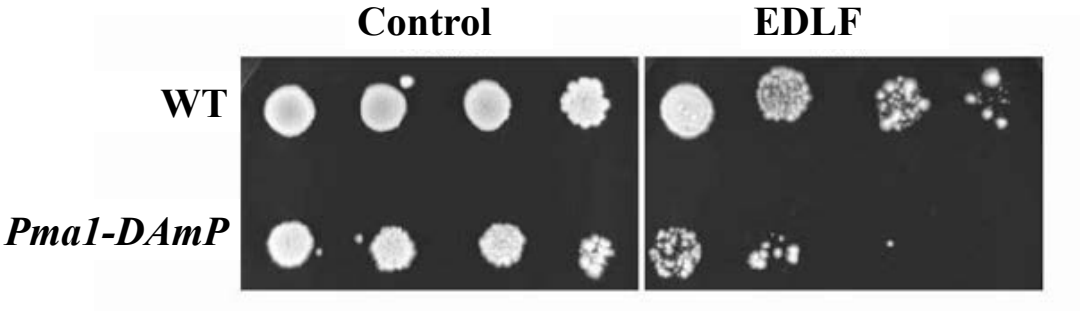

Figure 2.7: A hypoxmorphic allele of *PMA1* confers hypersensitivity to edelfosine A yeast strain with the *PMA1-DAmP* (**D**ecreased **A**bundance by **m**RNA **P**erturbation) allele displays increased sensitivity to edelfosine (EDLF = edelfosine).

The enrichment of genes related to maintenance of pH homeostasis in our sensitivity screen is in line with our previous findings involving Pma1 as the main target of edelfosine interaction with the yeast PM. Since Pma1 is an essential protein, it was not expected to be found in the screen for edelfosine-sensitive mutants using the *S. cerevisiae* non-essential gene deletion collection. We tested the sensitivity of cells carrying a hypomorphic allele of *PMA1*, *PMA1-DAmP* (Decreased Abundance by mRNA Perturbation) that results in substantially reduced levels of the protein (111). Consistent with our above results, *PMA1-DAmP* cells displayed increased sensitivity towards edelfosine (Figure 2.7).

2.4 Concluding remarks

The genome wide screens presented in this chapter provided a greater insight into the mode of action of edelfosine as well as to cellular processes that modulate sensitivity and resistance to this ATL. Vesicular trafficking was identified to be a critical process in mediating edelfosine resistance. It was also elucidated that it is the recycling of proteins back to the PM and not inhibition of drug uptake that provides edelfosine resistance. The sensitive screen highlighted the importance of pH homeostasis in edelfosine sensitivity, which was in line with previous findings that identified Pma1 internalization as a main consequence of edelfosine interaction with the PM. In the following chapter we further investigate how intracellular pH is affected upon edelfosine treatment.

Chapter Three: Edelfosine alters pH homeostasis

3.1 Introduction

The results obtained from the most recent sensitive genetic screen showed enrichment in genes known to participate in pH homeostasis, transcription and lipid biosynthesis (Chapter 2). Mutants lacking proper V-ATPase function (*vma* mutants), as well as those lacking a functional K^+ pump, *trk1,* were among those identified to be hypersensitive to edelfosine. Previous evidence showed that Pma1 is internalized upon edelfosine treatment (78), and we also saw that a hypomorphic allele (*PMA1-DAmP*) of Pma1 showed increased sensitivity to edelfosine (Figure 2.7, Chapter 2).

It is also well known that Pma1, V-ATPase and Trk1 work together to regulate pH homeostasis in yeast (100). Interestingly, the resistance screen identified mutants of genes coding for subunits of the F1-F0 ATPase as resistant to edelfosine (Chapter 2) (106). The F1-F0 ATPase is localized to the inner mitochondrial membrane and is able to either synthesize or hydrolyze ATP, depending on the metabolism of the cell. Under respiratory conditions, the F1-F0 ATPase synthesizes ATP from adenosine di-phosphate (ADP) and phosphate (Pi) in a process that is powered by the electrochemical gradient produced by the activity of the electron transport chain. Therein, during respiration the F1-F0 ATPase pumps protons from the inter-membrane space to the mitochondrial matrix (125-128). Conversely, during fermentation, the F1-F0 ATPase works in reverse to hydrolyze ATP, and causes the export of protons into the inter-membrane space (128).

Altogether the results of the genetic screens as well as previous work on the effect of edelfosine in yeast have implicated the three proton pumps present in the cell: P-type ATPase Pma1 at PM, V-type vacuolar ATPase (14 subunits) and the F-type pump F1-F0 ATPase (7 subunits) in the

mitochondria. A decrease in Pma1 levels and defects in the V-ATPase conferred hypersensitivity to edelfosine, while strains with mutations in the F1-F0 ATPase displayed resistance to the drug. Since all of the studies have been conducted in yeast in the presence of glucose, we reasoned that fermentation is the predominant metabolic pathway being used by these cells. During fermentation, we expect each of the aforementioned pumps to contribute to cytosolic pH in a manner illustrated in Figure 3.1.

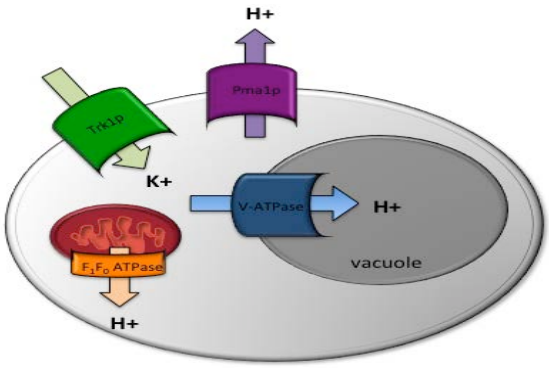

Figure 3.1: Contributions of the major yeast proton pumps to cytosolic pH during fermentation V-ATPase (blue), Pma1 (purple) function to export protons out of the cytosol, therein increasing cytosolic pH; Trk1 (green) maintains the electrochemical gradient at the PM which aids in Pma1 function; F1-F0 ATPase (orange) pumps protons from the matrix to the inter-membrane space potentially contributing to cytosolic acidification.

Pma1 and the V-ATPase collaborate to maintain an alkaline cytosolic pH (7.2 +/- 0.2), while the F1-F0 ATPase works in reverse, and hydrolyzes ATP, creating an influx of protons in the inter-membrane space, which may contribute to cytosolic acidification, while simultaneously causing the alkalinization of the mitochondrial matrix (98, 128). Therefore the contradictory contributions to pH homeostasis by the F1-F0 ATPase and Pma1 and V-ATPase pumps may correlate to their opposing phenotypes. As such, we decided to investigate the effect edelfosine has on the maintenance of pH homeostasis in wild type, hypersensitive and resistant yeast strains.

3.2 Materials and methods

Yeast strains, plasmids and growth conditions

Detailed information on yeast strains and primers used is provided in Table 3.1 and 3.2 respectively. Yeast were grown in yeast complex medium (YPD; 1% yeast extract, 2% bacto-peptone and 2% glucose) or in synthetic defined medium (SD; 0.67% yeast nitrogen base without amino acids, 2% glucose), or in low fluorescence media (LF-YNB; 0.67% yeast nitrogen base without amino acids, 2% glucose) with amino acids supplied to complement strain auxotrophies. Where needed, the pH of media was adjusted to acidic pH conditions using, 5M hydrochloric acid (HCl) or for alkaline pH conditions using 5M sodium hydroxide (NaOH). For plates, 2% agar was added to desired media prior to autoclaving, wherein glucose (2% or 4%) was added from a concentrated sterile stock after media was autoclaved. For acidic plates, those with pH < 5, pH was adjusted using 5M HCl after autoclaving. When necessary, plates were supplemented with 5μM copper, from a 100x concentrated stock of $CuSO_4\,5H_2O$ and 5μM iron from a 100x concentrated stock of $(NH_4)_2\,Fe\,(SO_4)_2\,.6\,H_2O$. Growth of cells in liquid media was measured using UV-Vis Spectrophotometer (Shimadzu UV-2450) by optical density at a wavelength of 600nm (OD_{600}).

Edelfosine was a kind gift from Medmark Pharma GmbH. A 10 mg/ml stock solution in ethanol was prepared fresh every time and used within two days. The final ethanol concentration in control (ethanol) and edelfosine containing (edelfosine in ethanol) plates never exceeded 0.2%. Growth on control (with ethanol) plates was indistinguishable from that of control plates lacking ethanol. Edelfosine was added after autoclaving and cooling of the media to at least 60 °C.

Table 3.1: List of yeast strains used in this chapter

Strain Name	Genotype	Source
BY4741	*MATa his3 leu2 met15 ura3*	Euroscarf
YMS084	*MATα can1Δ::MFa1pr-HIS3-MFα1pr-LEU2 his3Δ0 leu2Δ0 ura3Δ0 met1Δ0 lyp1Δ0*	(111)
PMA1-DAmP	YMS084 *YGL008C::3NATB*	(111)
vma2Δ	*MATa his3Δ1 leu2Δ0 met15Δ0 ura3Δ0 YBR127c::kanMX4*	Euroscarf
snf1Δ	*MATa his3Δ1 leu2Δ0 met15Δ0 ura3Δ0 YDR477w::kanMX4*	Euroscarf
trk1Δ	*MATa his3Δ1 leu2Δ0 met15Δ0 ura3Δ0 YJL129c::kanMX4*	Euroscarf
vps35Δ	*MATa his3Δ1 leu2Δ0 met15Δ0 ura3Δ0 YJL154c::kanMX4*	Euroscarf
lem3Δ	*MATa his3Δ1 leu2Δ0 met15Δ0 ura3Δ0 YNL323w::kanMX4*	Euroscarf

Table 3.2: List of plasmids used in this chapter

Plasmid	Description	Source
cytosolic pHluorin	pYES expressing pHluorin from *ACT1* promoter	(98)
mitochondrial pHluorin	pYES expressing mitochondrial pHluorin from *ACT1* promoter	(98)
empty	pYES	Invitrogen

Serial dilutions

Yeast cells were grown to mid-log phase (OD_{600}= 0.4-0.6) in YPD or SD media and concentrated in order to obtain OD_{600} =1. Three subsequent 1/10 dilutions were carried out to obtain, OD_{600} = 0.1, 0.01 and 0.001. Five µl of each dilution was spotted onto desired solid media plates in the absence or presence of the indicated concentrations of edelfosine. Each plate growth assay experiments was done in triplicates and repeated two times. Plates were incubated at 30 °C for the indicated periods of time and imaged using a GelDoc system (BioRad).

Yeast Transformations

The Lithium Acetate method was used to transform yeast cells with desired plasmids. Yeast cells were grown in 15 ml YPD media, at 30ºC overnight with shaking and diluted to 2 X 10^6 cells/ml (OD_{600} = 0.1-0.2) in 50 ml fresh YPD the next morning and incubated 3-4 hours more (time varied depending on strain), for log phase (OD_{600} = 0.4-0.6). Cells were harvested by centrifugation at room temperature in a 50ml FALCON tube (3,000 rpm/5 min) and resuspended in 1 ml 1M sorbitol, transferred to a 1.5ml tube and spun for 1 minute @ 10,000rpm. Pelleted cells were washed with 1 ml 1X TE/1X LiAc and then resuspended in 500µl 1X TE/1X LiAc. From this suspension, 50 µl cells was added to tubes containing transforming DNA (at least 600 ng) and 50 µg single-stranded carrier DNA (salmon sperm DNA, (Invitrogen, boiled and iced immediately before use). Furthermore, 350 µl 40% PEG/1X TE/1X LiAc was added to the cells, mixed, and incubated at 30°C with shaking for 60 minutes. Cells were then heat-shocked at 42°C for 10 minutes, spun for 1min @10,000rpm in microcentrifuge (Eppendorf) and resuspended in 150 µl 1X TE. Transformed cells were plated on selective plates, based on selection marker on used plasmid. Plates were incubated at 30ºC for 2-3 days. Single colonies were selected from these plates and re-streaked onto fresh plates.

pH luorin measurements

A green fluorescent protein (GFP) derivative named pH luorin was used to measure intracellular pH. This protein is mutated at the following residues: S202H, E132D, S147E, N149L, N164I, K166Q, I167V, R168H and L220F as compared to wild type GFP and shows a quick reversible excitation ratio between pH 5.5 to 7.5(129). Yeast transformed with pYES (Empty), pYES-ACT-pHluorin (Cytosolic pH luorin), pYES-ACT-pHluorin (Mitochondrial pH

luorin) were grown to OD_{600} = 0.5 at 30°C in LF-YNB media at pH 7. In order to obtain standard curves, ~15 OD's of cells transformed with each cytosolic pH luorin, mitochondrial pH luorin and empty vector were collected, re-suspended in 15 ml PBS and treated with 100 mg/ml digitonin (Sigma). From here, 1 ml (1 OD) of cells was re-suspended in one of ten buffers with pH values ranging from 5.95-7.8.

Measurements were done following the procedure outlined in *Orij et al.* (98). Briefly, samples were excited at 390 and 470 nm, and fluorescence emission was measured at 512nm in a Cary Eclipse Fluorescence Spectrometer (Varian). Emission values were obtained using Cary Eclipse Ratio Application software, where data and statistical analysis was done using Microsoft Excel and GraphPad Prism software. In order to obtain standard curves, the ratio between emission intensities resulting from excitation at 390nm and 470nm (R390/470) was plotted against the corresponding pH buffer. In all experiments, emission intensity values obtained from the empty vector transformants (pYES) (which accounted for background fluorescence) were subtracted.

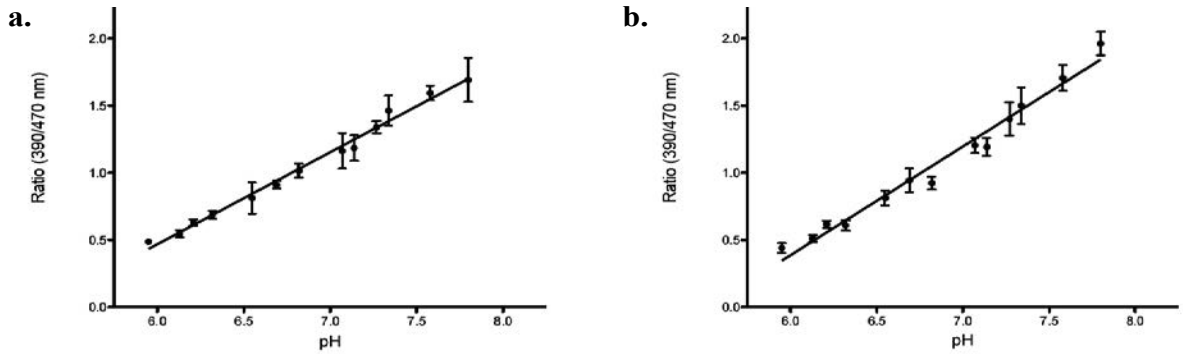

Figure 3.2: Standard curves for pH luorin (a) Cytosolic pH luorin (b) Mitochondrial pH luorin Cells treated with digitonin (100 mg/ml) were resuspended in buffers of pH from 5.95 to 7.8 and excited at 390 nm and 470 nm and emission fluorescence was measured from each at 512 nm. The ratio of emission values R390/470 is plotted against the corresponding buffer pH.

In order to measure changes in pH caused by edelfosine, fluorescence measurements were taken for cells treated with edelfosine (19μM final concentration in 0.1% ethanol) and un-treated cells (0.1% ethanol). Measurements were taken at 15 minute intervals up to and including 90 minutes. After which, cells were treated with 100 μg/ml digitonin for 15 minutes to allow for equilibration with the media pH, and then another measurement was taken. Corresponding emission values for 390 and 470 nm excitation wavelengths were used to obtain R390/R470 and the corresponding cytosolic or mitochondrial pH values were determined using standard curves (Figure 3.2). Each experiment was carried out a minimum of three times and contained at least four replicates.

Mitochondrial Fragmentation

Cells containing pYES-ACT-mitochondrial pHluorin plasmid were grown in LF-YNB media at pH 7. After reaching OD_{600} = 0.1-0.2, cultures were split and cells were either treated with edelfosine (19μM final concentration in 0.1% ethanol) or left untreated (0.1% ethanol) and incubated at 30^{o}C for 15 minutes. Cells were then concentrated and placed on slabs of solid medium made from LF-YNB and 2% agar. Coverslips were sealed and digital images were obtained using epifluorescence microscope (DMR; Leica, Germany) fitted with a Plan Apo ×100 oil immersion objective lens. Images were captured using a cooled CCD camera (Retiga 1350 EX, QImaging, Burnaby, British Columbia, Canada) and Volocity Software 5.0.2, aligned using Adobe Photoshop Elements (9.0). Mitochondrial morphology was categorized for edelfosine treated, (19μM final concentration in 0.1% ethanol) and untreated cells (0.1% ethanol) at 0 minutes and 15 minutes. Only cells expressing mitochondrial pHluorin, and none containing auto-fluorescence (due to cell death) were visually classified based on morphology as

fragmented or non-fragmented. A minimum of 100 cells was quantified for each condition; final quantification was based on 3 separate experiments.

3.3 Results

3.3.1 Edelfosine induces cytosolic and mitochondrial acidification

We measured the effect that edelfosine had on intracellular pH by using a pH sensitive green fluorescent protein, ratiometric pH luorin (98). This protein allows for the accurate determination of organelle specific pH, and has been used to successfully measure intracellular pH in yeast (98, 100, 107, 111, 130). We decided to express a cytosol targeted, or mitochondrial (matrix) targeted pHluorin in wild type cells as well as hypersensitive and resistant mutants, *vma2Δ* and *vps35Δ*, respectively, to measure the changes in pH in these compartments, during edelfosine treatment. Vma2 is a subunit of the vacuolar ATPase and we observed that its deletion resulted in a strong sensitivity to edelfosine (Table 2.4, Figure 2.5 from Chapter 2). On the other hand, Vps35 is a component of the yeast retromer and cells with an inactivated *VPS35* gene, show normal drug uptake, but are still edelfosine resistant (106). We chose to monitor edelfosine induced pH changes over a 90 minute time frame, as we have previously determined that this precedes cell death (78).

We treated wild type (WT, BY4741) hypersensitive mutant *vma2* and resistant mutant *vps35* expressing a cytosolic pH luorin with 19μM edelfosine to determine the effect of edelfosine on intracellular pH. Treatment of WT cells with 19mM edelfosine caused cytosolic acidification as early as 45 minutes after drug addition, compared to untreated cells. It is important to note that due to the sensitivity of the pH luorin measurements, the first hour of treatment shows great fluctuations in pH indicating the cells may be attempting to re-establish pH homeostasis after

initial edelfosine administration. After 90 minutes, the cytosolic pH of untreated cells reached 7.36 +/- 0.13, where the pH in edelfosine treated cells dropped to 6.89 +/- 0.04, a drop of 0.43-0.51 pH units (Figure 3.3). Edelfosine treatment also caused a decrease in the cytosolic pH of both hypersensitive deletion mutant, *vma2* and resistant deletion mutant, *vps35* (Figure 3.3). The pH decrease with edelfosine treatment was most pronounced in *vma2*. Untreated cells reached a pH of 7.23 +/- 0.06, while after 90 minutes, edelfosine treated cells were acidified to a pH of 6.76 +/- 0.06, which corresponds to an additional 0.12-0.14 pH unit decrease when compared to the WT cells. Conversely, *vps35*, showed greater buffering capacity compared to WT and *vma2*, having an overall decrease of 0.29-0.37 pH units. After 90 minutes following edelfosine treatment, the final pH in *vps35* cells was 7.05 +/- 0.04, as compared to the untreated *vps35* pH being 7.38 +/- 0.08.

We also looked at the effect edelfosine had on the mitochondrial pH of WT, *vma2* and *vps35* strains. Treatment of WT cells with 19mM edelfosine showed mitochondrial acidification at 60 minutes, and after 90 minutes of drug treatment, edelfosine treated cells dropped to a pH of 6.98 +/- 0.02 as compared to untreated cells which maintained pH 7.47 +/- 0.15, a difference of 0.47-0.51 pH units (Figure 3.4). Edelfosine also caused a decrease in the mitochondrial pH of hypersensitive mutant *vma2* and resistant mutant *vps35* (Figure 3.4). The final pH of edelfosine treated *vma2* mutants was 6.57 +/- 0.05 as compared to untreated cells, which maintained a pH of 7.17 +/- 0.08, indicating acidification of 0.55-0.65 pH units (Figure 3.4). The resistant mutant *vps35* showed greater buffering capacity in comparison to WT and *vma2* with pH decreasing only 0.06 – 0.30 pH units after 90 minute edelfosine treatment. The final pH in *vps35* untreated cells was 7.32 +/- 0.11 compared to edelfosine treated, 7.14 +/- 0.12 (Figure 3.4).

Table 3.3: Final pH values of WT, *vma2* and *vps35* after 90 minutes in the presence and absence of edelfosine

		WT	***vma2***	***vps35***
Cytosolic pH	Control	7.36 +/- 0.13	7.23 +/- 0.06	7.38 +/- 0.08
	Edelfosine	6.89 +/- 0.04	6.76 +/- 0.06	7.05 +/- 0.04
Mitochondrial pH	Control	7.47 +/- 0.15	7.17 +/- 0.08	7.32 +/- 0.11
	Edelfosine	6.98 +/- 0.02	6.57 +/- 0.05	7.14 +/- 0.12

As expected, mitochondrial pH in control (untreated) WT and *vps35* strains was more alkaline compared to the cytosolic pH, where the *vma2* strain showed no significant difference between cytosolic and mitochondrial pH (Figure 3.5). It is worth noting that the drop in cytosolic pH preceded mitochondrial acidification.

In summary, edelfosine treatment induces acidification in both the cytosol and the mitochondria in all three strains. Comparison of overall pH decreases due to drug treatment indicates that acidification in both the mitochondria and cytosol is comparable in WT cells. These results indicate that the hypersensitive *vma2* strain has the lowest buffering capacity, showing the largest drop in pH in both the cytosol and the mitochondria, wherein resistant mutant *vps35* displayed the greatest buffering capacity. Altogether the evidence obtained supports the hypothesis that the buffering capacity of the cell influences its ability to handle the disturbance in pH homeostasis induced by edelfosine, further pointing at an important role for intracellular acidification in mediating the cytotoxic activity of edelfosine in *S. cerevisiae.*

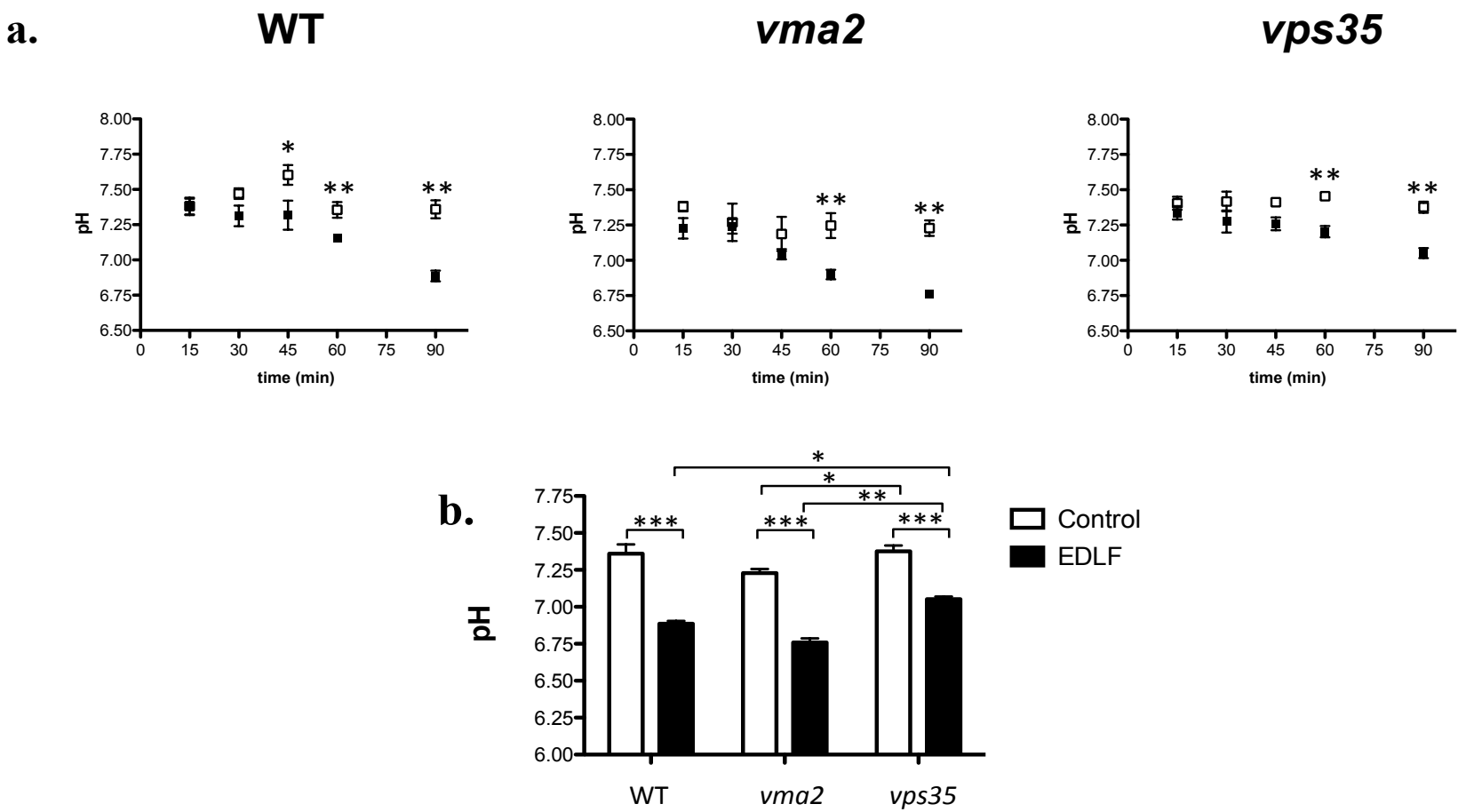

Figure 3.3: Measuring intracellular pH changes after edelfosine treatment Cytosolic measurements were performed using cells expressing pHluorin **(a)** Intracellular pH was monitored during a 90 minute period in untreated (0.1% ethanol, open squares) and edelfosine (19μM edelfosine, 0.1% ethanol, closed squares). Time course shown for wild type (WT, BY4741), *vma2, vps35* **(b)** Comparison of values obtained for control (0.1% ethanol, white bars) and edelfosine treated (EDLF, black bars, 19mM edelfosine, 0.1% ethanol, black bars) 90 minute treatment. Data shows mean values +/- SD representative of 3 experiments. [p< 0.001 (***), p<0.01 (**), p<0.05 (***)].

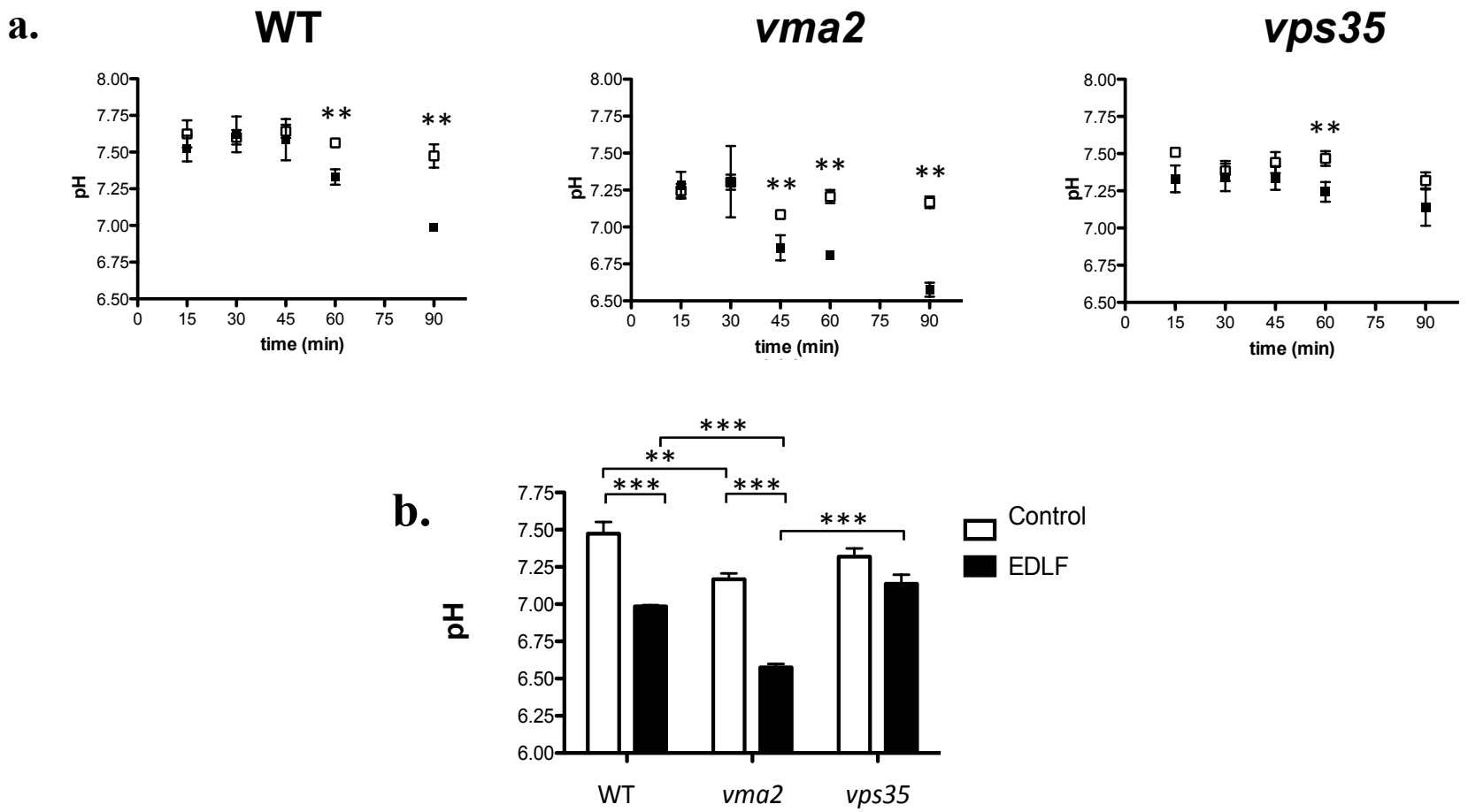

Figure 3.4: Measuring mitochondrial pH changes after edelfosine treatment Mitochondrial measurements were performed using cells expressing mitochondrial pHluorin **(a)** Mitochondrial pH was monitored during a 90 minute period in untreated (0.1% ethanol, open squares) and edelfosine (19μM edelfosine, 0.1% ethanol, closed squares). Time course shown for wild type (WT, BY4741), *vma2, vps35* **(b)** Comparison of values obtained for control (0.1% ethanol, white bars) and edelfosine treated (EDLF, black bars, 19mM edelfosine, 0.1% ethanol, black bars) 90 minute treatment. Data shows mean values +/- SD representative of 3 experiments. [$p < 0.001$ (***), $p<0.01$ (**), $p<0.05$ (***)].

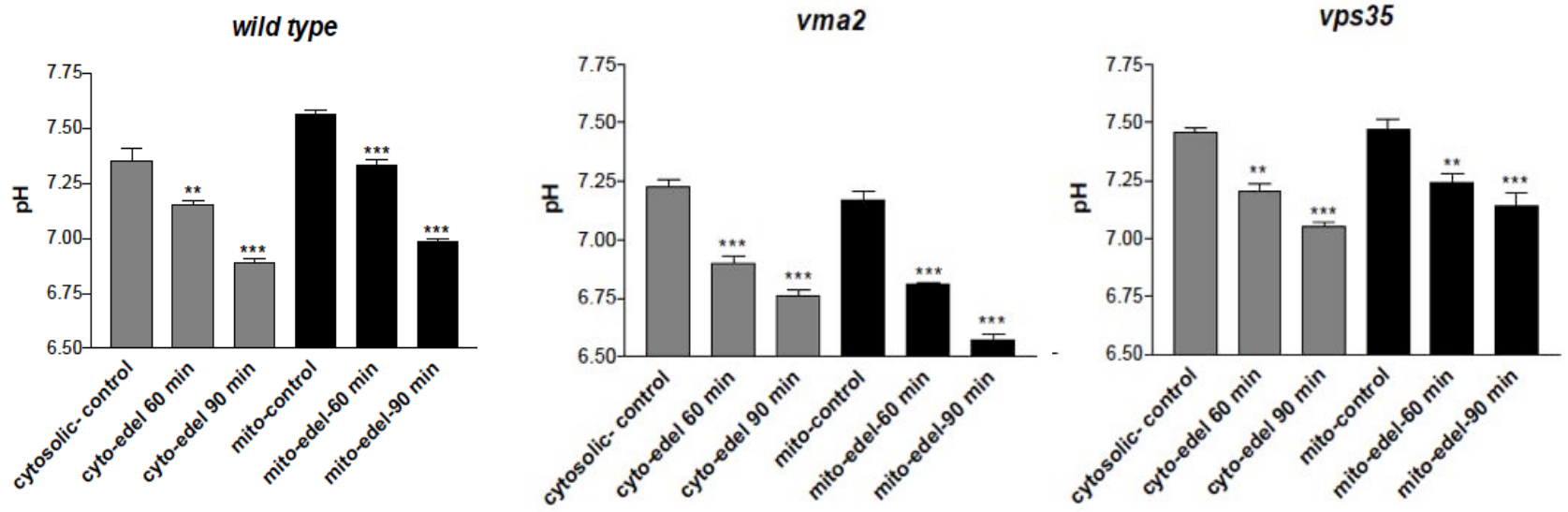

Figure 3.5: Edelfosine treatments caused cytosolic and mitochondrial acidification Comparison of the effect of edelfosine treatment (19mM, 0.1% ethanol) on cytosolic (grey bars) and mitochondrial (black bars) pH inWT, *vma2*, *vps35* using pH luorin analysis as seen at 0, 60 and 90 minutes after drug treatment. Data shows mean values +/- SD representative of 3 experiments [p< 0.001 (***), p<0.01 (**), p<0.05 (***)].

3.3.2 Edelfosine induces mitochondrial fragmentation

Since pH-luorin is a green fluorescent protein derivative, we were able to use the fluorescence signal of the mitochondrial targeted pH luorin to visualize mitochondrial morphology *in vivo*. We saw that the mitochondria of cells expressing the mitochondrial targeted pH luorin showed a network-like morphology, a phenotype typical for yeast grown on glucose (Figure 3.6a) (131). Interestingly, mitochondrial morphology of wild type cells was severely affected by edelfosine treatment, displaying a high degree of fragmentation (Figure 3.6a). We therefore expanded our analysis to include the hypersensitive and resistant mutant strains *vma2* and *vps35* respectively. We also decided to include the resistant *lem3* mutant, which is unable to uptake edelfosine (89, 106).

We observed mitochondrial fragmentation in cells treated with edelfosine as early as 15 minutes following drug treatment (Figure 3.5b). Interestingly, hypersensitive mutant *vma2* showed that even in control conditions, 28% of cells displayed fragmented mitochondria, as compared to only 13% in WT and less than 5% in both *vps35* and *lem3* resistant mutants. After 15 minutes, mitochondrial fragmentation was detected in more than 80% of WT and *vma2* treated cells. Comparatively, the resistant mutant *vps35* displayed mitochondrial fragmentation in 54% of the cells, while fragmented mitochondria were detected in only 17% of *lem3* mutant cells. These results suggest that cells with impeded drug uptake are less likely to exhibit mitochondrial fragmentation. Since this change in mitochondria morphology precedes cytosol acidification (Figure 3.3), we speculated that mitochondrial fragmentation could be a mechanism to maintaining pH homeostasis in the presence of edelfosine.

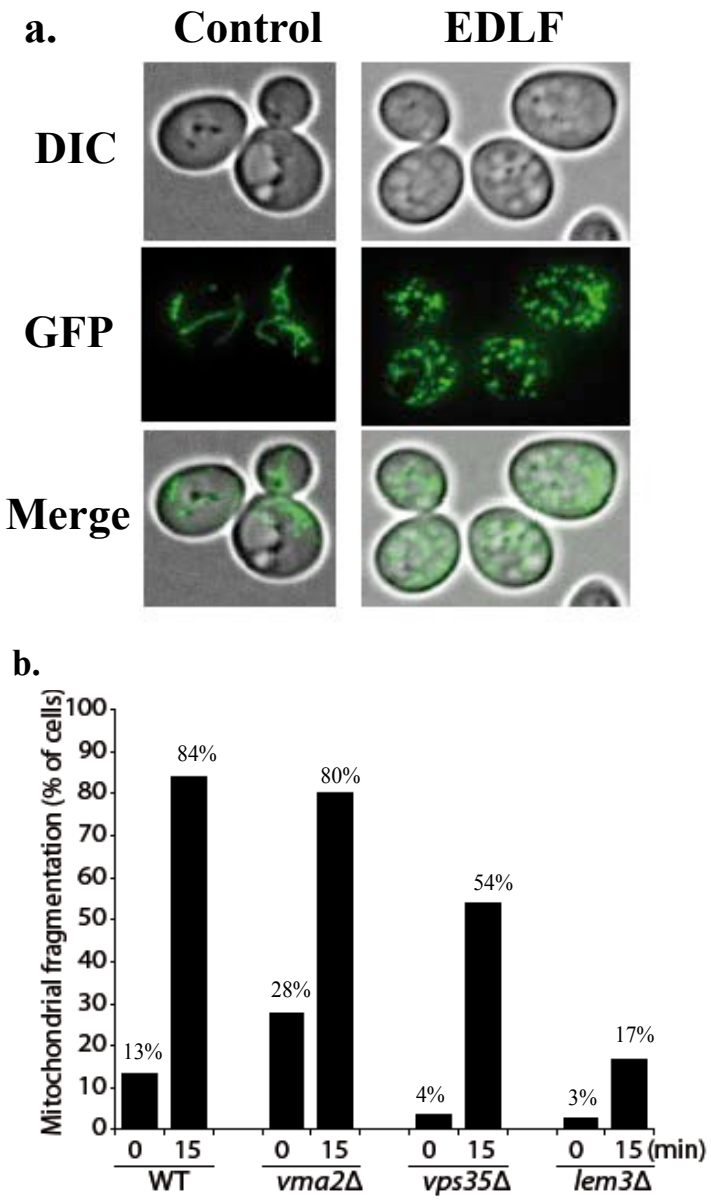

Figure 3.6: Quantification of mitochondrial fragmentation after edelfosine treatment (a) Comparison of different mitochondrial morphology observed in cells expressing mitochondrial pH luorin. Fragmentation is observed in edelfosine treated cells (19μM, 0.1% ethanol, right), where non-fragmented mitochondrial morphology is seen in the untreated cells (0.1% ethanol, left) **(b)** Quantification of mitochondrial fragmentation in WT cells, hypersensitive *vma2,* and resistant *vps35, lem3* strains 15 minutes following edelfosine addition. Values represent the percentage of total cells that are showing fragmented mitochondria and are a composite of 100 cells of 3 separate trials (DIC = differential interference contrast; EDLF = edelfosine).

3.3.3 Extracellular pH modulates edelfosine cytotoxicity

We considered that if edelfosine compromises pH homeostasis an aggravated phenotype should be displayed when cells are grown under stress conditions, like in tolerance to extreme extracellular pH. The lower and upper pH tolerance limits for yeast growth are 2.5 and 8 respectively (132). Due to the tight control of intracellular pH, the kinetics of growth and fermentation are not affected at extracellular pH between 3.5 and 6.0 (132). We therefore decided to test sensitivity to edelfosine at extracellular pH of 3.0 and 7.5, which still allowed for significant cell growth, despite causing considerable stress (133). The hypomorphic strain *PMA1-DAmP* was included in the analysis to monitor the impact that the chosen pH conditions would have on a strain that should (partially) mimic the effect of edelfosine. A decrease in Pma1 activity and expression has been previously described in yeast grown at pH 2.5 and 3 (132, 133). As expected, growth of the *PMA1-DAmP* strain was impaired at pH 3, when compared to its isogenic wild type (Figure 3.7). Interestingly, a similar delay was also observed in control plates with a pH of 7.5, while no major differences were detected at pH 5. As expected, the effect of edelfosine was stronger for strains grown at an extracellular pH of 3 but surprisingly, was even more potent at a slightly alkaline extracellular pH of 7.5 (Figure 3.7). These results suggest that additional compensatory pathway/s uniquely triggered by alkaline media are either impaired by treatment with edelfosine or result in enhanced sensitivity to the drug.

We further examined the effect of extracellular pH in the hypersensitive mutants *vma2* and *trk1* (Figure 3.8). As expected, all strains were able to grow at an extracellular pH of 5. The *vma2* mutant strain showed impaired growth in both the slightly alkaline and the acidic growth conditions, wherein the growth of *trk1* was comparable to that of the WT at an extracellular pH of 7.5 but was impaired at the acidic pH of 3 (Figure 3.8). Treatment with a sub-lethal

concentration of edelfosine (9.5 μM), showed that the effect of the drug was exacerbated at the alkaline pH, while cells grown at an extracellular pH of 5 and 3 had growth comparable to untreated cells (Figure 3.8).

We decided to further investigate the effect that medium alkalinization had on the potency of edelfosine. It has been shown that increased extracellular pH is linked to the decreased uptake of Cu^{2+}, Fe^{2+} and glucose (134). In addition, it has also been shown that supplementation of Cu^{2+}, Fe^{2+} to *vma* mutants helps in their growth at slightly alkaline pH (100). Therefore, we decided to supplement plates with 4% glucose and $CuSO_4\ 5H_2O$ (final concentration of 5μM Cu) and $(NH_4)_2Fe(SO_4)_2\ 6H_2O$ (final concentration of 5 μM Fe). We also decided to include resistant strains *vps35* and *lem3,* as positive controls.

The supplementation of plates with increased glucose (4%) alone at an extracellular pH of 7.5 did not revert the sensitive phenotype of WT, *vma2* or *trk1* in the presence of edelfosine, but was able to increase the growth in the *lem3* and *vps35* resistant mutants (Figure 3.9). Furthermore, supplementation of plates with glucose (4%), $CuSO_4\ 5H_2O$ (final concentration of 5μM Cu) and $(NH_4)_2Fe(SO_4)_2\ 6H_2O$ (final concentration of 5 μM Fe) showed improved growth in all strains at sub-lethal concentrations of edelfosine (9.5 μM) and increased resistance of *lem3* and *vps35* strains at cytotoxic concentrations of edelfosine (19μM, 38μM) (Figure 3.9).

These results suggest that cells with impaired mechanisms for controlling intracellular pH homeostasis (*vma2*, Pma1-DAmP) are already sensitive to growth at alkaline pH, therein making them even more sensitive to edelfosine treatment. Additionally, the improvement in growth after nutrient supplementation suggests that edelfosine may also be responsible for impairing nutrient uptake at alkaline pH.

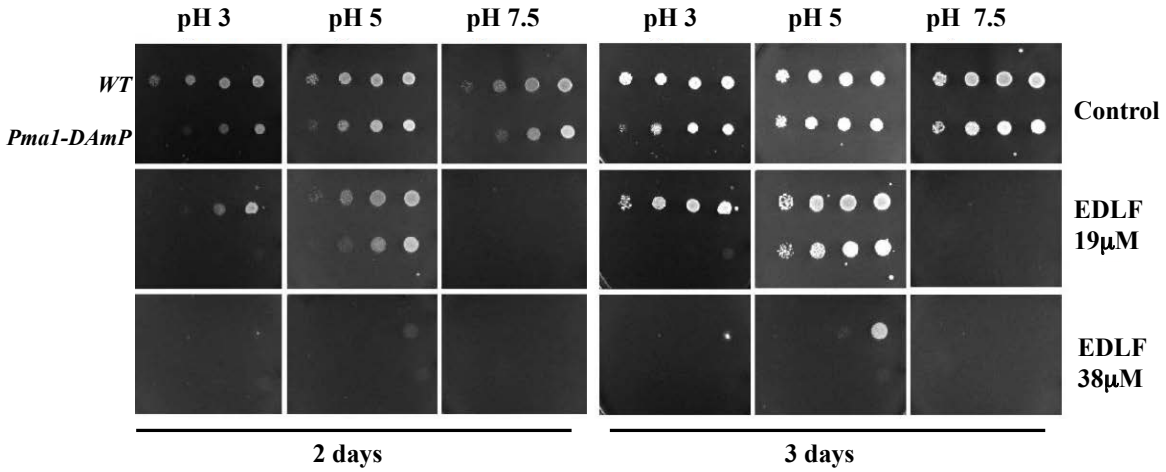

Figure 3.7: Edelfosine sensitivity of *PMA1-DAmP* at various extracellular pH conditions The yeast strain *PMA1-DAmP* and its isogenic wild type were grown to log phase in SD medium (pH 5.2) and then serial diluted onto SD plates of pH = 3, 5 or 7.5 containing the indicated concentrations of edelfosine. Plates were incubated at 30°C for 2-3 days. Data is representative of 3 separate experiments (EDLF = edelfosine).

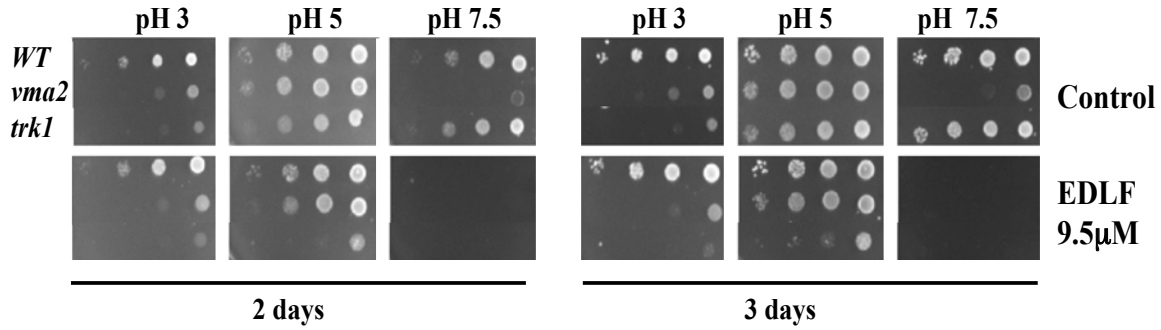

Figure 3.8: Edelfosine sensitivity in hypersensitive mutants at various extracellular pH conditions Sensitive yeast strains representative of different gene clusters, *vma2* (pH homeostasis), *trk1* (ion transport), were grown to log phase in SD medium (pH 5.2) and then serial diluted onto SD plates of pH = 3, 5 or 7.5 containing a sub-lethal concentration (9.5 mM) of edelfosine. Plates were incubated at 30°C for 2-3 days. Data is representative of 2 separate experiments (EDLF = edelfosine).

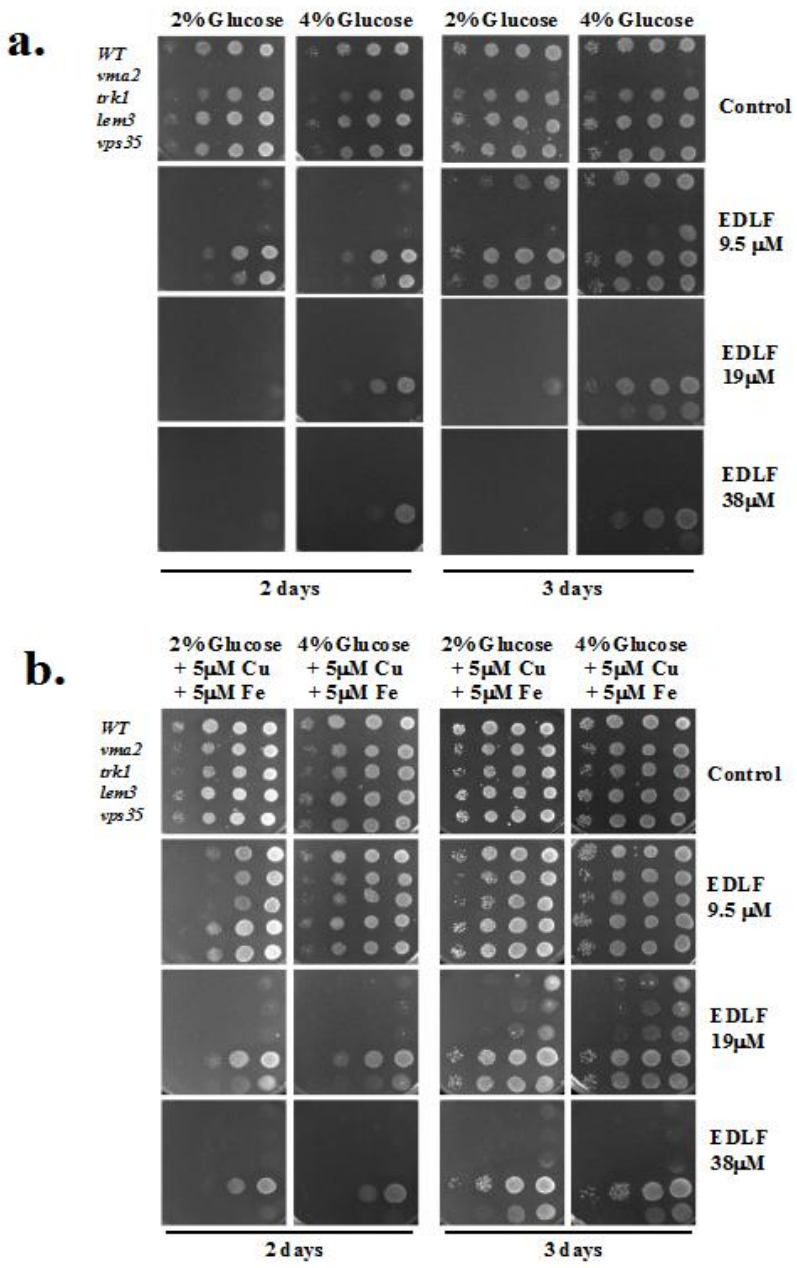

Figure 3.9: Edelfosine sensitivity in plates supplemented with glucose, 5mM Cu^{2+} and 5 mM Fe^{2+} at pH= 7.5 (a) Plates were supplemented with either 2 or 4 % glucose **(b)** Plates were supplemented with 5µM Cu and 5 µM Fe, at either 2 or 4 % glucose. Sensitive mutant strains *vma2* (pH homeostasis), *trk1* (ion transport), and resistant mutant strains were grown to log phase in SD medium (pH 5.2) and then serial diluted onto SD plates of pH = 7.5, with indicated concentrations of edelfosine. Plates were incubated at 30^{o}C for 2-3 days. Data is representative of 2 separate experiments (EDLF = edelfosine).

3.4 Concluding Remarks

The results shown here further highlight the role of intracellular acidification in mediating edelfosine cytotoxicity. We demonstrate that it is the buffering capacity of a cell that dictates how well it handles disturbances in pH homeostasis caused by edelfosine treatment. Therein, cells such as *PMA1-DAmP* and *vma2*, which have impaired mechanisms for controlling pH homeostasis, show hypersensitivity to edelfosine, an effect that is exacerbated when cells are grown in alkaline pH. The ability to alleviate some of edelfosines cytotoxicity by increasing nutrient availability suggests that the drug may also be impeding nutrient uptake in response to pH signaling. In the following chapter we investigate the effect edelfosine has on nutrient PM transporters.

Chapter Four: Edelfosine alters plasma membrane architecture

4.1 Introduction

The yeast PM is laterally compartmentalized into specific micro-domains, and membrane proteins distribute in one of three distinct patterns i) discrete patches, ii) mesh-like (existing between discrete patches) or iii) homogeneously distributed among both (103, 104). Edelfosine interacts with lipid rafts at the PM, which results in the internalization of ergosterol and the essential proton pump Pma1, which is associated with the mesh-like compartment that has received the name of Membrane Compartment of Pma1 (MCP). While Pma1 is the only resident of the MCP compartment, over 20 different PM proteins have been shown to associate instead with the discrete patched Membrane Compartment of Can1 (MCC) named after the arginine transporter, Can1 (103, 104). Since we identified edelfosine uptake to be endocytosis-independent, yet mutants with impaired endocytosis combined with decreased proteolysis in the vacuole (*end4^{ts}pep4Δ*) are edelfosine resistant, we postulated that endocytosis of Pma1 is a key component of edelfosine mediated cytotoxicity (106). Our current model proposes that Pma1 internalization is a consequence of lipid raft disruption by edelfosine. Ergosterol is displaced from the PM and this seems to precede Pma1 internalization (Chapter 5) (107). Since the MCC compartment is even richer in ergosterol than the MCP (104, 105) we wanted to investigate whether edelfosine was also able to cause the internalization of proteins from other PM domains. Using fluorescence microscopy live imaging, we investigated the effect of edelfosine on the localization of several proteins known to be associated with the discrete patch-like MCC domain: arginine transporter Can1, uracil transporter Fur4 and a protein associated with endocytosis, the eisosome marker Sur7. In addition, we also analyzed how edelfosine affects the homogeneously distributed hexose transporters, Hxt1 and Hxt2p (non MCP or MCC proteins).

4.2 Materials and methods

Yeast strains, plasmids and growth conditions

Detailed information on yeast strains and plasmids used is provided in Table 4.1 and 4.2 respectively. Yeast were grown in yeast complex medium (YPD; 1% yeast extract, 2% bacto-peptone and 2% glucose) or in synthetic defined medium (SD; 0.67% yeast nitrogen base without amino acids, 2% glucose), with amino acids supplied to complement strain auxotrophies. For plates, 2% agarose was added to the desired media prior to autoclaving. Growth of cells in liquid media was measured using UV-Vis Spectrophotometer (Shimadzu UV-2450) by optical density at a wavelength of 600nm (OD_{600}). Edelfosine was a kind gift from Medmark Pharma GmbH. A 10 mg/ml stock solution in ethanol was prepared fresh every time and used within two days. The final ethanol concentration in control (ethanol) and edelfosine containing (edelfosine in ethanol) plates never exceeded 0.2%. Growth on control (with ethanol) plates was indistinguishable from that of control plates lacking ethanol. Edelfosine was added after autoclaving and cooling of the media to at least 60 °C.

Table 4.1: List of yeast strains used in this chapter

Strain Name	**Genotype**	**Source**
BY4741 (WT)	*MATa his3 leu2 met15 ura3*	Euroscarf
W303-1a	*MATa ura3-1 his3-11,15 leu2-3,112 trp1-1 ade2-1 can 1-100*	Euroscarf
Sur7-GFP	*W303 Sur7-GFP::HIS3*	(135)
Hxt2-GFP	*W303 Hxt2-GFP::HIS3*	(135)
SEY6210	*MATa ura3-52 leu2-3,112 his3-D100 trp1-D901 lys2-801 suc2- D9*	(103)
Pma1-RFP	SEY6210 *PMA1::tdimer2 (12) ::kanMX4*	(103)
Pma1RFP/Can1GFP	SEY6210 except *PMA1::tdimer2(12):: kanMX4CAN1::GFP::kanMX4*	(103)

Table 4.2: List of plasmids used in this chapter

Plasmid	Description	Source
Fur4-GFP	pRS315 expressing Fur4-GFP from *CUP1* promoter	(136)
Hxt1-GFP	pRS315 expressing Hxt1-GFP from *HXT1* promoter	(136)
Fur4-GFP-DUb	pRS316 expressing Fur4-GFP-Ubp7^{CD} from *CUP1* promoter	(136)
Hxt1-GFP-DUb	pRS316-Hxt1-GFP-Ubp7^{CD} from *HXT1* promoter	(136)

Yeast Transformations

Transformation of yeast cells with plasmids was done following the procedure outlined in Chapter 3.2.

Serial Dilutions

Serial dilutions of Fur4-GFP, Fur4-GFP-DUb , Hxt1-GFP and Hxt1-GFP-DUb were done following the procedure outlined in Chapter 3.2.

Microscopy

Cells carrying plasmids containing *FUR4-GFP, FUR4-GFP-DUb, HXT1-GFP,* or *HXT1-GFP-DUb,* were grown in selective SD media to early log phase and 100μM $CuCl_2$ was added for 2-3 hours, to induce the expression of all genes under the *CUP1* promoter. Although neither *HXT1-GFP,* or *HXT1-GFP-DUB* require copper induction, this was added for consistency. After reaching OD_{600} = 0.1-0.2, cultures were split and cells were either treated with edelfosine (19μM final concentration in 0.1% ethanol) or left untreated (0.1% ethanol) and incubated at 30^{o}C for

one hour. Cells were then concentrated and placed on slabs of solid medium made from LF-YNB and 2% agar. Coverslips were sealed and digital images were obtained using Leica SP5 Confocal Laser Scanning system (Leica, Germany). Fluorescence signals of RFP (excitation 543 nm, HeNe laser) were detected at emission range 565-635 nm, and fluorescence signals of GFP (excitation 488 nm, HeNe laser) were detected at emission range 499-561 nm. Images were aligned using Adobe Photoshop Elements (9.0) software and statistical analysis was done using Graph Pad Prism (5.0). A minimum of 100 cells was quantified for each condition; final quantification was based on 3 independent experiments.

Cell Lysates

Cells were grown to OD_{600} = 0.1-0.2 in defined media, under appropriate conditions. Around 20 OD_{600} cell equivalents were collected, washed and resuspended in 500 μL of TNE buffer [50 mM Tris-HCl, pH 7.4, 150 mM NaCl, 5mM EDTA, protease inhibitor mixture (Roche), 2.5 mg/ml pepstatin, 1 mM phenylmethanesulfonylfluoride]. Cells were then broken using glass beads in a mini bead beater (Biospec) at maximum speed for about one minute at 4^{o}C. In order to remove unbroken cells and debris, samples were spun at 500g for 5 minutes at 4^{o}C. Protein concentration of the samples was determined using the Lowry method (137). Equal amounts of protein, were analyzed by 8% SDS-PAGE and transferred to polyvinylidene difluoride (PVDF) membranes and blots were incubated with antibodies to Pma1 (gift of Ramon Serrano, Universidad Politecnica de Valencia) or to ubiquitin (Invitrogen) and then with horseradish peroxidase-conjugated secondary antibodies, which were detected using enhanced chemiluminescence.

4.3 Results

4.3.1 Edelfosine induces internalization of nutrient transporters

In order to examine protein localization upon edelfosine treatment *in vivo,* we used proteins containing green fluorescent protein (GFP) or red fluorescent protein (RFP) expressed in wild type yeast strains. In all cases, the GFP and RFP were fused to the carboxy-end of each protein, which have been previously shown to yield functional proteins. The list of PM proteins studied is summarized in Table 4.3.

Table 4.3: Plasma membrane proteins studied in this thesis

Protein	Role	Transmembrane Domains	Membrane Compartment
Pma1	Proton pump ATPase (essential)	10	MCP
Can1	Arginine permease	12	MCC
Fur4	Uracil permease	12	MCC
Sur7	Eisosome marker	4	MCC
Hxt1	Low affinity glucose transporter	12	Homogeneous
Hxt2	High affinity glucose transporter	12	Homogeneous

When available, endogenously expressed Pma1-RFP was used as a positive control, as previous results have already confirmed edelfosine treatment induced its internalization (78). We further investigated the effect of edelfosine on proteins localized to the MCC compartment. We first looked at Sur7-GFP, a structural protein of eisosomes known to be involved in endocytosis (135). While edelfosine induced internalization of Pma1 and its accumulation in the vacuole, Sur7p remained associated with the PM in a patch like distribution. (Figure 4.1b). However, closer observation of Sur7p in edelfosine treated cells revealed the formation of larger patches in the form of rings, which were not observed in control cells (Figure 4.1a).

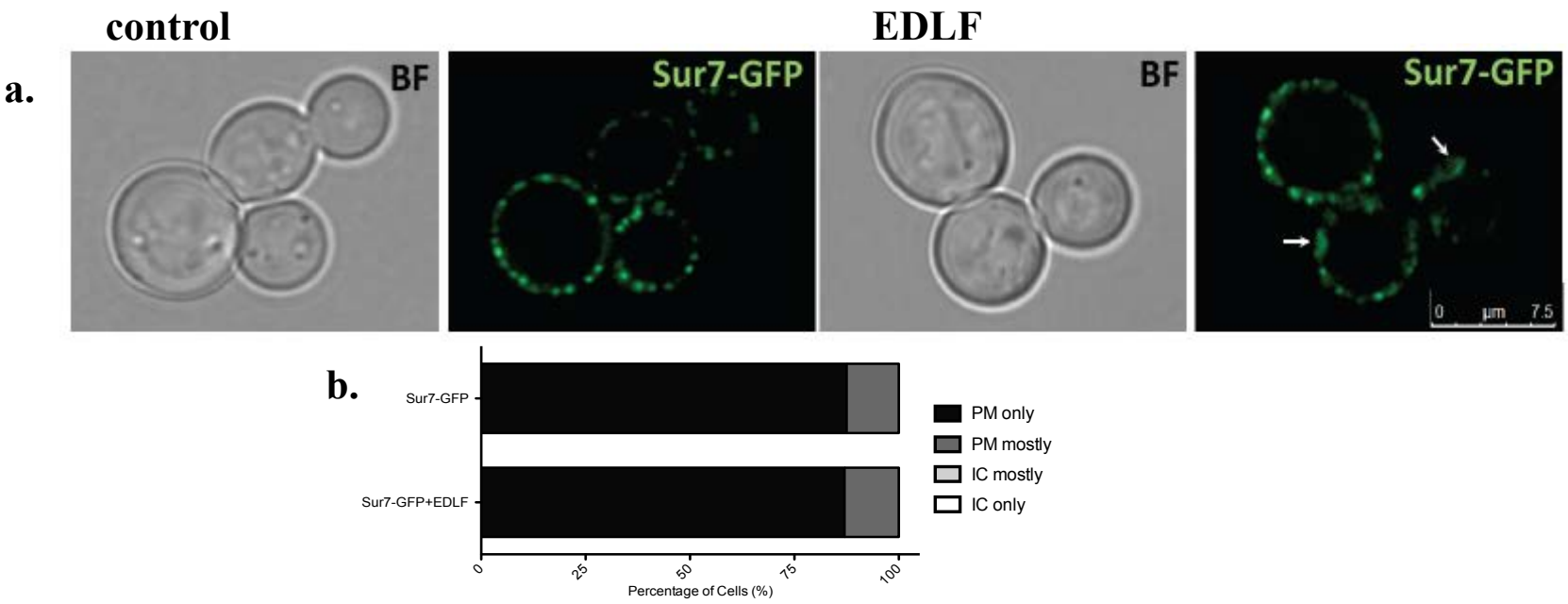

Figure 4.1: Edelfosine does not induce internalization of the MCC resident protein Sur7 (a) Cells with endogenously expressed Sur7-GFP were grown to log phase in the presence of absence of edelfosine (19µM) for 1 hour at 30°C before imaging using confocal microscopy. **(b)** Quantitation of at least 100 cells from each condition (EDLF= edelfosine, PM = plasma membrane, IC = intracellular, BF= brightfield).

We further examined the distribution of two nutrient H^+ symporters, Can1-GFP and Fur4-GFP, known to co-localize with Sur7 in MCC compartments. In contrast to Sur7 and similar to Pma1, edelfosine induced the internalization of Can1-GFP (Figure 4.2) and Fur4-GFP (Figure 4.3) after one hour treatment. It is important to note that while distinct Pma1-RFP domains that did not overlap with either Can1-GFP or Fur4-GFP were observed in control samples, internalized Pma1, Can1 and Fur4 partially co-localized to the vacuole in edelfosine treated ones (Figures 4.2 and 4.3).

Altogether, these results indicate that edelfosine alters the organization of the yeast PM by selectively inducing the internalization of Pma1 as well as the MCC resident nutrient H^+-symporters Can1 and Fur4, but not the structural eisosome protein Sur7p.

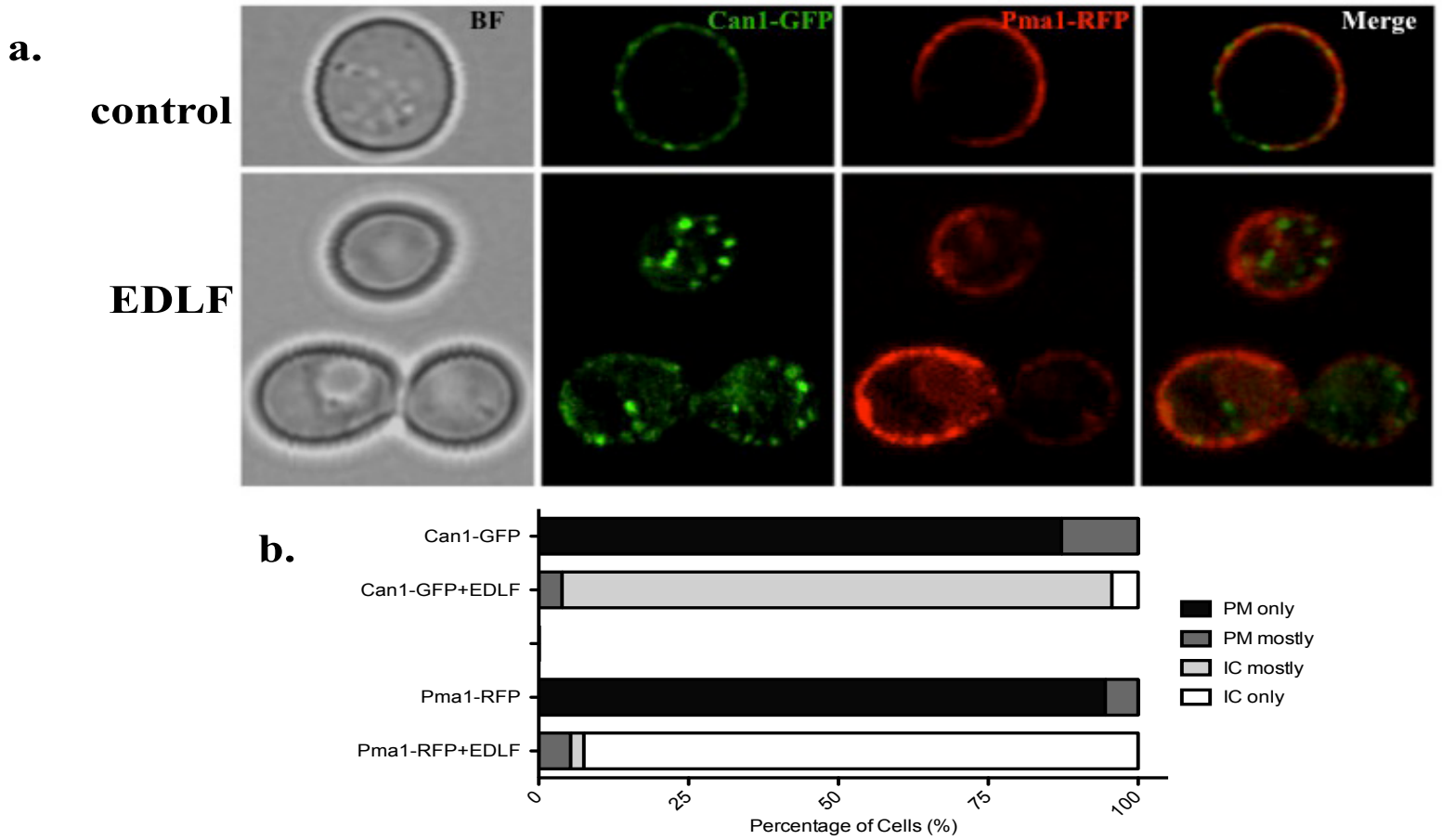

Figure 4.2: Edelfosine induces internalization of the H^+-symporter Can1 of the MCC (a) Cells co-expressing Pma1-RFP and Can1-GFP were grown to log phase in the presence or absence of edelfosine (19μM) for 1 hour at 30°C before imaging using confocal microscopy **(b)** Quantitation of at least 100 cells from each condition (EDLF= edelfosine, PM = plasma membrane, IC = intracellular, BF= brightfield).

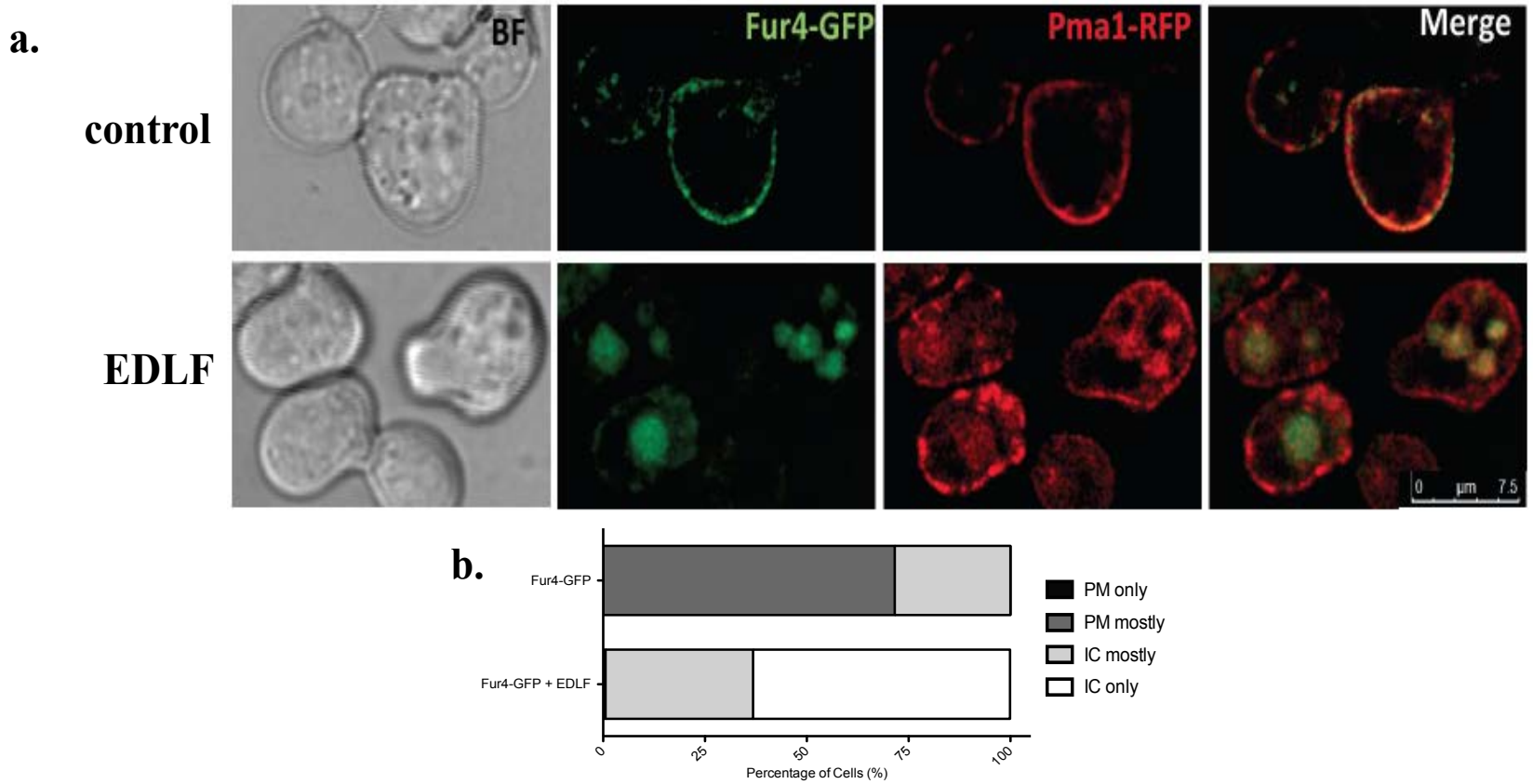

Figure 4.3: Edelfosine induces internalization of the H^+ uracil symporter Fur4 of the MCC (a) Cells co-expressing Pma1-RFP and Fur4-GFP were grown to log phase in the presence or absence of edelfosine (19µM) for 1 hour at 30°C before imaging using confocal microscopy **(b)** Quantitation of at least 100 cells from each condition (EDLF= edelfosine, PM = plasma membrane, IC = intracellular, BF= brightfield).

Finally, we also investigated the effect of edelfosine on two glucose transporters that are homogeneously distributed within both MCP and MCC domains (103). Edelfosine caused the internalization of the low affinity hexose transporter, Hxt1-GFP (Figure 4.4 b,c) and the high affinity hexose transporter, Hxt2-GFP from the PM (Figure 4.4 a,c), although the effect was stronger in the case of Hxt1.

These results indicate that edelfosine causes the alteration of the yeast PM by internalization of proteins from the MCP domain: Pma1, the MCC domain: Fur4, Can1 and homogeneously distributed proteins: Hxt1 and Hxt2. However, since edelfosine did not cause the internalization of Sur7, this suggests that PM protein internalization induced by edelfosine is not global but rather selective.

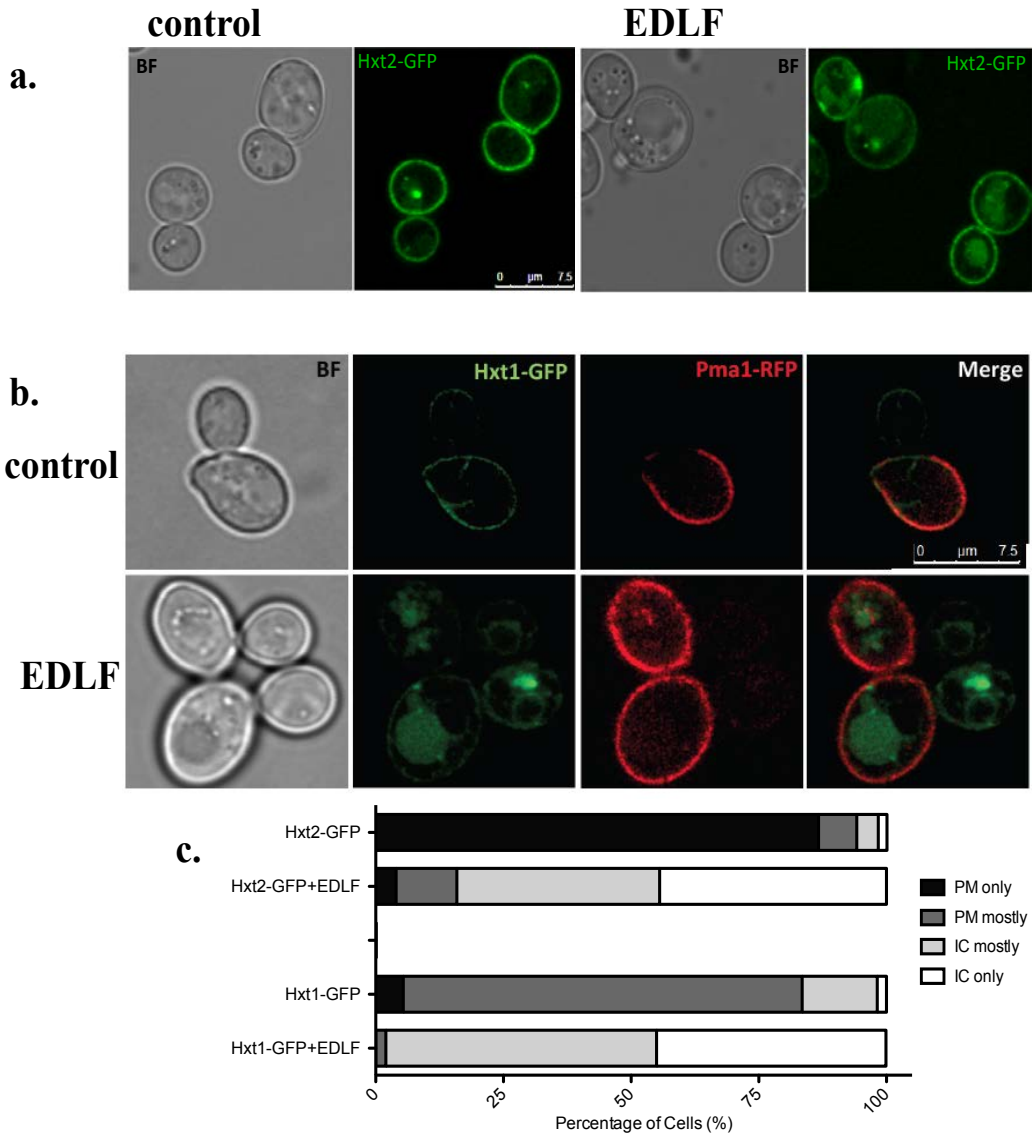

Figure 4.4: Edelfosine induces internalization of the hexose transporters Hxt1 and Hxt2 (a) Cells with endogenously expressed Hxt2-GFP and **(b)** cells co-expressing Pma1-RFP and Fur4-GFP were grown to log phase in the presence or absence of edelfosine (19µM) for 1 hour at 30^{o}C before imaging using confocal microscopy. **(c)** Quantitation of at least 100 cells from each condition (EDLF= edelfosine, PM = plasma membrane, IC = intracellular, BF= brightfield).

4.3.2 Ubiquitination mediates edelfosine-induced internalization of nutrient transporters

Endocytosis-mediated internalization and subsequent vacuolar degradation of PM proteins often requires protein ubiquitination (5). In accordance to this, the resistance screen also identified mutants with deficient ubiquitin pools (*doa4Δ*), E3-ubiquitin ligase adaptor proteins as well as mutants of pathways that recognize ubiquitinated cargo like the ESCRT and retromer systems to be edelfosine resistant (5). Interestingly, a Pma1 mutant (*pma1-7*) that fails to associate with sphingolipid and ergosterol-rich membrane microdomains en route to the PM is known to be targeted to the endosomal/ vacuolar system (138) in a ubiquitin-dependent process (139). Since the effect of edelfosine resembles that of the *pma1-7* mutant, the effect of edelfosine on Pma1 ubiquitination was investigated. When cell extracts were immunoprecipitated with protein A-Sepharose beads coupled to an antibody against Pma1, an extra band with a molecular weight ~8 kDa higher than the Pma1 band from untreated cells was observed at early time points (1-2 hours) (Fig. 4.5a). This is compatible with a mono-ubiquitination signal and was further supported by the immunoprecipitation of ubiquitinated proteins followed by western blot using an anti-Pma1 antibody (Figure 4.5b). Here, ubiquitinated Pma1 was readily detected after drug treatment, whereas it was absent in untreated cells (Figure 4.5b). Since ubiquitination is required for the internalization of most membrane proteins in yeast, including nutrient transporters (140), we determined whether ubiquitin-mediated endocytosis was essential for protein internalization in cells treated with edelfosine.

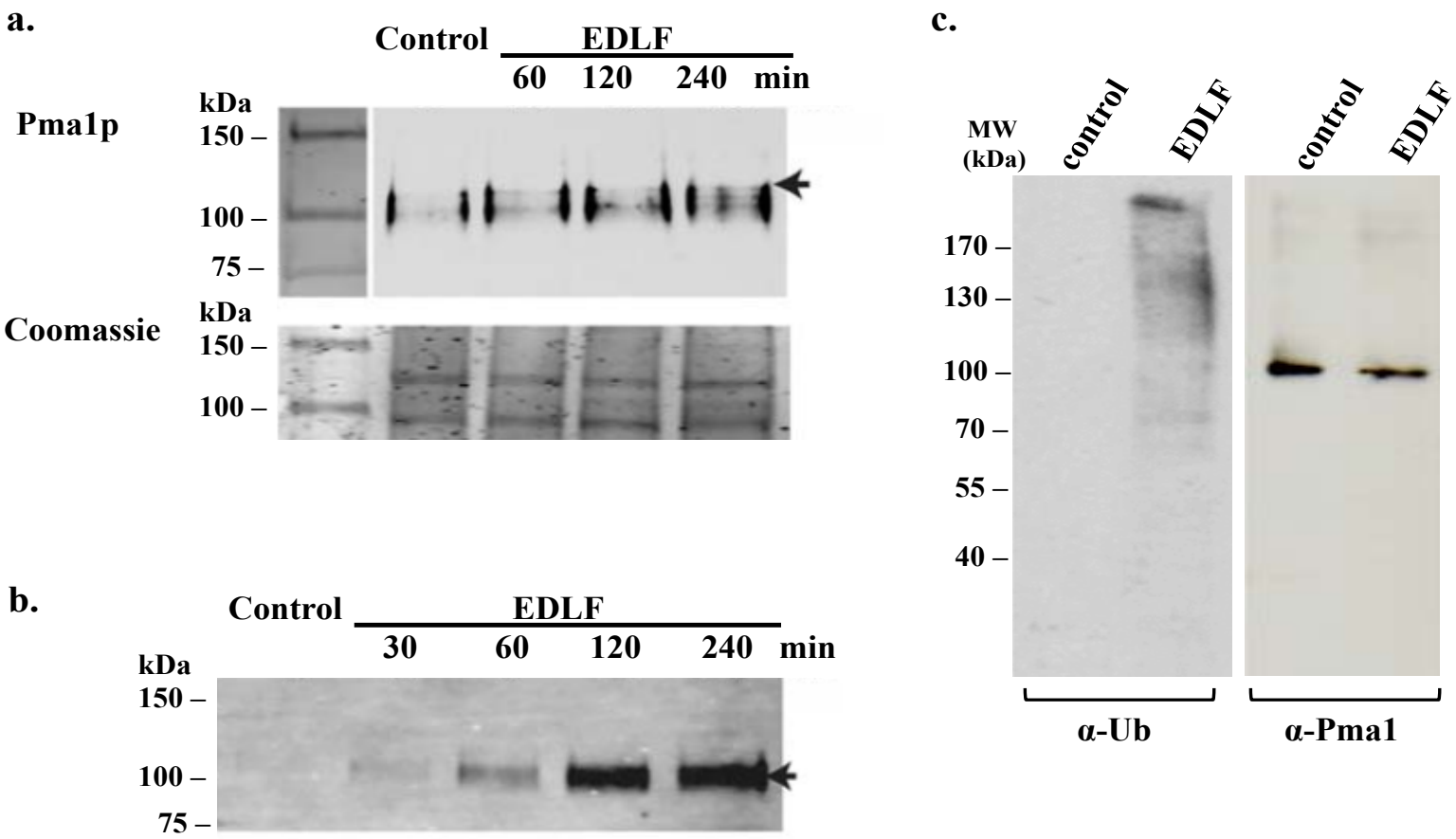

Figure 4.5: Edelfosine induces Pma1 ubiquitination (a) Pma1 immunoprecipitation allows for detection of a discrete band ~ 8KDa larger than Pma1 (arrow) when treated with edelfosine. Coomassie stained gels are below as loading controls **(b)** Western blot for Pma1 after immunoprecipitation of total ubiquitinated proteins **(c)** Western blots of cell lysates of wild type cells grown in absence or presence of edelfosine (19 μM) blotted against ubiquitin (left panel) or Pma1 (right panel) (EDLF= edelfosine) [**(a)** and **(b)** done by Dr. Mollinedo; **(c)** done by Ola Czyz].

First, an analysis of total cell lysates treated with edelfosine indicated that Pma1 was not the only protein being ubiquitinated (Figure 4.5c). We then expressed Fur4p-GFP fused to the catalytic domain of the deubiquitinating peptidase Ubp7p (DUb) which has been shown to be a constitutive non-ubiquitinatable form of Fur4p (136). These cells were also expressing Pma1-RFP to allow for co-localization studies (Figure 4.6a). In contrast to Pma1-RFP and Fur4p-GFP the presence of the DUb catalytic domain abolished Fur4p internalization induced by edelfosine. Similar results were obtained for the glucose transporter Hxt1 (Figure 4.6b).

Although the addition of the de-ubiquitinase domain enabled Fur4 and Hxt1 to remain at the PM, their distribution pattern was altered, and became patchier. A similar pattern was observed for the Pma1-RFP. Interestingly, the retention of either of these transporters at the PM was unable to revert the cytotoxic effect of edelfosine (Figure 4.7). These results indicate that the internalization of nutrient transporters, represented here by Fur4p and Hxt1, is in fact mediated by edelfosine-induced ubiquitination.

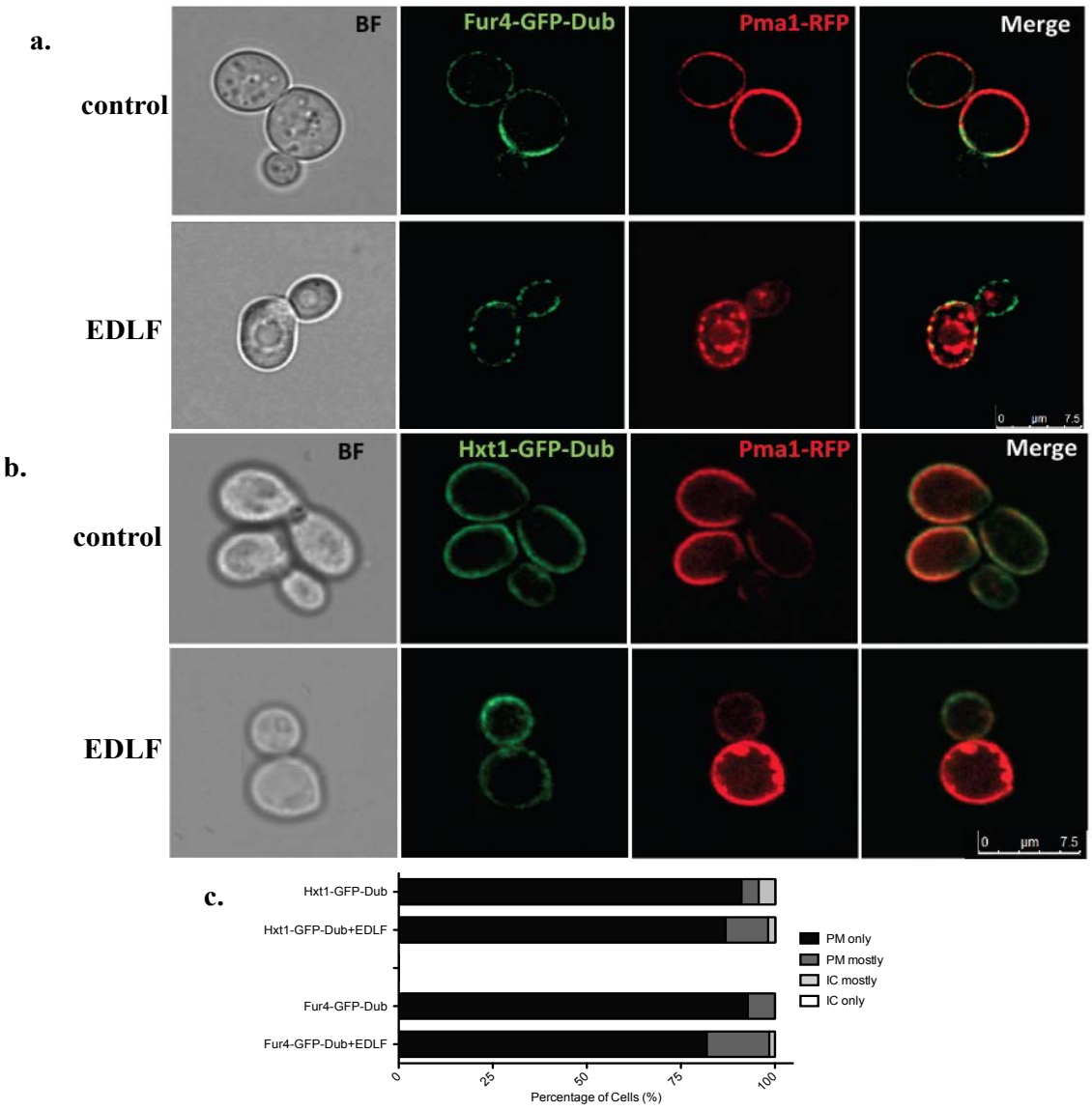

Figure 4.6: Ubiquitination mediates internalization of Fur4 and Hxt1 induced by edelfsoine **(a)** Cells co-expressing Pma1-RFP and Hxt1-GFP-DUb or Fur4-GFP-DUb **(b)** were grown to log phase in the presence or absence of edelfosine (19μM) for 1 hour at 30°C before imaging using confocal microscopy. **(c)** Quantitation of at least 100 cells from each condition (EDLF= edelfosine, PM = plasma membrane, IC = intracellular, BF= brightfield).

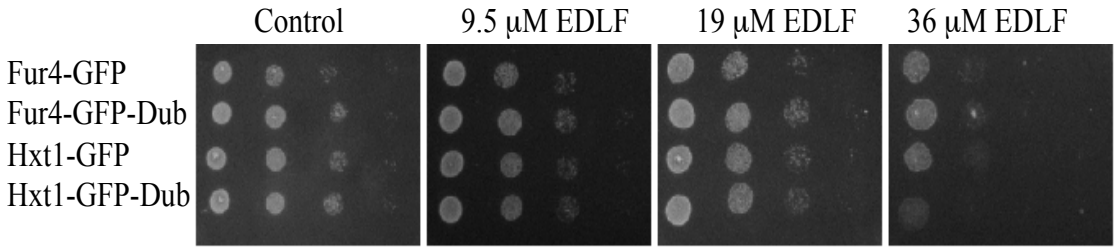

Figure 4.7: Edelfosine sensitivity of cells carrying Fur4-DUb or Hxt1-DUb Cells were grown to mid-log phase in defined media to maintain plasmids and serial diluted on control or edelfosine containing plates. Plates were incubated at 30^{o}C for 2 days (EDLF= edelfosine).

4.4 Concluding Remarks

The results presented here further demonstrate that edelfosine alters lateral organization of the PM by inducing internalization of not only Pma1 but also nutrient transporters, Fur4, Can1, Hxt1 and Hxt2 from membrane micro-domains. However, edelfosine did not induce the internalization of the structural protein, Sur7 but did alter its distribution pattern, indicating that protein internalization from the PM is a selective process. Following this, it was observed that edelfosine increased overall ubiquitination levels of proteins, and that edelfosine-mediated ubiquitination was required for the endocytosis of PM transporters. Therein, edelfosine causes the mis-localization of PM proteins and induces their internalization by stimulating protein ubiquitination. In obtaining a greater understanding of the way in which edelfosine alters PM organization, we wanted to see whether the same effects were seen in other members of the ATL family. In the following chapter we begin to look at the mode of action of the second generation of ATLs miltefosine and perifosine in yeast.

Chapter Five: Effects of second-generation antitumor lipids on plasma membrane organization

5.1 Introduction

It is evident that membrane re-organization and intracellular acidification play a detrimental role, eliciting the cytotoxic effect of edelfosine. By expanding research to members of the second generation of ATLs, it becomes possible to not only test the relevance of the internalization of Pma1, sterols and intracellular acidification on drug cytotoxicity but provide a greater insight into the mode of action for this entire drug family. Currently, there is no available data demonstrating whether the other members of this drug family, miltefosine, perifosine, and erucylphosphocholine are also able to affect lipid raft integrity.

Edelfosine is cytotoxic to yeast cells at concentrations similar to those used in cancer cells. As minimal work had been done with yeast and the other ATLs, our first course of action was to determine their minimal inhibitory concentrations (MIC), establish if their effect was cytostatic or cytotoxic and investigate if they were able to affect PM lateral domain organization in a way similar to edelfosine.

5.2 Materials and Methods

Yeast strains, plasmids and growth conditions

Detailed information on yeast strains used is provided in Table 5.1. Yeast were grown in yeast complex medium (YPD; 1% yeast extract, 2% bacto-peptone and 2% glucose) For plates, 2% agarose was added to the desired media prior to autoclaving. Growth of cells in liquid media was measured using UV-Vis Spectrophotometer (Shimadzu UV-2450) by optical density at a wavelength of 600nm (OD_{600}). Edelfosine was a kind gift from Medmark Pharma GmbH,

perifosine and erucylphosphocholine were provided by ÆEterna Zentaris and miltefosine was commercially available from Cayman Chemical Company. Fresh drug stocks were prepared prior to each experiment using absolute ethanol to obtain final stock concentrations of 19 mM for edelfosine, 10 mM for perifosine, 10 mM for miltefosine and 10mM for erucylphosphocholine.

Table 5.1: List of yeast strains used in this chapter

Strain Name	**Genotype**	**Source**
BY4741	*MATa his3 leu2 met15 ura3*	Euroscarf
Pma1-RFP	SEY6210 *PMA1::tdimer2 (12) ::kanMX4*	(103)
Pma1RFP/Can1GFP	SEY6210 except *PMA1::tdimer2(12)::kanMX4CAN1::GFP::kanMX4*	(103)

Minimal inhibitory concentration and cell viability

Wild type (BY4741) cells were grown to OD_{600} = 0.1 in YPD at 30^{o}C. From this culture, aliquots were treated with ethanol (control) or with the indicated concentrations of edelfosine, miltefosine, perifosine or erucylphosphocholine. Growth was measured by optical density at a wavelength of 600nm (OD_{600}) hourly for 8 hours and after an overnight incubation (18 hours). Additionally, aliquots were removed at the indicated time points and cells counted using a hemacytometer. Two hundred cells were then plated onto rich media (YPD) to assess cellular viability. Experiments were performed in triplicate and repeated at least twice. For viability experiments, plates were incubated at 30^{o}C for three days, colonies counted, and results expressed in percentages relative to control plates.

Microscopy

Strains Pma1-RFP, Pma1-RFP/Can1-GFP were grown in YPD media**.** After reaching OD_{600} = 0.1-0.2, cultures were split and cells were either treated with edelfosine (19mM final concentration in 0.1% ethanol), miltefosine (8μM final concentration in 0.1% ethanol), perifosine (4 μM final concentration in 0.1% ethanol) or left untreated (0.1% ethanol) and incubated at 30^{o}C for one hour. Cells were then concentrated and placed on slabs of solid medium made from LF-YNB and 2% agarose (refer to Chapter 4.2) Coverslips were sealed and digital images were obtained using Leica SP5 Confocal Laser Scanning system (Leica, Germany). Fluorescence signals of RFP (excitation 543 nm, HeNe laser) were detected at emission range 565-635 nm, and fluorescence signals of GFP (excitation 488 nm, HeNe laser) were detected at emission range 499-561 nm. Images were aligned using Adobe Photoshop 7.0 software and statistical analysis was done using Graph Pad Prism 5.0.

Detergent resistant membrane isolation, western blots, silver stains

Wild type (BY4741) cells were grown to OD_{600} = 0.1 in YPD at 30^{o}C. After reaching OD_{600} = 0.1-0.2, cultures were split and cells were either treated with edelfosine (19μM final concentration in 0.1% ethanol), miltefosine (8 μM final concentration in 0.1% ethanol), perifosine (4 μM final concentration in 0.1% ethanol) or left untreated (0.1% ethanol) and incubated at 30^{o}C for one hour. Yeast DRM's were isolated following the method previously described by Zaremberg *et al.* 2005 (78). Approximately 20 OD_{600} cell equivalents were collected from each treatment. Cells were washed and resuspended in 500 μL of TNE buffer [50 mM Tris-HCl, pH 7.4, 150 mM NaCl, 5mM EDTA, protease inhibitor mixture (Roche), 2.5 mg/ml pepstatin, 1 mM phenylmethanesulfonylfluoride]. Cells were then broken using glass

beads in a mini bead beater (Biospec) at maximum speed for about one minute at 4°C. In order to remove unbroken cells and debris, samples were spun at 500g for 5 minutes at 4°C. Protein concentration of the samples was determined using the Lowry method (137) and 200-300 μg of protein in 500 mL of TNE buffer was incubated with Triton X-100 (1% final concentration, Pierce) for 30 minutes on ice. Afterwards, 1 ml of 60% Optiprep (Axis-Shield PoC AS) was added to the lysate to obtain a final concentration of 40% Optiprep. This solution was overlayed with 2.4 ml of 30% Optiprep in TXNE (TNE with 0.1% Triton X 100) and subsequently with 400 mL of 0.1% TXNE.

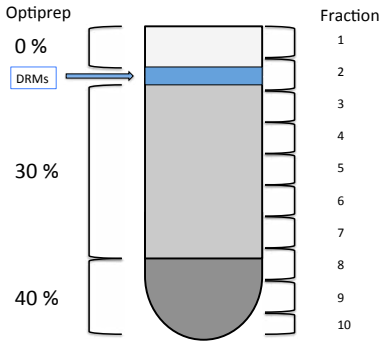

Figure 5.1: Schematic demonstrating DRM isolation fractions Concentrations of Optiprep are shown on the left, and the interface between 0 and 30% (blue) indicates DRMs. Right hand side depicts fractions taken out post centrifugation.

Samples were then centrifuged at 166 000 g for 2 hours in a swinging bucket TLS55 rotor (Beckman). Ten or twelve fractions were collected from the top of the gradient, however Fraction 2 always corresponded to DRMs. The interface between the 0 and 30% Optiprep contained a layer of DRMs and was easily identified and collected as Fraction 2. Aliquots of each fraction were analyzed by 8% SDS-PAGE, followed by silver staining or western blot as indicated. Proteins were transferred to polyvinylidene difluoride (PVDF) membranes and blots were incubated with antibodies to Pma1 (gift of Ramon Serrano, Universidad Politecnica de

Valencia) or 3-phosphoglycerate (Pgk1) as a loading control (Molecular Probes). Pgk1 is highly abundant in the cytosol as it catalyzes the transfer of phosphoryl groups from 1,3-bisphosphoglycerate to ADP to produce ATP in glycolysis. Blots were further incubated with horseradish peroxidase-conjugated secondary antibodies, and signals were detected using enhanced chemiluminescence. Once developed, images were scanned and Image J was used for densitometric analysis.

Lipid Extractions

Lipid extracts were obtained using a modified Folch's extraction protocol adapted for yeast (141). Briefly, approximately 20 OD_{600} of cells were concentrated by centrifugation at 2500 g for 5min. Cells were washed twice with cold 1M sorbitol, transferred to screw cap tubes, following re-suspension in 1ml $CHCl_3/CH_3OH$ (1:1, v/v). Fifty micrograms of phosphatidyldimethylethanolamine (PDME) was added to each sample to be used as internal standard followed by 0.5 mm acid-washed glass beads (~ 1/8 volume of the liquid). Cells were homogenized for 1 min at 4°C using a mini bead beater (BioSpec). Samples were then transferred to test tubes using a glass Pasteur pipette. The beads were washed with 1ml) $CHCl_3/CH_3OH$ (2:1, v/v), and the supernatant was combined with the corresponding cell extract. Lipids were extracted by sequential additions of 0.5 ml $CHCl_3/CH_3OH$ (2:1, v/v), 0.5ml $CHCl_3$ and 1.5ml of water. After vortexing well phases were separated by centrifugation at 2500 g for 10 min at room temperature. The aqueous (top) phase and the interphase containing proteins were aspirated off. The organic phase was transferred to a clean test tube using a 1 ml Hamilton syringe and washed twice with 2.5 ml of artificial upper phase $CHCl_3/CH_3OH/H_2O$ (3:48:47

v/v/v). The organic phase of eight independent replicates were combined at the end. Samples were dried in glass vials under Argon gas and weighed to determine the lipid mass obtained.

Lipid Analysis Protocol

Based on the obtained weights, each sample was re-dissolved in $CHCl_3$/isooctane (1:1 v/v) to give a final concentration of 1μg lipid/μl. The samples were then transferred to high-performance-liquid-chromatography (HPLC) vials (Agilent), and stored at -20^{o}C. Samples were analyzed by HPLC using an Agilent 1100 series equipped with a quaternary pump and an evaporative light-scattering detector (Alltech ELSD 2000). The column used was an Onyx monolithic silica (Phenomenex). The solvent system used consisted of: solvent A: isooctane:ethylacetate (99.8:0.2); solvent B: acetone:ethylacetate (2:1) with 0.02% acetic acid; solvent C: isopropanol:water (85:15) with acetic acid and ethanolamine each at 0.05%. The gas flow was 3.0 L/min and drift tube temperature was set at 60^{o}C. Retention peaks were analyzed using Agilent Chemstation software and quantified using calibration curves prepared with commercial lipid standards (Sigma, Avanti Polar Lipids).

5.3. Results

5.3.1. Growth inhibitory effect of miltefosine, perifosine and erucylphosphocholine in yeast

We determined the minimal inhibitory concentration (MIC) for the different ATLs: miltefosine, perifosine and erucylphosphocholine using wild type (BY4741) cells grown in rich medium. Edelfosine (19 μM) was used as reference point. We found both miltefosine and perifosine to be more potent than edelfosine while ErPC did not inhibit growth of yeast in the micromolar range.

Miltefosine

While the MIC for miltefosine was 4mM, this concentration had a cytostatic effect, as viability assays done in parallel with the growth curves showed that cells treated with 4 μM miltefosine for up to 4 hours were viable when miltefosine was removed (Figure 5.2). On the other hand, a 10 μM concentration of miltefosine displayed a cytotoxic effect as yeast cells lost viability under this condition (Figure 5.2).

Perifosine

The MIC for perifosine was 3μM, but this concentration was cytostatic as yeast growth was inhibited but the cells remained viable (Figure 5.3). On the other hand, a 12μM concentration of perifosine displayed a cytotoxic effect as yeast cells lost viability under this condition (Figure 5.3).

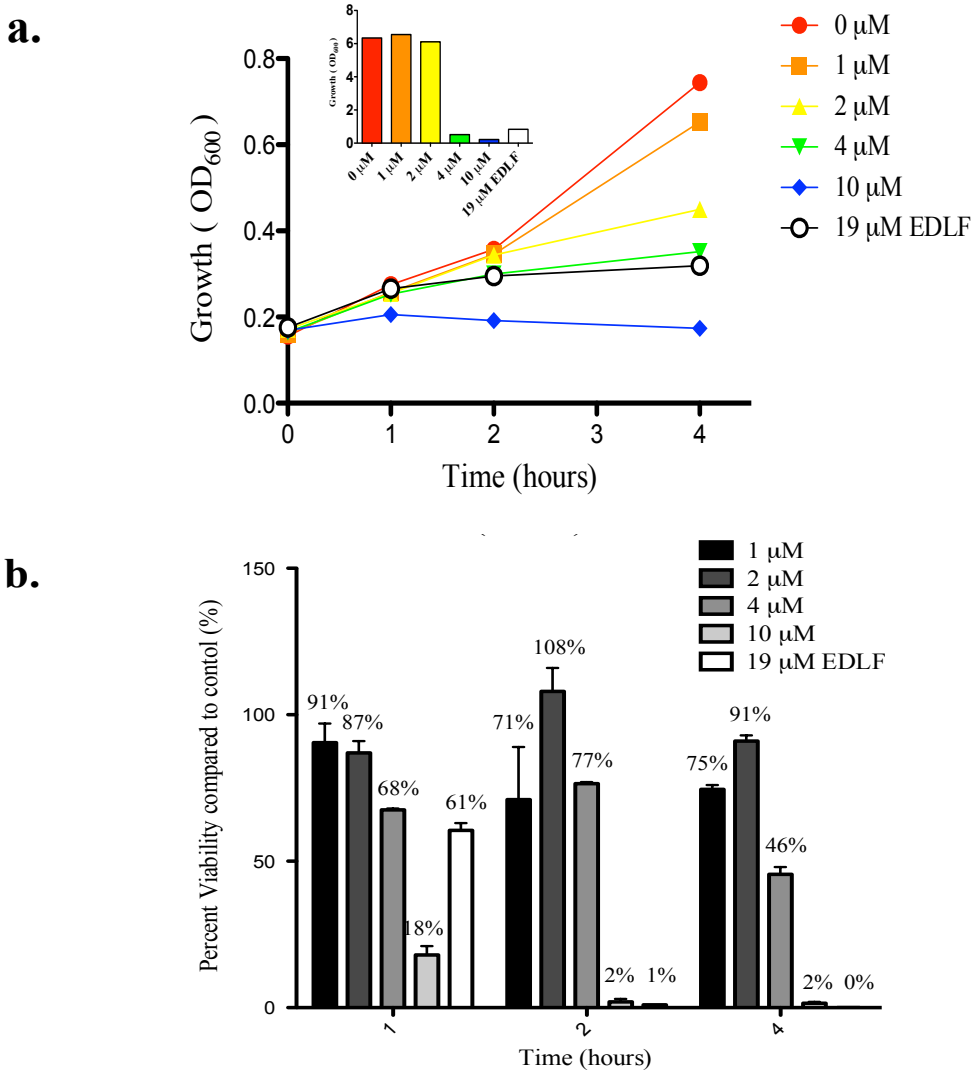

Figure 5.2: Growth curves and corresponding viability assays for miltefosine treated cells **(a)** Cells grown in rich medium to early log phase were treated with the indicated concentrations of miltefosine or edelfosine and growth was monitored over 4 hours. The inset displays overnight growth reached for each condition **(b)** To determine cell viability, equal amounts of cells were plated at the indicated time points onto rich medium plates in the absence of drug. Plates were incubated for 3 days at 30 °C, colonies were counted, and results expressed as percentage of control plates.

a.

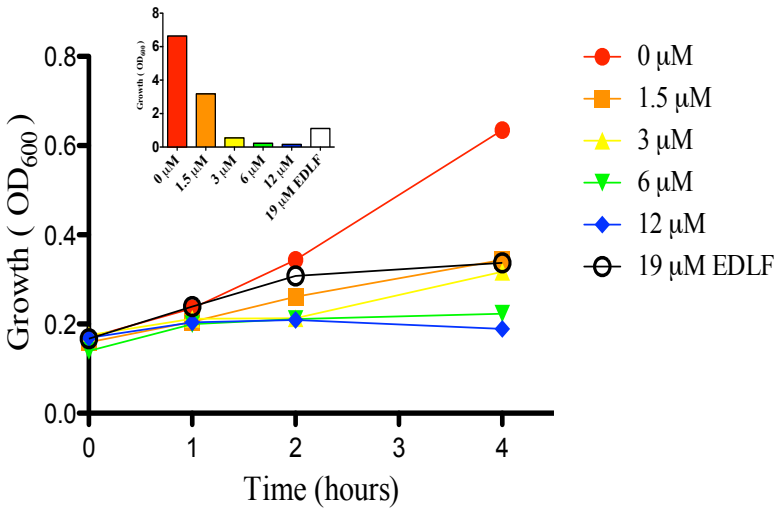

b.

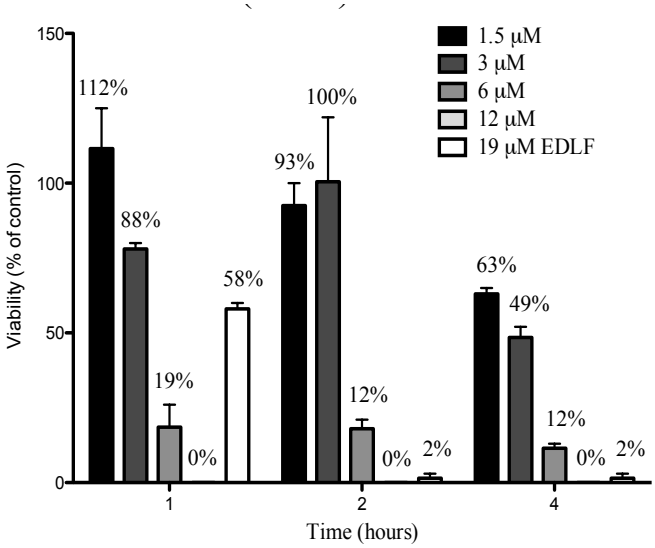

Figure 5.3: Growth curves and corresponding viability assays for perifosine treated cells **(a)** Cells grown in rich medium to early log phase were treated with the indicated concentration of perifosine or edelfosine and growth was monitored over 4 hours. The inset displays overnight growth reached for each condition **(b)** To determine cell viability, equal amounts of cells were plated at the indicated time points onto rich medium plates in the absence of drug. Plates were incubated for 3 days at 30 °C, colonies were counted, and results expressed as percentage of control plates.

Erucylphosphocholine

In a first attempt to determine the MIC of erucylphosphocholine we used a similar concentration range to that investigated for other ATLs. Surprisingly, growth was not inhibited up to concentrations of 10 μM (Figure 5.4a). Therefore concentrations were increased up to 800 μM due to limiting amount of drug. Cells treated with > 400μM erucylphosphocholine were able to partially inhibit yeast growth (Figure 5.4b). Due to the possibility of erucylphosphocholine having a detergent effect at the high concentrations necessary to inhibit growth this drug was eliminated from subsequent investigations.

Table 5.2: Cytostatic and cytotoxic (MIC) concentrations of ATL's

Drug	**Cytostatic effect (μM)**	**Cytotoxic Concentration (μM)**
Edelfosine	-	19
Miltefosine	4	10
Perifosine	3	12
Erucylphosphocholine	> 500 μM	> 500 μM

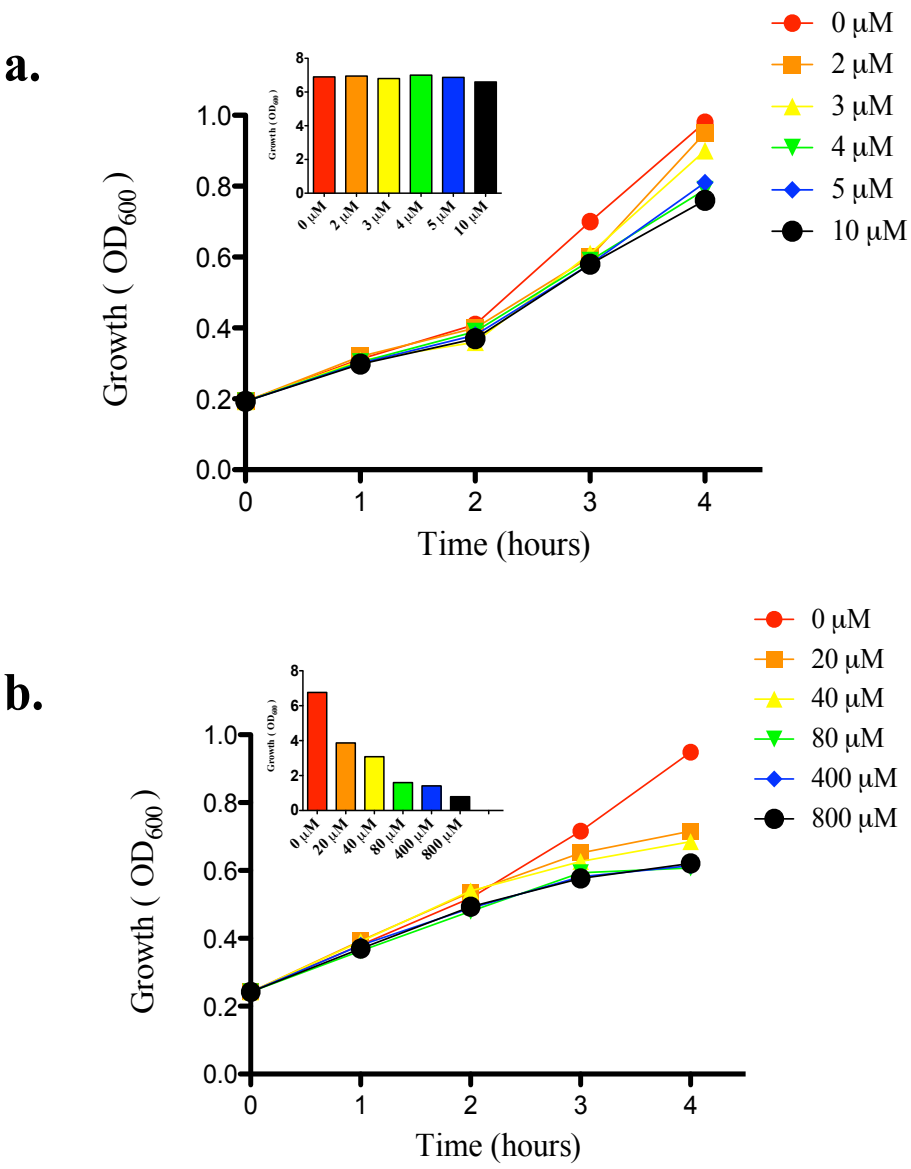

Figure 5.4: Growth curves for erucylphosphocholine treated cells Cells grown in rich medium to early log phase were treated with the indicated concentration of erucylphosphocholine and growth was monitored over 4 hours. The inset displays overnight growth reached for each condition **(a)** Low range concentrations were tested first **(b)** the concentration range was then expanded to 800 µM.

5.3.2 Miltefosine and perifosine induce internalization of Pma1 and Can1

In order to determine whether miltefosine and perifosine had similar modes of action to edelfosine, we wanted to see the effect that these ATLs would have on the localization of the essential proton pump, Pma1. We used cells expressing Pma1-RFP and Can1-GFP at endogenous levels to study the effect of these ATLs *in vivo*, using live imaging confocal microscopy. Miltefosine and perifosine were able to induce Pma1-RFP and Can1-GFP internalization in as early as 15 minutes after drug treatment, comparable to edelfosine (Figure 5.5). Interestingly, no co-localization was observed between these proteins during internalization, suggesting they may follow different endocytic pathways. We completed these investigations by analyzing the levels of Pma1 associated with DRMs upon treatment with miltefosine and perifosine. Results showed that Pma1 association with DRMs decrease upon treatment with miltefosine and perifosine in a similar manner to that displayed by cells treated with edelfosine (Figure 5.6). These results suggested that the ATLs may share a common mechanism of action.

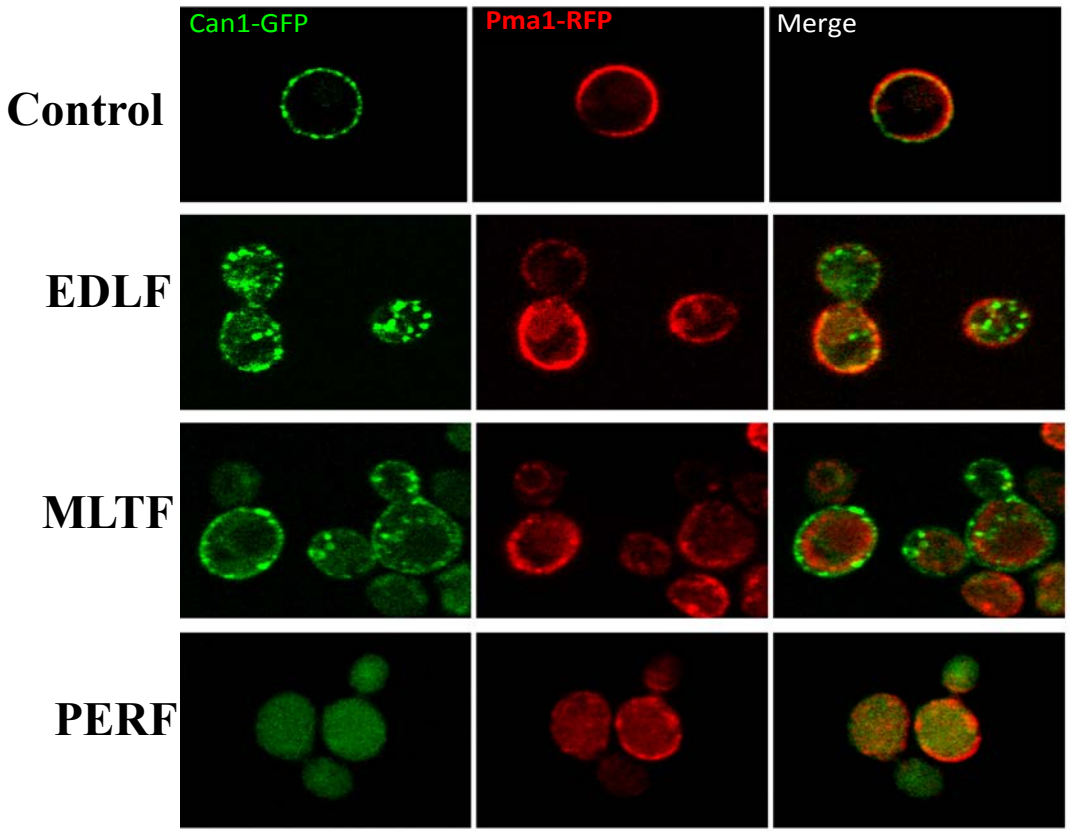

Figure 5.5: Localization of essential proton pump Pma1 (MCP) and H^+ arginine symporter Can1 (MCC) after ATL treatment. Cells co-expressing Pma1-RFP and Can1-GFP were grown to early log phase in defined media and then treated with edelfosine (19μM), miltefosine (8 μM), or perifosine (4μM) for 15 minutes at 30°C. Cells were imaged live using confocal microscopy. Images are representative of one independent experiment performed twice (EDLF= edelfosine, MLTF= miltefosine, PERF = perifosine).

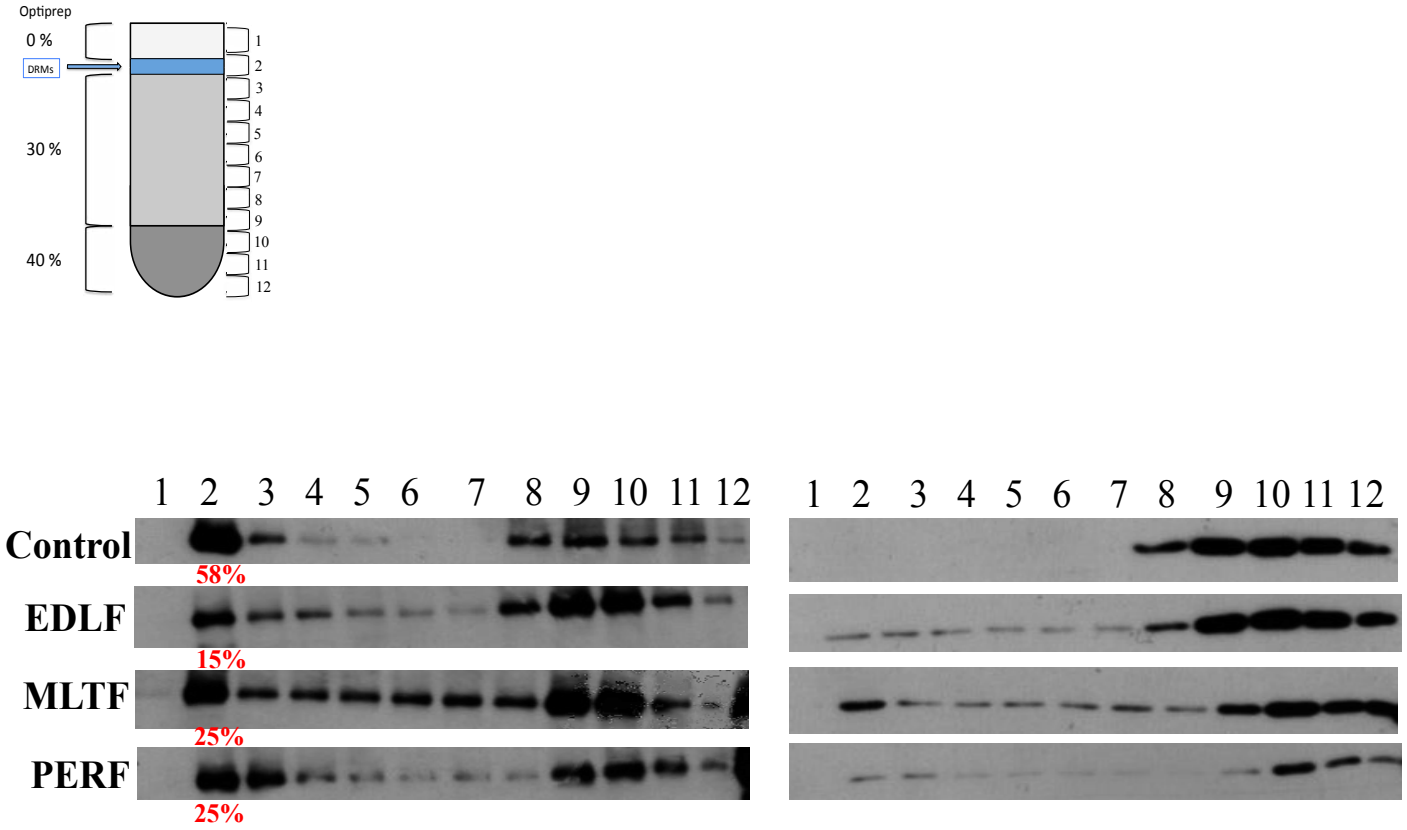

Figure 5.6: ATLs displace Pma1 from detergent resistant membranes Wild type (BY4741) cells were grown to early log phase in rich media at 30°C and t treated with edelfosine (19 μM), miltefosine (8 μM) or perifosine (4μM) for 1 hour. DRMs were then prepared as indicated in Materials and Methods **(a)** Western blot against Pma1 **(b)** Same western blot showing loading control Pgk1. Percentages of Pma1 associated with Fraction 2 (containing DRMs) were determined by densitometry using ImageJ (EDLF= edelfosine, MLTF= miltefosine, PERF = perifosine).

5.3.3 Lipid profiles of cells treated with different antitumor lipids

Finally, we wanted to determine how ATLs affected total cell lipid composition. We treated cells for one hour with cytotoxic concentrations of edelfosine, miltefosine and perifosine and extracted lipids using a modified Folch's protocol adapted for yeast. Lipids were then analyzed by high performance liquid chromatography (HPLC) and retention times were compared to a set of available standards. Prior to extraction we added a known amount of an internal standard to each sample, to assess the efficiency of the extraction protocol. This also allowed us to normalize the results despite variations in the efficiency of the extraction between samples. Analysis of the data was limited to major lipid species, and although preliminary, general trends indicated that treatment with ATLs decreased the levels of phosphatidylcholine, as well as those of the neutral lipids sterol esters and triacylglycerides. Interestingly ergosterol levels remained unchanged (Figure 5.7).

The effect of ATLs on neutral lipid metabolism seemed to be highly reproducible and represents a novel aspect of the response of cells to ATL treatment worth further investigation.

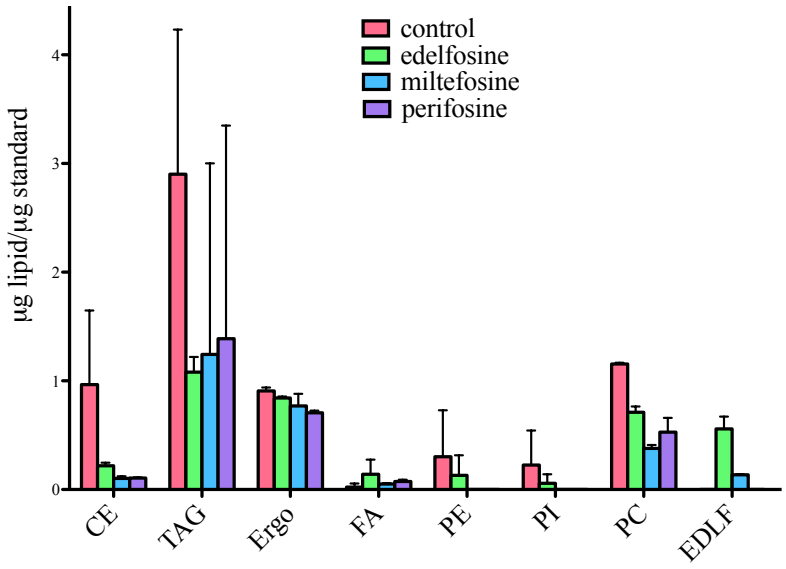

Figure 5.7: Comparison of lipid profiles from lipid extracts of cells treated with ATLs Cells were grown in rich media to early log phase and treated with edelfosine (19µM), miltefosine (8µM) and perifosine (4µM) for 2 hours. Lipids were extracted using the modified Folch's method described in Materials and Methods. Equal mass of lipids for each sample was analyzed by HPLC. Lipids were identified based on retention times of available standards (CE = cholesteryl esters, TAG = triacylglycerides, Ergo = ergosterol, FA = free fatty acids, PE = phosphatidylethanolamine, PI= phosphatidylinositol, PC= phosphatidylcholine, EDLF= edelfosine).

5.4 Concluding remarks

The second generation ATLs miltefosine and perifosine showed to be more potent towards yeast than edelfosine, as they were cytotoxic at lower drug concentrations. Interestingly, erucylphosphocholine did not show the same effects as the other ATLs and was not cytotoxic to the yeast at similar concentrations. Further work with miltefosine and perifosine showed they both caused the mis-localization of Pma1 and Can1 from the PM. Moreover, it seems that these ATLs have similar effects on lipid metabolism, showing decreases in PC, and neutral lipids, sterol esters and TAGs while maintaining similar ergosterol levels. These preliminary results suggest that the ATLs edelfosine, miltefosine, perifosine may have similar modes of action in yeast.

Chapter Six: Discussion

Edelfosine and pH homeostasis

It has been well established that the displacement of the essential proton pump, Pma1 from lipid rafts is a critical event that mediates edelfosine cytotoxicity (78). Pma1 collaborates with the vacuolar V-ATPase, as well as the K^+ pump, Trk1 to regulate pH homeostasis within the cell (100). In these studies, we demonstrated that the disruption of pH homeostasis is a major contributor of a cells sensitivity towards edelfosine. We showed that cells defective in V-ATPase activity (*vma* mutants) were more susceptible to edelfosine than wild type cells and showed increased intracellular acidification after drug treatment. As untreated *vma* mutants already display an aberrant cytosolic pH and decreased Pma1 activity, we were able to see how this effect was strengthened after edelfosine treatment, emphasizing the importance of pH homeostasis in regulating drug sensitivity (100). Interestingly, cytosolic acidification has been shown to affect the sorting of cargo proteins and Pma1 from the Golgi, which helps to highlight the role intracellular pH plays in PM protein localization, and in the case of edelfosine how it may mediate communication from the PM to internal cellular compartments (149). We further demonstrated that the resistant mutant *vps35,* involved in retrograde transport, displays a higher buffering capacity when treated with edelfosine. The obtained results indicated that mutants lacking components in several endocytotic and trafficking pathways conferred resistance to edelfosine. As edelfosine uptake is endocytosis independent, we propose that the impairments in the retrograde transport pathway results in the recycling of Pma1, and other proteins to the PM. Proper localization of Pma1 would not only help to re-establish proper V-ATPase function, and

therein pH homeostasis, it would also allow for the re-establishment of the electrochemical gradient at the PM, which is essential for the function of many PM nutrient transporters (106).

Role of mitochondria

Alterations of intracellular pH can also regulate cellular metabolism and yeast growth rates (133). Since our resistance screen was enriched in mitochondrial function categories, including proteins responsible for F1-F0 ATPase function and those involved in cellular respiration pathways, this suggested that the inability for a cell to respire may increase tolerance to edelfosine (106). We further observed that cells treated with edelfosine showed an increase in the acidification of the mitochondrial matrix. The influx of protons into the mitochondrial matrix is necessary to establish an electrochemical gradient, which allows the F1-F0 ATPase to synthesize ATP during respiration (125-127). Therein, the influx of protons may be indicative of the cells shift from fermentation to respiration, upon treatment with edelfosine, identifying the role of respiration in edelfosine cytotoxicity.

We further observed that cells show mitochondrial fragmentation as early as 15 minutes after edelfosine addition. The maintenance of mitochondrial morphology within the cell is tightly regulated by the opposing processes of fission and fusion (142, 143). Mitochondrial fragmentation (or fission) has been linked to the loss of mitochondrial membrane potential, increased outer mitochondrial membrane permeability and slowed growth, as well as an initiation of programmed cell death (142, 144). Interestingly, in *C. elegans* and some mammalian cells it has been postulated that fragmentation of mitochondria may actually cause cytosolic acidification (143). However, since the mitochondrion are much smaller in size than the cytosol, the contribution to cytosolic acidification remains unclear. Interestingly, the resistance screen

found that the deletion of Dnm1, a GTPase responsible for the mitochondria fission (145, 146), suggesting that the maintenance of functional mitochondria is essential to regulate processes beyond respiration that may confer drug resistance.

Nutrient Uptake

It has also been reported that cells lacking Snf1 and Snf4, which regulate cellular metabolism based on nutrient availability are sensitive to growth on acidic pH (120), and that Snf1 may have a role in response to alkaline pH stress (124). We determined that edelfosine sensitivity was exacerbated when cells were grown at either acidic (pH =3) or slightly alkaline (pH = 7.5) extracellular pH. It has been shown that cells grown in acidic conditions are more susceptible to intracellular acidification (133). Therefore, the inhibition of Pma1 function by edelfosine further impedes the ability for cells to maintain pH homeostasis, leading to impaired growth at low extracellular pH. Interestingly, *vma* mutants also had impaired growth at acidic pH. It is known that cells with impaired V-ATPase function show decreased amounts of Pma1 at the PM as compared to normal cells (100), further demonstrating that cells with impaired pH homeostasis mechanisms are hypersensitive to edelfosine.

On the other hand, the impairment of cellular growth at pH = 7.5 may be explained by a metabolic switch by the cells from fermentation to respiration that occurs at more alkaline pH (124). This phenotype is expected, as cells with impaired respiration confer resistance to edelfosine. Therein, this evidence further suggests that respiration can be attributed to edelfosine cytotoxicity.

In order to alleviate the growth defects seen at alkaline pH, we increased the availability of extracellular glucose, copper and iron (124, 134). We saw that supplementation of copper, iron

with glucose, but not glucose alone was able to improve the overall fitness of the yeast in edelfosine resistant mutants, *lem3* and *vps35* at high extracellular pH. We also saw that hypersensitive mutants, *vma2* and *trk1* were more resistant to edelfosine when supplemented with nutrients, suggesting that edelfosine may be affecting the same pathways that are triggered by cell growth in alkaline conditions. We suggest that high extracellular pH may be impairing nutrient availability, which may further mediate edelfosine sensitivity.

Therein, we further observed that along with Pma1 internalization, edelfosine treatment also caused the displacement of certain nutrient transporters from the PM, arginine-H^+ symporter, Can1, uracil-H^+ symporter Fur4, and hexose transporters, Hxt1 and Hxt2. We hypothesize that the inability for cells to form an electrochemical gradient at the PM due to Pma1 internalization causes a depolarization of the PM, which leads to the mis-localization of membrane proteins. It has been observed in other studies that PM depolarization results in the exit of both ergosterol and resident symporters Fur4 and Can1 out of MCC patches, an effect which results in growth inhibition (104, 105). We further postulated that the internalization of sterols caused by edelfosine may also play a role in the mis-localization of PM transporters. We hypothesize that edelfosine induces changes in the sterol retention capacity of the PM by interfering with the interaction between sterols and sphingolipids, a perturbation that has been associated with reduced protein segregation (147, 148). Since edelfosine induces the internalization of ergosterol, we speculate that certain ergosterol rich membrane domains, such as the MCC can be readily re-organized with the addition of drug. This may result in the de-mixing of different micro-domains, which would explain the lateral movement or the increased "patchiness" observed in certain PM proteins that occurs after edelfosine treatment. Interestingly, lipid analysis profiles

indicate that edelfosine does not alter the amount of ergosterol present within the cell, suggesting that ergosterol may be accumulating in other intracellular membranes.

It is worth highlighting that the changes in lateral segregation of proteins targeted for internalization precede protein ubiquitination, as Fur4-GFP-Dub alters its PM distribution upon treatment with edelfosine, coinciding with that of Pma1 *en route* to being internalized. It is interesting that edelfosine induces the displacement of transporter proteins from the PM via ubiquitination mechanisms, which lead to subsequent protein internalization and vacuolar degradation. In addition to causing Pma1 ubiquitination, we show that the internalization of Fur4 and Hxt1 is also mediated by edelfosine- induced ubiquitination, as we observe the non-ubiquitinable forms of the transporters to remain at the PM. It is not clear at this point whether changes in intracellular pH can be sensed by the ubiquitination machinery.

Furthermore, the inhibition of glucose uptake due to the internalization of hexose transporters may have further effects on both Pma1 and V-ATPase function. Since in glucose-deprived conditions the function of Pma1 is reduced, and the Vo and V1 subunits of the V-ATPase preferentially disassemble, cytosolic acidification should be further exacerbated (100). Here we present preliminary evidence that the Vma2 (from the V1 subunit) of the V-ATPase accumulated in the DRMs of cells treated with ATLs, as compared to untreated cells (Figure 6.1).

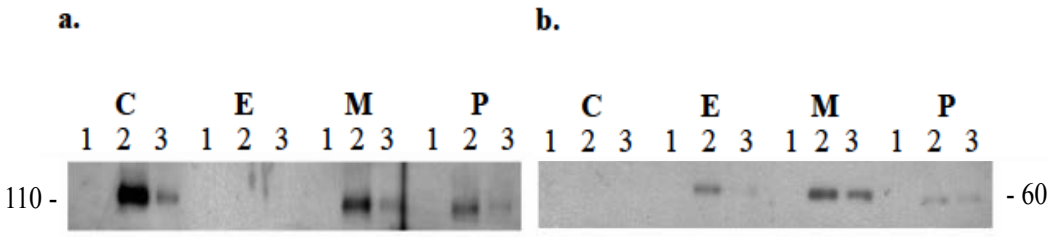

Figure 6.1: Pma1 and Vma2 localization in cells treated with ATLs WT (BY4741) cells were grown to early log phase in rich media at 30°C and then treated with ; edelfosine (19 μM), miltefosine (8 μM) or perifosine (4μM) for 2 hours . Cells were then lysed and equal amounts of protein were subjected to DRM preparation using equilibrium density gradients. Twelve fractions were obtained, and 20μl aliquots of the first three fractions containing DRMs were analyzed by SDS-PAGE **(a)** Western blot against Pma1 (110 kDa) **(b)** Same western blot against Vma2 (60 kDa).

We also examined the MCC/eisosome marker Sur7, a protein known to function in endocytosis (103). Interestingly, edelfosine treatment did not cause the internalization of this protein, but did alter its lateral distribution, an effect that may be caused by the mis-localization of sterols and sphingolipids described earlier. Alternatively, Sur7p retention at the PM may be necessary in order to facilitate endocytotic mechanisms. To date, it is unclear whether Sur7 ever becomes ubiquitinated, and this may also factor into why its internalization is not triggered by edelfosine treatment. Overall, we suggest that the endocytic-mediated internalization of PM transporters, and the resultant inhibition of nutrient uptake may be a secondary effect of Pma1 and sterol internalization caused by edelfosine.

Updated model of edelfosine cytotoxicity

The updated model (Figure 6.2) further emphasizes the importance of pH homeostasis in edelfosine cytotoxicity. Edelfosine internalization is essential for drug cytotoxicity, and this is mediated by a P4-type ATPase containing a Lem3 β-subunit at the PM. Within the first fifteen

minutes following drug treatment, the mitochondria becomes fragmented, a response mechanism that is only seen in cells with proper drug uptake. Although the purpose of this mitochondrial fragmentation remains unknown, we speculate it is a response mechanism to the presence of edelfosine. At the PM edelfosine may induce de-mixing of sterols and sphingolipids inducing the subsequent internalization of sterols from the PM. This leads to changes in the lateral organization of the PM, which causes the displacement of PM proteins from their respective micro-domains. The proton pump Pma1 is then internalized and degraded in the vacuole. The movement of Pma1 out of the PM induces cytosolic acidification, which results in disruption of the electrochemical gradient at the PM. These events occurring at the PM may also impact the function of the V-ATPase, further decreasing cytosolic pH. A consequence of the lack of electrochemical gradient caused by Pma1 internalization is the ubiquitination and subsequent internalization and degradation of PM transporters, which ultimately decreases the amount of nutrients being up-taken by the cell. The lack of nutrient availability will undoubtedly impede cellular growth. Persistent cytosolic acidification should eventually lead to cell death.

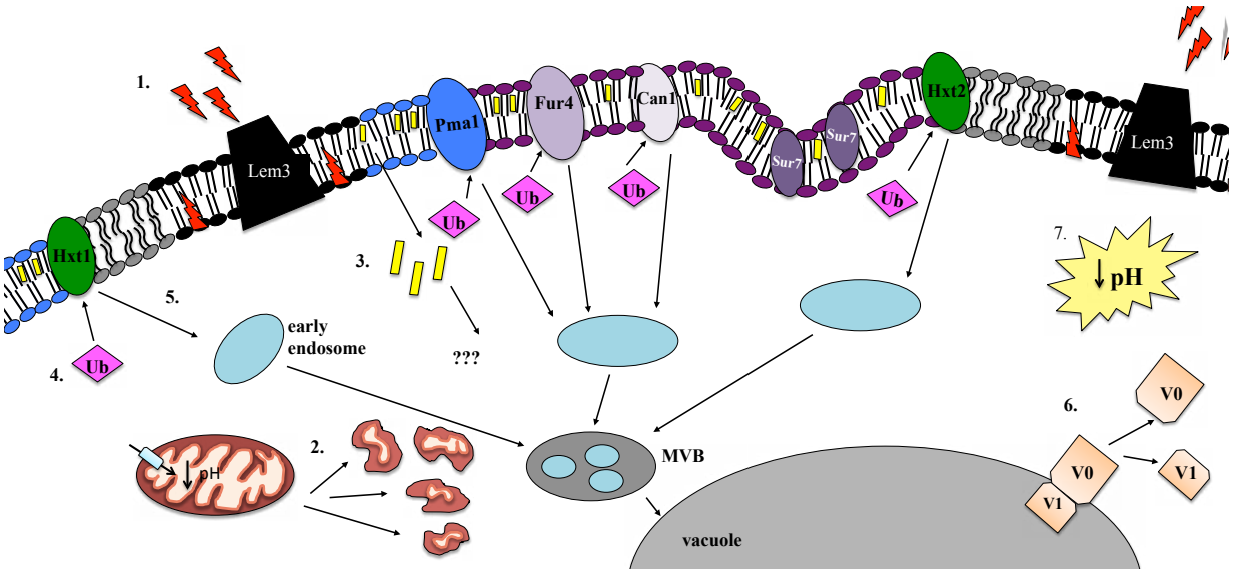

Figure 6.2: Updated model of edelfosine mode of action Edelfosine (red) inserts into lipid rafts in the PM, and is flipped into the inner leaflet of the PM via a flippase that is regulated by Lem3 **(2)** Mitochondrial fragmentation is observed at early time points **(3)** Edelfosine interaction with the PM also causes the internalization of sterols (yellow) and **(4)** induces the ubiquitination of PM transporters resulting in their **(5)** displacement from lipid rafts and, internalization and subsequent degradation in the vacuole **(6)** Intracellular conditions induce disassembly of the V-ATPase and all these events lead to **(7)** cellular acidification and eventual cell death.

Conclusions from the second generation anti-tumor lipids

Finally, investigations into second-generation ATLs miltefosine and perifosine showed they were more potent than edelfosine in yeast cells. Despite this, miltefosine and perifosine were still able to induce the internalization of Can1 and Pma1 from the PM. In addition the preliminary results with Vma2 suggest that the mis-localization of this V-ATPase component is a consequence of ATL treatment (Figure 6.1). Taken together, this suggests that disruption of pH homeostasis is a characteristic mode of action of this drug family, however more research needs to be conducted in this area.

Chapter Seven: Future directions

7.1: Relevance of Pma1 in mediating anti-tumor lipid cytotoxicity

The work done in this thesis has shown that the uptake of edelfosine, a lysoPC analogue causes ubiquitination and selective internalization of PM transporters. Our results with the non-ubiquitinatable forms of Fur4 (Fur4-GFP-DUb) and Hxt1 (Hxt1-GFP-DUb) suggest that alterations in lateral membrane organization precede the ubiquitination and internalization of PM transporters. Although speculative at this point, our work suggests that pH may play a role in signaling changes at the PM which may regulate ubiquitination and the subsequent removal of proteins from the PM. Edelfosine has also been shown to cause the ubiquitination of an essential PM protein, Pma1, which is known to be extremely stable, with a half-life of 11-12 hours (101). Therein, these results further support the PM as an early target of the drug. It is worth noting that ubiquitination is not always necessary for Pma1 to be targeted to the vacuole for degradation (149). Therefore, it would be relevant to determine if the internalization and targeting of PM Pma1 to the vacuole induced by edelfosine is mediated by ubiquitination.

- It would be of interest to examine whether maintaining Pma1 at the PM would confer edelfosine resistance. For this, we propose to generate a non-ubiquitinatable form of Pma1, by attaching a de-ubiquitinase domain (DUb), in order to prevent its internalization. We speculate that addition of the DUb domain would still allow for the proper localization of, Pma1-DUb to the PM, although we cannot predict if it will maintain its activity.

Our lab has previously shown that overexpression of Pma1 alleviates sensitivity of wild type cells to edelfosine (78). The downside of dealing with overexpression of Pma1 is that the protein is made in large quantities, and does not entirely localize to the PM and as such, the excess is sent to the vacuole for degradation (our own unpublished results and Annick M. Breton personal communication). Therefore we decided to perform the experiments of acidic and alkaline pH media using the hypomorphic Pma1 strain (Pma1-DAmP) and its isogenic wild type (Chapter 3; Figure 3.7). Based on what is known from the literature it was expected that an acidic external pH of 3 would decrease expression of Pma1 and would result in a stronger sensitivity effect. This was in fact the case, but surprisingly, sensitivity to the drug was even stronger at external pH of 7.5. Altogether these results further highlight the role of pH homeostasis in modulating edelfosine sensitivity. We further hypothesize that additional mechanisms operating under alkaline stress may be responsible for the enhanced sensitivity to the drug. The increased uptake of glucose, iron and copper has been shown to be critical in improving fitness of yeast at alkaline pH (124, 134). Indeed, we saw that supplementation of glucose, iron and copper reverted the hypersensitivity to edelfosine displayed by yeast (Chapter 3; Figure 3.9). As we have already shown that edelfosine alters localization of glucose transporters Hxt1 and Hxt2 (Chapter 4; Figure 4.4), we speculate that it may also affect proper partitioning of iron and copper transporters into their unique coexisting microdomains at the PM (147).

- It would be of interest to study the effect that edelfosine has on the localization of iron transporter Fet3 and copper transporters, Ctr1 and Ctr3 of the PM.

While completing the work done in this thesis, we also participated in a study that was aimed at investigating the role the yeast oxysterol binding protein Kes1 played in maintaining normal sphingolipid homeostasis (150). A summary of the experiments and the results obtained during these investigations is presented in Appendix 1. It is worth noting that lack of Kes1 leads to the mis-localization of Pma1 from the PM, presumably due to altered sphingolipid metabolism in the Golgi apparatus. Interestingly, we found that despite being localized to an internal compartment, Pma1 remains associated with DRMs, suggesting the presence of intracellular lipid rafts that may differ from those present at the PM. Since we know that edelfosine preferentially associates with lipid rafts at the PM, and we have recently determined that upon uptake, edelfosine accumulates in the ER (106) we speculate that a proportion of the drug is able to associate with internal DRM's.

- It would be of interest to further study the effect of ATLs on Pma1 and sterol distribution in a *kes1* mutant.

7.2 Examining intracellular pH changes and sterol distribution in miltefosine and perifosine treated yeast

The second generation ATLs, miltefosine and perifosine showed mis-localization of Pma1 in a manner similar to that of edelfosine (Chapter 5, Figure 5.5 and 5.6). This prompted the idea that a characteristic of this drug family may be to induce cytotoxicity by means of disrupting pH homeostasis in the same way as edelfosine. In knowing that V-ATPase plays a role in mediating pH homeostasis, we wanted to observe whether it remained localized to the vacuole during ATL treatment. Following this, preliminary results indicated that upon drug treatment, the Vma2 subunit of the V-ATPase associates with DRMs, but in differing proportions for each

drug. Although still preliminary this may indicate that the effect on pH homeostasis varies depending on the ATL, suggesting slightly different modes of action.

- It would be of interest to examine changes in intracellular pH for treatment with miltefosine and perifosine, and in addition, further investigate the effect of miltefosine and perifosine on sterol distribution.

References

1. Van Meer, G., Voelker, D.R., and Feigenson, G.W. (2008) Membrane lipids: where they are and how they behave. *Nature reviews molecular cell biology.* **9,** 112-124

2. Vance, J.E., and Vance, D.E. (2008) *Biochemistry of lipids, lipoproteins and membranes,* Elsevier Science

3. Singer, S., and Nicolson, G.L. (1972) The fluid mosaic model of the structure of cell membranes. *Landmark Papers in Cell Biology.* 296-307

4. Vigh, L., Escribá, P.V., Sonnleitner, A., Sonnleitner, M., Piotto, S., Maresca, B., Horváth, I., and Harwood, J.L. (2005) The significance of lipid composition for membrane activity: new concepts and ways of assessing function. *Prog.Lipid Res.* **44,** 303-344

5. Israelachvili, J., Marčelja, S., and Horn, R.G. (1980) Physical principles of membrane organization. *Q.Rev.Biophys.* **13,** 121-200

6. Holthuis, J.C., and Levine, T.P. (2005) Lipid traffic: floppy drives and a superhighway. *Nature Reviews Molecular Cell Biology.* **6,** 209-220

7. Epand, R.M. (1998) Lipid polymorphism and protein–lipid interactions. *Biochimica et Biophysica Acta (BBA)-Reviews on Biomembranes.* **1376,** 353-368

8. Janmey, P., and Kinnunen, P. (2006) Biophysical properties of lipids and dynamic membranes. *Trends Cell Biol.* **16,** 538-546

9. Escribá, P.V., González-Ros, J.M., Goñi, F.M., Kinnunen, P.K.J., Vigh, L., Sánchez-Magraner, L., Fernández, A.M., Busquets, X., Horváth, I., and Barceló-Coblijn, G. (2008) Membranes: a meeting point for lipids, proteins and therapies. *J.Cell.Mol.Med.* **12,** 829-875

10. Shindou, H., and Shimizu, T. (2009) Acyl-CoA: lysophospholipid acyltransferases. *J.Biol.Chem.* **284,** 1-5

11. Bloch, K.E. (1983) Sterol, Structure and Membrane Functio. *Crit.Rev.Biochem.Mol.Biol.* **14,** 47-92

12. Robinson, J., and Karnovsky, M. (1980) Evaluation of the polyene antibiotic filipin as a cytochemical probe for membrane cholesterol. *Journal of Histochemistry & Cytochemistry.* **28,** 161-168

13. Tanford, C. (1978) The hydrophobic effect and the organization of living matter. *Science.* **200,** 1012-1018

14. Escribá, P.V. (2006) Membrane-lipid therapy: a new approach in molecular medicine. *Trends Mol.Med.* **12,** 34-43

15. Gennis, R.B. (1989) *Biomembranes: molecular structure and function,* , Springer-Verlag New York

16. Lingwood, D., and Simons, K. (2010) Lipid rafts as a membrane-organizing principle. *Science.* **327,** 46-50

17. Van Meer, G. (1989) Lipid traffic in animal cells. *Annu.Rev.Cell Biol.* **5,** 247-275

18. Sprong, H., Van Der Sluijs, P., and Van Meer, G. (2001) How proteins move lipids and lipids move proteins. *Nature Reviews Molecular Cell Biology.* **2,** 504-513

19. Simons, K., and Toomre, D. (2000) Lipid rafts and signal transduction. *Nature Reviews Molecular Cell Biology.* **1,** 31-39

20. Vereb, G., Szöllősi, J., Matko, J., Nagy, P., Farkas, T., Vigh, L., Matyus, L., Waldmann, T., and Damjanovich, S. (2003) Dynamic, yet structured: the cell membrane three decades after the Singer–Nicolson model. *Proceedings of the National Academy of Sciences.* **100,** 8053-8058

21. Fridriksson, E.K., Shipkova, P.A., Erin, D., Holowka, D., Baird, B., and McLafferty, F.W. (1999) Quantitative analysis of phospholipids in functionally important membrane domains from RBL-2H3 mast cells using tandem high-resolution mass spectrometry. *Biochemistry (N.Y.).* **38,** 8056-8063

22. Simons, K., and Ikonen, E. (1997) Functional rafts in cell membranes. *Nature.* **387,** 569

23. Brachwitz, H., and Vollgraf, C. (1995) Analogs of alkyllysophospholipids: chemistry, effects on the molecular level and their consequences for normal and malignant cells. *Pharmacol.Ther.* **66,** 39-82

24. Munder, P., Modolell, M., Andreesen, R., Weltzien, H., and Westphal, O. (1979) Lysophosphatidylcholine (lysolecithin) and its synthetic analogues. Immunemodulating and other biologic effects **2,** 187-203

25. Vink, S.R., van Blitterswijk, W.J., Schellens, J.H.M., and Verheij, M. (2007) Rationale and clinical application of alkylphospholipid analogues in combination with radiotherapy. *Cancer Treat.Rev.* **33,** 191-202

26. Berdel, W.E. (1982) Antineoplastic activity of synthetic lysophospholipid analogs. *Ann.Hematol.* **44,** 71-78

27. Eibl, H., Arnold, D., Weltzien, H.U., and Westphal, O. (1967) Synthesen von Cholinphosphatiden, I. Zur Synthese von α-und β-Lecithinen und ihren Ätheranaloga. *Justus Liebigs Ann.Chem.* **709,** 226-230

28. Eibl, H., and Westphal, O. (1967) Synthesen von Cholinphosphatiden, V. Palmitoyl-propandiol-(1.3)-phosphorylcholin (2-Desoxylysolecithin) und ω. ω′-Alkandiol-Analoga. *Justus Liebigs Ann.Chem.* **709,** 244-247

29. Hilgard, P., Klenner, T., Stekar, J., and Unger, C. (1993) Alkylphosphocholines: a new class of membrane-active anticancer agents. *Cancer Chemother.Pharmacol.* **32,** 90-95

30. Arnold, D., Weltzien, H.U., and Westphal, O. (1967) Concerning the synthesis of lysolecithin and its ether analogs. *Justus Liebigs Ann.Chem.* **709,** 234-239

31. Weltzien, H.U., and Westphal, O. (1967) Synthesen von Cholinphosphatiden, IV. O-Methylierte und O-acetylierte Lysolecithine. *Justus Liebigs Ann.Chem.* **709,** 240-243

32. Andreesen, R., Osterholz, J., Luckenbach, G.A., Costabel, U., Schulz, A., Speth, V., Munder, P.G., and Löhr, G.W. (1984) Tumor cytotoxicity of human macrophages after incubation with synthetic analogues of 2-lysophosphatidylcholine. *J.Natl.Cancer Inst.* **72,** 53-59

33. Andreesen, R., Osterholz, J., Bross, K.J., Schulz, A., Luckenbach, G.A., and Löhr, G.W. (1983) Cytotoxic effector cell function at different stages of human monocyte-macrophage maturation. *Cancer Res.* **43,** 5931-5936

34. Mollinedo, F., de la Iglesia-Vicente, J., Gajate, C., de Mendoza, A.E.H., Villa-Pulgarin, J.A., de Frias, M., Roué, G., Gil, J., Colomer, D., and Campanero, M.A. (2010) In vitro and in vivo selective antitumor activity of edelfosine against mantle cell lymphoma and chronic lymphocytic leukemia involving lipid rafts. *Clinical Cancer Research.* **16,** 2046-2054

35. Modolell, M., Andreesen, R., Pahlke, W., Brugger, U., and Munder, P.G. (1979) Disturbance of phospholipid metabolism during the selective destruction of tumor cells induced by alkyl-lysophospholipids. *Cancer Res.* **39,** 4681-4686

36. Tarnowski, G.S., Mountain, I.M., Stock, C.C., Munder, P.G., Weltzien, H.U., and Westphal, O. (1978) Effect of lysolecithin and analogs on mouse ascites tumors. *Cancer Res.* **38,** 339-344

37. Mollinedo, F., Gajate, C., Martin-Santamaria, S., and Gago, F. (2004) ET-18-OCH3 (edelfosine): a selective antitumour lipid targeting apoptosis through intracellular activation of Fas/CD95 death receptor. *Curr.Med.Chem.* **11,** 3163-3184

38. Andreesen, R., Modolell, M., Weltzien, H.U., Eibl, H., Common, H.H., Löhr, G.W., and Munder, P.G. (1978) Selective destruction of human leukemic cells by alkyl-lysophospholipids. *Cancer Res.* **38,** 3894-3899

39. Tidwell, T., Guzman, G., and Vogler, W.R. (1981) The effects of alkyl-lysophospholipids on leukemic cell lines. I. Differential action on two human leukemic cell lines, HL60 and K562. *Blood.* **57,** 794-797

40. Hoffman, D.R., Hoffman, L.H., and Snyder, F. (1986) Cytotoxicity and metabolism of alkyl phospholipid analogues in neoplastic cells. *Cancer Res.* **46,** 5803-5809

41. van der Luit, A.H., Vink, S.R., Klarenbeek, J.B., Perrissoud, D., Solary, E., Verheij, M., and van Blitterswijk, W.J. (2007) A new class of anticancer alkylphospholipids uses lipid rafts as membrane gateways to induce apoptosis in lymphoma cells. *Molecular cancer therapeutics.* **6,** 2337-2345

42. Runge, M.H., Andreesen, R., Pfleiderer, A., and Munder, P.G. (1980) Destruction of human solid tumors by alkyl lysophospholipids. *J.Natl.Cancer Inst.* **64,** 1301-1306

43. Scherf, H., Schuler, B., Berger, M., and Schmähl, D. (1987) Therapeutic activity of ET-18-OCH 3 and hexadecylphosphocholine against mammary tumors in BD-VI rats. *Lipids.* **22,** 927-929

44. Berdel, W.E., Fink, U., and Rastetter, J. (1987) Clinical phase I pilot study of the alkyl lysophospholipid derivative ET-18-OCH 3 1. *Lipids.* **22,** 967-969

45. Drings, P., Günther, I., Gatzemeier, U., Ulbrich, F., Khanavkar, B., Schreml, W., Lorenz, J., Brugger, W., Schick, H., and Pawel, J. (1992) Final Evaluation of a Phase II Study on the Effect of Edelfosine (an Ether Lipid) in Advanced Non-Small-Cell Bronchogenic Carcinoma. *Onkologie.* **15,** 375-382

46. Vogler, W.R., Olson, A.C., Okamoto, S., Somberg, L.B., and Glasser, L. (1987) Experimental studies on the role of alkyl lysophospholipids in autologous bone marrow transplatation. *Lipids.* **22,** 919-924

47. Hilgard, P., Kampherm, E., Nolan, L., Pohl, J., and Reissmann, T. (1991) Investigation into the immunological effects of miltefosine, a new anticancer agent under development. *J.Cancer Res.Clin.Oncol.* **117,** 403-408

48. Unger, C., Eibl, H., Von Heyden, H., Peukert, M., Sindermann, H., and Nagel, G. (1990) Phase I study with daily hexadecylphosphocholine in patients with malignant disease. *Onkologie.* **13,** 56

49. Verweij, J., Planting, A., van der Burg, M., and Stoter, G. (1992) A dose-finding study of miltefosine (hexadecylphosphocholine) in patients with metastatic solid tumours. *J.Cancer Res.Clin.Oncol.* **118,** 606-608

50. Berdel, W., Becher, R., Edler, L., Bremer, K., Essers, U., Drozd, A., Zafferani, M., Klee, M., Bachmann, P., and Korfel, A. (1992) Daily oral Miltefosine (hexadecyl-phosphocholine) in patients with advanced non-small cell lung cancer. A phase II study. *Onkologie.* **15,** 238-242

51. Sindermann, H., and Engel, J. (2006) Development of miltefosine as an oral treatment for leishmaniasis. *Trans.R.Soc.Trop.Med.Hyg.* **100,** S17-S20

52. Unger, C., Damenz, W., Fleer, E., Kim, D., Breiser, A., Hilgard, P., Engel, J., Nagel, G., and Eibl, H. (1989) Hexadecylphosphocholine, a New Ether Lipid Analogue Studies on the Antineoplastic Activity in Vitro and in Vivo. *Acta Oncol.* **28,** 213-217

53. Terwogt, J.M.M., Mandjes, I., Sindermann, H., Beijnen, J., and ten Bokkel Huinink, W. (1999) Phase II trial of topically applied miltefosine solution in patients with skin-metastasized breast cancer. *Br.J.Cancer.* **79,** 1158

54. Smorenburg, C., Seynaeve, C., Bontenbal, M., Planting, A.S.T., Sindermann, H., and Verweij, J. (2000) Phase II study of miltefosine 6% solution as topical treatment of skin metastases in breast cancer patients. *Anticancer Drugs.* **11,** 825-828

55. Dummer, R., Krasovec, M., Röger, J., Sindermann, H., and Burg, G. (1993) Topical administration of hexadecylphosphocholine in patients with cutaneous lymphomas: results of a phase I/II study. *J.Am.Acad.Dermatol.* **29,** 963-970

56. Hilgard, P., Klenner, T., Stekar, J., Nössner, G., Kutscher, B., and Engel, J. (1997) D-21266, a new heterocyclic alkylphospholipid with antitumour activity. *Eur.J.Cancer.* **33,** 442-446

57. Van Ummersen, L., Binger, K., Volkman, J., Marnocha, R., Tutsch, K., Kolesar, J., Arzoomanian, R., Alberti, D., and Wilding, G. (2004) A phase I trial of perifosine (NSC 639966) on a loading dose/maintenance dose schedule in patients with advanced cancer. *Clinical Cancer Research.* **10,** 7450-7456

58. Crul, M., Rosing, H., De Klerk, G., Dubbelman, R., Traiser, M., Reichert, S., Knebel, N., Schellens, J., Beijnen, J., and ten Bokkel Huinink, W. (2002) Phase I and pharmacological study of daily oral administration of perifosine (D-21266) in patients with advanced solid tumours. *Eur.J.Cancer.* **38,** 1615-1621

59. Jendrossek, V., Hammersen, K., Erdlenbruch, B., Kugler, W., Krügener, R., Eibl, H., and Lakomek, M. (2002) Structure-activity relationships of alkylphosphocholine derivatives: antineoplastic action on brain tumor cell lines in vitro. *Cancer Chemother.Pharmacol.* **50,** 71-79

60. Erdlenbruch, B., Jendrossek, V., Gerriets, A., Vetterlein, F., Eibl, H., and Lakomek, M. (1999) Erucylphosphocholine: pharmacokinetics, biodistribution and CNS-accumulation in the rat after intravenous administration. *Cancer Chemother.Pharmacol.* **44,** 484-490

61. Kötting, J., Berger, M.R., Unger, C., and Eibl, H. (1992) Alkylphosphocholines: influence of structural variation on biodistribution at antineoplastically active concentrations. *Cancer Chemother.Pharmacol.* **30,** 105-112

62. Croft, S.L., Seifert, K., and Duchêne, M. (2003) Antiprotozoal activities of phospholipid analogues. *Mol.Biochem.Parasitol.* **126,** 165-172

63. Escobar, P., Matu, S., Marques, C., and Croft, S.L. (2002) Sensitivities of< i> Leishmania species to hexadecylphosphocholine (miltefosine), ET-18-OCH< sub> 3</sub>(edelfosine) and amphotericin B. *Acta Trop.* **81,** 151-157

64. Achterberg, V., and Gercken, G. (1987) Cytotoxicity of ester and ether lysophospholipids on *Leishmania donovani* promastigotes. *Mol.Biochem.Parasitol.* **23,** 117-122

65. Jha, T., Sundar, S., Thakur, C., Bachmann, P., Karbwang, J., Fischer, C., Voss, A., and Berman, J. (1999) Miltefosine, an oral agent, for the treatment of Indian visceral leishmaniasis. *N.Engl.J.Med.* **341,** 1795-1800

66. Mollinedo, F. (2007) Antitumour ether lipids: proapoptotic agents with multiple therapeutic indications

67. Schmidt-Ott, R., Klenner, T., Overath, P., and Aebischer, T. (1999) Topical treatment with hexadecylphosphocholine (Miltex ® efficiently reduces parasite burden in experimental cutaneous leishmaniasis. *Trans.R.Soc.Trop.Med.Hyg.* **93,** 85-90

68. Soto, J., Toledo, J., Gutierrez, P., Nicholls, R., Padilla, J., Engel, J., Fischer, C., Voss, A., and Berman, J. (2001) Treatment of American cutaneous leishmaniasis with miltefosine, an oral agent. *Clinical Infectious Diseases.* **33,** e57-e61

69. van Blitterswijk, W.J., and Verheij, M. (2012) Anticancer mechanisms and clinical application of alkylphospholipids. *Biochimica et Biophysica Acta (BBA)-Molecular and Cell Biology of Lipids.*

70. Ruiter, G.A., Zerp, S.F., Bartelink, H., van Blitterswijk, W.J., and Verheij, M. (1999) Alkyl-lysophospholipids activate the SAPK/JNK pathway and enhance radiation-induced apoptosis. *Cancer Res.* **59,** 2457-2463

71. Ferguson, L.R., and Pearson, A.E. (1996) The clinical use of mutagenic anticancer drugs. *Mutation Research/Fundamental and Molecular Mechanisms of Mutagenesis.* **355,** 1-12

72. Swinnen, J.V., Brusselmans, K., and Verhoeven, G. (2006) Increased lipogenesis in cancer cells: new players, novel targets. *Current Opinion in Clinical Nutrition & Metabolic Care.* **9,** 358-365

73. Berdel, W. (1991) Membrane-interactive lipids as experimental anticancer drugs. *Br.J.Cancer.* **64,** 208

74. van Blitterswijk, W.J., and Verheij, M. (2008) Anticancer alkylphospholipids: mechanisms of action, cellular sensitivity and resistance, and clinical prospects. *Curr.Pharm.Des.* **14,** 2061-2074

75. Boggs, K.P., Rock, C.O., and Jackowski, S. (1995) Lysophosphatidylcholine and 1-O-octadecyl-2-O-methyl-rac-glycero-3-phosphocholine inhibit the CDP-choline pathway of phosphatidylcholine synthesis at the CTP: phosphocholine cytidylyltransferase step. *J.Biol.Chem.* **270,** 7757-7764

76. Wright, M.M., Howe, A.G., and Zaremberg, V. (2004) Cell membranes and apoptosis: role of cardiolipin, phosphatidylcholine, and anticancer lipid analogues. *Biochemistry and cell biology.* **82,** 18-26

77. Cui, Z., and Houweling, M. (2002) Phosphatidylcholine and cell death. *Biochimica et Biophysica Acta (BBA)-Molecular and Cell Biology of Lipids.* **1585,** 87-96

78. Zaremberg, V., Gajate, C., Cacharro, L.M., Mollinedo, F., and McMaster, C.R. (2005) Cytotoxicity of an anti-cancer lysophospholipid through selective modification of lipid raft composition. *J.Biol.Chem.* **280,** 38047-38058

79. Samadder, P., Richards, C., Bittman, R., Bhullar, R., and Arthur, G. (2003) The antitumor ether lipid 1-Q-octadecyl-2-O-methyl-rac-glycerophosphocholine (ET-18-OCH3) inhibits the association between Ras and Raf-1. *Anticancer Res.* **23,** 2291

80. Ruiter, G.A., Verheij, M., Zerp, S.F., Moolenaar, W.H., and Van Blitterswijk, W.J. (2002) Submicromolar doses of alkyl-lysophospholipids induce rapid internalization, but not activation, of epidermal growth factor receptor and concomitant MAPK/ERK activation in A431 cells. *International journal of cancer.* **102,** 343-350

81. Ruiter, G.A., Zerp, S.F., Bartelink, H., van Blitterswijk, W.J., and Verheij, M. (2003) Anti-cancer alkyl-lysophospholipids inhibit the phosphatidylinositol 3-kinase-Akt/PKB survival pathway. *Anticancer Drugs.* **14,** 167-173

82. Kondapaka, S.B., Singh, S.S., Dasmahapatra, G.P., Sausville, E.A., and Roy, K.K. (2003) Perifosine, a novel alkylphospholipid, inhibits protein kinase B activation. *Molecular Cancer Therapeutics.* **2,** 1093-1103

83. Verheij, M., van Blitterswijk, W.J., and Bartelink, H. (1998) Radiation-induced apoptosis: The ceramide-SAPK signaling pathway and clinical aspects. *Acta Oncol.* **37,** 575-581

84. Shen, Y.H., Godlewski, J., Zhu, J., Sathyanarayana, P., Leaner, V., Birrer, M.J., Rana, A., and Tzivion, G. (2003) Cross-talk between JNK/SAPK and ERK/MAPK Pathways: Sustained activation of JNK blocks ERK activation by mitogenic factors. *J.Biol.Chem.* **278,** 26715-26721

85. Nieto-Miguel, T., Gajate, C., and Mollinedo, F. (2006) Differential targets and subcellular localization of antitumor alkyl-lysophospholipid in leukemic versus solid tumor cells. *J.Biol.Chem.* **281,** 14833-14840

86. Patra, S.K. (2008) Dissecting lipid raft facilitated cell signaling pathways in cancer. *Biochimica et Biophysica Acta (BBA)-Reviews on Cancer.* **1785,** 182-206

87. Riekhof, W.R., and Voelker, D.R. (2009) The yeast plasma membrane P_4-ATPases are major transporters for lysophospholipids. *Biochimica et Biophysica Acta (BBA)-Molecular and Cell Biology of Lipids.* **1791,** 620-627

88. Saito, K., Fujimura-Kamada, K., Furuta, N., Kato, U., Umeda, M., and Tanaka, K. (2004) Cdc50p, a protein required for polarized growth, associates with the Drs2p P-type ATPase implicated in phospholipid translocation in Saccharomyces cerevisiae. *Mol.Biol.Cell.* **15,** 3418-3432

89. Hanson, P.K., Malone, L., Birchmore, J.L., and Nichols, J.W. (2003) Lem3p is essential for the uptake and potency of alkylphosphocholine drugs, edelfosine and miltefosine. *J.Biol.Chem.* **278,** 36041-36050

90. van der Luit, A.H., Budde, M., Ruurs, P., Verheij, M., and van Blitterswijk, W.J. (2002) Alkyl-lysophospholipid accumulates in lipid rafts and induces apoptosis via raft-dependent endocytosis and inhibition of phosphatidylcholine synthesis. *J.Biol.Chem.* **277,** 39541-39547

91. Kato, U., Emoto, K., Fredriksson, C., Nakamura, H., Ohta, A., Kobayashi, T., Murakami-Murofushi, K., Kobayashi, T., and Umeda, M. (2002) A novel membrane protein, Ros3p, is required for phospholipid translocation across the plasma membrane in Saccharomyces cerevisiae. *J.Biol.Chem.* **277,** 37855-37862

92. Mager, W.H., and Winderickx, J. (2005) Yeast as a model for medical and medicinal research. *Trends Pharmacol.Sci.* **26,** 265-273

93. Simon, J.A., and Bedalov, A. (2004) Yeast as a model system for anticancer drug discovery. *Nature Reviews Cancer.* **4,** 481-487

94. Botstein, D., Chervitz, S.A., and Cherry, M. (1997) Yeast as a model organism. *Science.* **277,** 1259-1260

95. Smith, A.M., Ammar, R., Nislow, C., and Giaever, G. (2010) A survey of yeast genomic assays for drug and target discovery. *Pharmacol.Ther.* **127,** 156

96. Warburg, O. (1956) On the origin of cancer cells. *Science.* **123,** 309-314

97. Diaz-Ruiz, R., Rigoulet, M., and Devin, A. (2011) The Warburg and Crabtree effects: On the origin of cancer cell energy metabolism and of yeast glucose repression. *Biochimica et Biophysica Acta (BBA)-Bioenergetics.* **1807,** 568-576

98. Orij, R., Postmus, J., Ter Beek, A., Brul, S., and Smits, G.J. (2009) In vivo measurement of cytosolic and mitochondrial pH using a pH-sensitive GFP derivative in Saccharomyces cerevisiae reveals a relation between intracellular pH and growth. *Microbiology.* **155,** 268-278

99. Vaupel, P., Kallinowski, F., and Okunieff, P. (1989) Blood flow, oxygen and nutrient supply, and metabolic microenvironment of human tumors: a review. *Cancer Res.* **49,** 6449-6465

100. Martínez-Muñoz, G.A., and Kane, P. (2008) Vacuolar and plasma membrane proton pumps collaborate to achieve cytosolic pH homeostasis in yeast. *J.Biol.Chem.* **283,** 20309-20319

101. Benito, B., Moreno, E., and Lagunas, R. (1991) Half-life of the plasma membrane ATPase and its activating system in resting yeast cells. *Biochimica et Biophysica Acta (BBA)-Biomembranes.* **1063,** 265-268

102. Kane, P.M. (1995) Disassembly and reassembly of the yeast vacuolar H -ATPase in vivo. *J.Biol.Chem.* **270,** 17025-17032

103. Malínská, K., Malínský, J., Opekarová, M., and Tanner, W. (2003) Visualization of protein compartmentation within the plasma membrane of living yeast cells. *Mol.Biol.Cell.* **14,** 4427-4436

104. Grossmann, G., Opekarová, M., Malinsky, J., Weig-Meckl, I., and Tanner, W. (2006) Membrane potential governs lateral segregation of plasma membrane proteins and lipids in yeast. *EMBO J.* **26,** 1-8

105. Grossmann, G., Malinsky, J., Stahlschmidt, W., Loibl, M., Weig-Meckl, I., Frommer, W.B., Opekarová, M., and Tanner, W. (2008) Plasma membrane microdomains regulate turnover of transport proteins in yeast. *J.Cell Biol.* **183,** 1075-1088

106. Cuesta-Marbán, A., Botet, J., Czyz, O., Cacharro, L.M., Gajate, C., Hornillos, V., Delgado, J., Zhang, H., Amat-Guerri, F., and Acuña, A.U. (2013) Drug uptake, lipid rafts and vesicle trafficking modulate resistance to an anticancer lysophosphatidylcholine analogue in yeast. *J.Biol.Chem.*

107. Czyz, O.A., Bitew, T., Cuesta-Marbán, A., McMaster, C.R., Mollinedo, F., and Zaremberg, V. (2013) Alteration of plasma membrane organization by an anticancer lysophosphatidylcholine analogue induces intracellular acidification and internalization of plasma membrane transporters in yeast. *J.Biol.Chem.*

108. Aouida, M., Leduc, A., Poulin, R., and Ramotar, D. (2005) AGP2 encodes the major permease for high affinity polyamine import in Saccharomyces cerevisiae. *J.Biol.Chem.* **280,** 24267-24276

109. Gajate, C., Gonzalez-Camacho, F., and Mollinedo, F. (2009) Involvement of raft aggregates enriched in Fas/CD95 death-inducing signaling complex in the antileukemic action of edelfosine in Jurkat cells. *PLoS One.* **4,** e5044

110. Shi, Y., Stefan, C.J., Rue, S.M., Teis, D., and Emr, S.D. (2011) Two novel WD40 domain–containing proteins, Ere1 and Ere2, function in the retromer-mediated endosomal recycling pathway. *Mol.Biol.Cell.* **22,** 4093-4107

111. Schuldiner, M., Collins, S.R., Thompson, N.J., Denic, V., Bhamidipati, A., Punna, T., Ihmels, J., Andrews, B., Boone, C., and Greenblatt, J.F. (2005) Exploration of the function and organization of the yeast early secretory pathway through an epistatic miniarray profile. *Cell.* **123,** 507-519

112. Winzeler, E.A., Shoemaker, D.D., Astromoff, A., Liang, H., Anderson, K., Andre, B., Bangham, R., Benito, R., Boeke, J.D., and Bussey, H. (1999) Functional characterization of the S. cerevisiae genome by gene deletion and parallel analysis. *Science.* **285,** 901-906

113. Giaever, G., Chu, A.M., Ni, L., Connelly, C., Riles, L., Veronneau, S., Dow, S., Lucau-Danila, A., Anderson, K., and Andre, B. (2002) Functional profiling of the Saccharomyces cerevisiae genome. *Nature.* **418,** 387-391

114. Fyrst, H., Oskouian, B., Kuypers, F.A., and Saba, J.D. (1999) The PLB2 gene of Saccharomyces cerevisiae confers resistance to lysophosphatidylcholine and encodes a phospholipase B/lysophospholipase. *Biochemistry (N.Y.).* **38,** 5864-5871

115. Fairn, G.D., and McMaster, C.R. (2005) Studying phospholipid metabolism using yeast systematic and chemical genetics. *Methods.* **36,** 102-108

116. Breitkreutz, B., Stark, C., and Tyers, M. (2003) Osprey: a network visualization system. *Genome Biol.* **4,** R22

117. Robinson, M.D., Grigull, J., Mohammad, N., and Hughes, T.R. (2002) FunSpec: a web-based cluster interpreter for yeast. *BMC Bioinformatics.* **3,** 35

118. Graham, L.A., Hill, K.J., and Stevens, T.H. (1998) Assembly of the yeast vacuolar H - ATPase occurs in the endoplasmic reticulum and requires a Vma12p/Vma22p assembly complex. *J.Cell Biol.* **142,** 39-49

119. Yenush, L., Merchan, S., Holmes, J., and Serrano, R. (2005) pH-responsive, posttranslational regulation of the Trk1 potassium transporter by the type 1-related Ppz1 phosphatase. *Mol.Cell.Biol.* **25,** 8683-8692

120. Young, B.P., Shin, J.J., Orij, R., Chao, J.T., Li, S.C., Guan, X.L., Khong, A., Jan, E., Wenk, M.R., and Prinz, W.A. (2010) Phosphatidic acid is a pH biosensor that links membrane biogenesis to metabolism. *Science Signalling.* **329,** 1085

121. Zhang, J., Vemuri, G., and Nielsen, J. (2010) Systems biology of energy homeostasis in yeast. *Curr.Opin.Microbiol.* **13,** 382

122. Portillo, F., Mulet, J.M., and Serrano, R. (2005) A role for the non-phosphorylated form of yeast Snf1: tolerance to toxic cations and activation of potassium transport. *FEBS Lett.* **579,** 512-516

123. Ariño, J., Ramos, J., and Sychrová, H. (2010) Alkali metal cation transport and homeostasis in yeasts. *Microbiology and Molecular Biology Reviews.* **74,** 95-120

124. Antonio, C., Raquel, S., Maria, P., Carlos, C., Amparo, R., and Joaquin, A. (2012) The role of the Snf1 kinase in the adaptive response of Saccharomyces cerevisiae to alkaline pH stress. *Biochem.J.* **444,** 39-49

125. Wilkens, S. (2005) Rotary molecular motors. *Adv.Protein Chem.* **71,** 345-382

126. Arnold, I., Pfeiffer, K., Neupert, W., Stuart, R.A., and Schägger, H. (1998) Yeast mitochondrial F1F0-ATP synthase exists as a dimer: identification of three dimer-specific subunits. *EMBO J.* **17,** 7170-7178

127. Weber, J., and Senior, A.E. (1997) Catalytic mechanism of F1-ATPase. *Biochim.Biophys.Acta.* **1319,** 19

128. Traba, J., Satrústegui, J., and del Arco, A. (2009) Transport of adenine nucleotides in the mitochondria of *Saccharomyces cerevisiae*: Interactions between the ADP/ATP carriers and the ATP-Mg/Pi carrier. *Mitochondrion.* **9,** 79-85

129. Miesenböck, G., De Angelis, D.A., and Rothman, J.E. (1998) Visualizing secretion and synaptic transmission with pH-sensitive green fluorescent proteins. *Nature.* **394,** 192-195

130. Orij, R., Brul, S., and Smits, G.J. (2011) Intracellular pH is a tightly controlled signal in yeast. *Biochimica et Biophysica Acta (BBA)-General Subjects.* **1810,** 933-944

131. Westermann, B., and Neupert, W. (2000) Mitochondria-targeted green fluorescent proteins: convenient tools for the study of organelle biogenesis in Saccharomyces cerevisiae. *Yeast.* **16,** 1421-1427

132. Carmelo, V., Santos, H., and Sá-Correia, I. (1997) Effect of extracellular acidification on the activity of plasma membrane ATPase and on the cytosolic and vacuolar pH of< i> Saccharomyces cerevisiae. *Biochimica et Biophysica Acta (BBA)-Biomembranes.* **1325,** 63-70

133. Orij, R., Urbanus, M.L., Vizeacoumar, F.J., Giaever, G., Boone, C., Nislow, C., Brul, S., and Smits, G.J. (2012) Genome-wide analysis of intracellular pH reveals quantitative control of cell division rate by pHc in Saccharomyces cerevisiae. *Genome Biol.* **13,** R80

134. Serrano, R., Bernal, D., Simón, E., and Ariño, J. (2004) Copper and iron are the limiting factors for growth of the yeast Saccharomyces cerevisiae in an alkaline environment. *J.Biol.Chem.* **279,** 19698-19704

135. Walther, T.C., Brickner, J.H., Aguilar, P.S., Bernales, S., Pantoja, C., and Walter, P. (2006) Eisosomes mark static sites of endocytosis. *Nature.* **439,** 998-1003

136. Stringer, D.K., and Piper, R.C. (2011) A single ubiquitin is sufficient for cargo protein entry into MVBs in the absence of ESCRT ubiquitination. *J.Cell Biol.* **192,** 229-242

137. Lowry, O.H., Rosebrough, N.J., Farr, A.L., and Randall, R.J. (1951) Protein measurement with the Folin phenol reagent. *J.Biol.Chem.* **193,** 265-275

138. Bagnat, M., Chang, A., and Simons, K. (2001) Plasma membrane proton ATPase Pma1p requires raft association for surface delivery in yeast. *Mol.Biol.Cell.* **12,** 4129-4138

139. Pizzirusso, M., and Chang, A. (2004) Ubiquitin-mediated targeting of a mutant plasma membrane ATPase, Pma1-7, to the endosomal/vacuolar system in yeast. *Mol.Biol.Cell.* **15,** 2401-2409

140. Horák, J. (2003) The role of ubiquitin in down-regulation and intracellular sorting of membrane proteins: insights from yeast. *Biochimica et Biophysica Acta (BBA)-Biomembranes.* **1614,** 139-155

141. Schneiter, R., and Daum, G. (2006) Extraction of yeast lipids 41-45

142. Chen, H., Chomyn, A., and Chan, D.C. (2005) Disruption of fusion results in mitochondrial heterogeneity and dysfunction. *J.Biol.Chem.* **280,** 26185-26192

143. Johnson, D., and Nehrke, K. (2010) Mitochondrial fragmentation leads to intracellular acidification in Caenorhabditis elegans and mammalian cells. *Mol.Biol.Cell.* **21,** 2191-2201

144. Chan, D.C. (2006) Mitochondria: dynamic organelles in disease, aging, and development. *Cell.* **125,** 1241-1252

145. Bleazard, W., McCaffery, J.M., King, E.J., Bale, S., Mozdy, A., Tieu, Q., Nunnari, J., and Shaw, J.M. (1999) The dynamin-related GTPase Dnm1 regulates mitochondrial fission in yeast. *Nat.Cell Biol.* **1,** 298-304

146. Fannjiang, Y., Cheng, W., Lee, S.J., Qi, B., Pevsner, J., McCaffery, J.M., Hill, R.B., Basañez, G., and Hardwick, J.M. (2004) Mitochondrial fission proteins regulate programmed cell death in yeast. *Genes Dev.* **18,** 2785-2797

147. Spira, F., Mueller, N.S., Beck, G., von Olshausen, P., Beig, J., and Wedlich-Söldner, R. (2012) Patchwork organization of the yeast plasma membrane into numerous coexisting domains. *Nat.Cell Biol.* **14,** 640-648

148. Baumann, N.A., Sullivan, D.P., Ohvo-Rekilä, H., Simonot, C., Pottekat, A., Klaassen, Z., Beh, C.T., and Menon, A.K. (2005) Transport of newly synthesized sterol to the sterol-enriched plasma membrane occurs via nonvesicular equilibration. *Biochemistry (N.Y.).* **44,** 5816-5826

149. Huang, C., and Chang, A. (2011) pH-dependent cargo sorting from the Golgi. *J.Biol.Chem.* **286,** 10058-10065

150. LeBlanc, M.A., Fairn, G.D., Russo, S.B., Czyz, O., Zaremberg, V., Cowart, L.A., and McMaster, C.R. (2013) The Yeast Oxysterol Binding Protein Kes1 Maintains Sphingolipid Levels. *PLoS One.*

151. Fairn, G., and McMaster, C. (2008) Emerging roles of the oxysterol-binding protein family in metabolism, transport, and signaling. *Cellular and Molecular Life Sciences.* **65,** 228-236

152. Levine, T. (2005) A new way for sterols to walk on water. *Mol.Cell.* **19,** 722-723

153. Im, Y.J., Raychaudhuri, S., Prinz, W.A., and Hurley, J.H. (2005) Structural mechanism for sterol sensing and transport by OSBP-related proteins. *Nature.* **437,** 154-158

154. Schulz, T.A., and Prinz, W.A. (2007) Sterol transport in yeast and the oxysterol binding protein homologue (OSH) family. *Biochimica et Biophysica Acta (BBA)-Molecular and Cell Biology of Lipids.* **1771,** 769-780

155. LeBlanc, M.A., and McMaster, C.R. (2010) Lipid binding requirements for oxysterol-binding protein Kes1 inhibition of autophagy and endosome-trans-Golgi trafficking pathways. *J.Biol.Chem.* **285,** 33875-33884

156. Klemm, R.W., Ejsing, C.S., Surma, M.A., Kaiser, H., Gerl, M.J., Sampaio, J.L., de Robillard, Q., Ferguson, C., Proszynski, T.J., and Shevchenko, A. (2009) Segregation of sphingolipids and sterols during formation of secretory vesicles at the trans-Golgi network. *J.Cell Biol.* **185,** 601-612

Appendix 1: Partitioning of Pma1 into detergent resistant membranes in mutants of the Kes1/Osh4 member of the yeast oxysterol binding proteins

Introduction

Working in collaboration with Dr. McMaster's lab from Dalhousie University we investigated the role of a member of the yeast oxysterol binding protein family (Osh family) in lipid raft formation and Pma1 localization. The oxysterol-binding-proteins (known as OSBP/Osh) are conserved from yeast to humans and have been linked to the regulation of sterol homeostasis as well as in signal transduction pathways (151). Yeast contains seven members of the Osh family of proteins, which possess some functional redundancy, but are known to localize to different cellular compartments (Table A1.1). The most studied member of this family in yeast is Osh4, also known as Kes1. Recently, the structure of Kes1/Osh4 was solved showing the protein is composed of a β-barrel tunnel where sterols accommodate and a lid that opens and closes depending on occupancy by sterols in the tunnel region (Figure A1.1). The protein also has a region that recognizes phosphoinositides, which allows the protein to cycle between sterol donor and acceptor membranes (Figure A1.2).

Table A1.1: Yeast Osh proteins

Name	Domains/Motifs	Localization
Osh1	Ank, FFAT, PH, ORD	Golgi & nucleus-vacuole junction
Osh2	Ank, FFAT, PH, ORD	Peripheral patches near the bud neck
Osh3	GOLD, FFAT, PH, ORD	Cytoplasm
Osh4/ Kes1	ALPS, ORD, PIP binding	Golgi & cytoplasm
Osh5	ORD	Cytoplasm
Osh6	ORD	Cytoplasm and plasma membrane
Osh7	ORD	Cytoplasm and plasma membrane

(Ank= ankyrin repeat; FFAT= two phenylalanines in an acidic tract; PH =pleckstrin homology domain; ORD= oxysterol binding protein related domain; GOLD =Golgi dynamics domain; ALPS= ArfGAP1= lipid packing sensor motif)

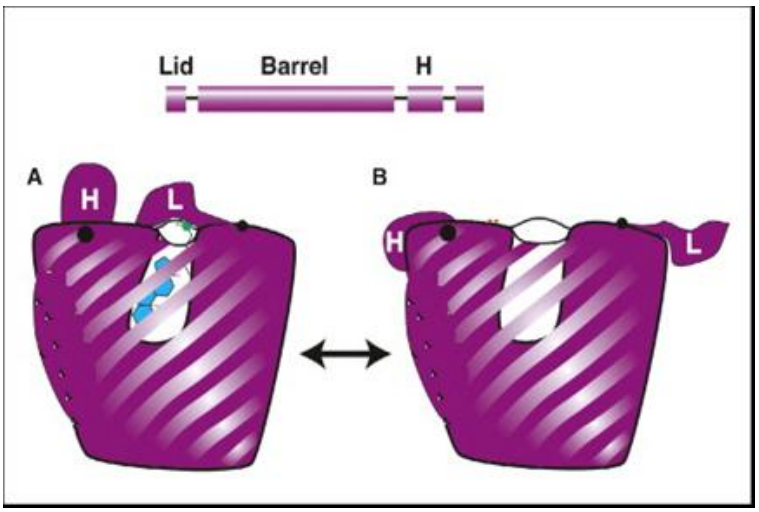

Figure A1.1: Cartoon structure of Kes 1 (a) Kes1 loaded with a sterol molecule with the lid (L) closed and the helical region (H) protruding. **(b)** Apo conformation of Kes1 with lid open and the helical region adopting a flat position that allows binding to membranes. Modified from (152).

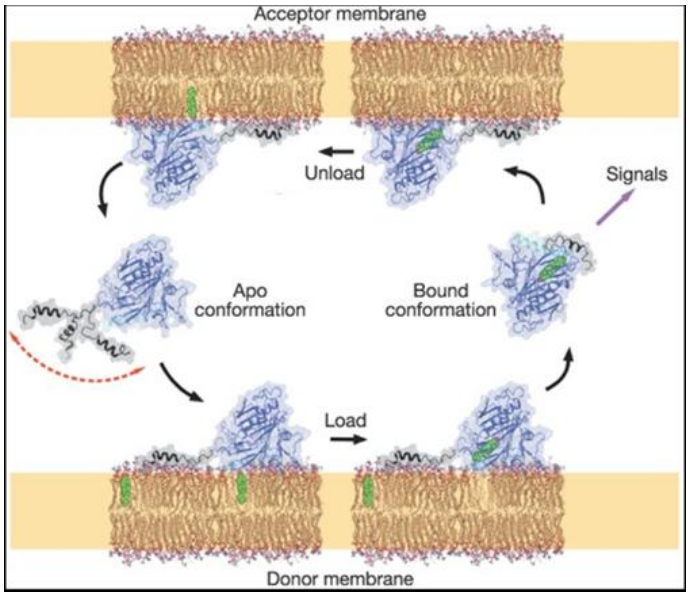

Figure A1.2: The proposed sterol transfer cycle mediated by Kes1 The apo conformation allows binding of Kes1 to a donor membrane, where sterols (green) are extracted. In its bound conformation the lid of the protein is closed protecting the sterol inside. In response to specific signals the protein would bind to a donor membrane releasing the sterol molecule. Modified from (153).

Work from the McMaster group identified a unique role of Kes1 in maintenance of sphingolipid homeostasis in the Golgi apparatus. Microscopy experiments indicated that cells lacking the Kes1, showed Pma1 mislocalization from the PM to an unidentified cellular compartment (150). Kes1 localizes to the Golgi, and has been associated with the regulation of sterol and sphingolipids synthesis, the main components of lipid rafts, as well as intracellular sterol trafficking (154, 155). In addition, many PM proteins, including Pma1 require lipid raft association at the Golgi for subsequent PM localization (138, 156). Therefore, we wanted to further investigate whether the lack of Kes1 impaired lipid raft formation, which therein resulted in the mis-localization of Pma1. Using several Kes1 mutants, we assessed whether impeding proper sterol (KES^{K109A}) or phosphatidylinositol-phosphate (PIP) binding activity (KES^{3E}) affected lipid raft formation (155). Finally, we examined if the deletion of all seven of the Osh family proteins affected lipid raft formation by monitoring association of Pma1 with DRMs. It is important to note that although DRMs obtained from whole cell lysates contain PM lipid rafts, they are not exclusively composed of them. After DRM isolation and subsequent western blot and silver stain analysis, we observed that the amount of Pma1 localized to DRMs in *kes1Δ* cells was comparable to that of WT cells (Figure A1.3), suggesting that despite mis-localization of Pma1 the protein remained associated with some internal lipid raft. We subsequently wanted to know whether impaired sterol binding (KES^{K109A}) or impaired PIP binding (KES^{3E}) would compromise Pma1 association with DRMs. Therefore, we transformed a mutant lacking the *KES1* gene with plasmids carrying KES^{K109A}, KES^{3E} as well as an empty vector, and a wild type *KES1* as negative and positive controls respectively. In accordance to the aforementioned results, *kes1Δ*[empty], the *kes1Δ*[KES^{K109A}], as well as the *kes1Δ*[KES1] transformants showed comparable amounts of Pma1 partitioning to DRMs (Figure A1.4). However, the *kes1Δ* [KES^{3E}]

showed Pma1 being distributed to other fractions (Figure A1.4) suggesting that lipid raft formation may be impaired in *kes1* mutants with compromised PIP binding capabilities.

Since yeast contains seven members of the Osh protein family (Osh), we postulated that deletion of *KES1* may be compensated by one of the other Osh family proteins. In order to better elucidate the role of Kes1 in lipid raft formation, we used an hepta-deletion mutant *osh-7Δ,* maintained alive by a functional Kes1 protein encoded in a plasmid, as well as a temperature sensitive mutant, $Kes1^{TS}$ which is only able to grow at 25°C (permissive temperature) but not at 37 °C (restrictive temperature). The growth of *osh-7Δ* [*KES1*] or *osh-7Δ* [$KES1^{TS}$] at 25°C showed comparable amounts of proteins in the silver stain (Figure A1.5), wherein, the shift to 37°C clearly indicated a decrease in protein expression in the temperature sensitive mutant, *osh-7Δ*[$kes1^{TS}$] (Figure A1.5). Further analysis showed that growth of *osh7-Δ*[$KES1^{TS}$] at 37°C, does not impede Pma1 partitioning into DRMs (Figure A1.6), but taken together with the results from Figure 4.11b, may impact the localization or expression of other proteins. These results suggest that the lack of *KES1* does not impede lipid raft formation, but may actually impede lipid raft transport to the PM, suggesting the possible presence of lipid rafts in other intracellular membranes.

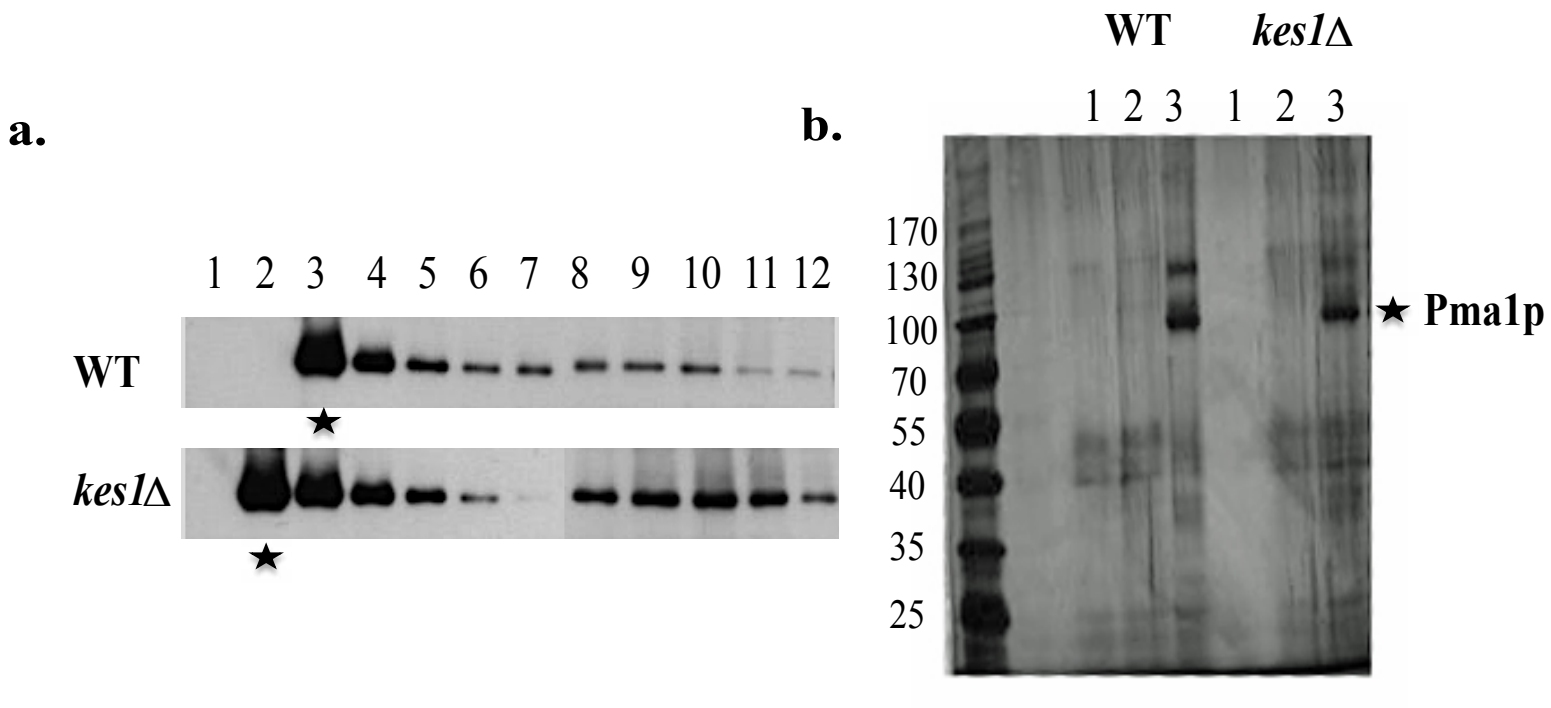

Figure A1.3: Pma1 localization in WT (BY4741) and *kes1Δ* Cells were grown to mid log phase at 30^{o}C, then lysed and equal amounts of protein were subjected to 1% Triton-X 100 incubation followed by Optiprep density gradient centrifugation. Twelve fractions were obtained, and 20ml aliquot of each fraction was analyzed by SDS-PAGE and silver staining **(a)** Western blot against Pma1 **(b)** Silver stain of the same samples (stars indicated Pma1).

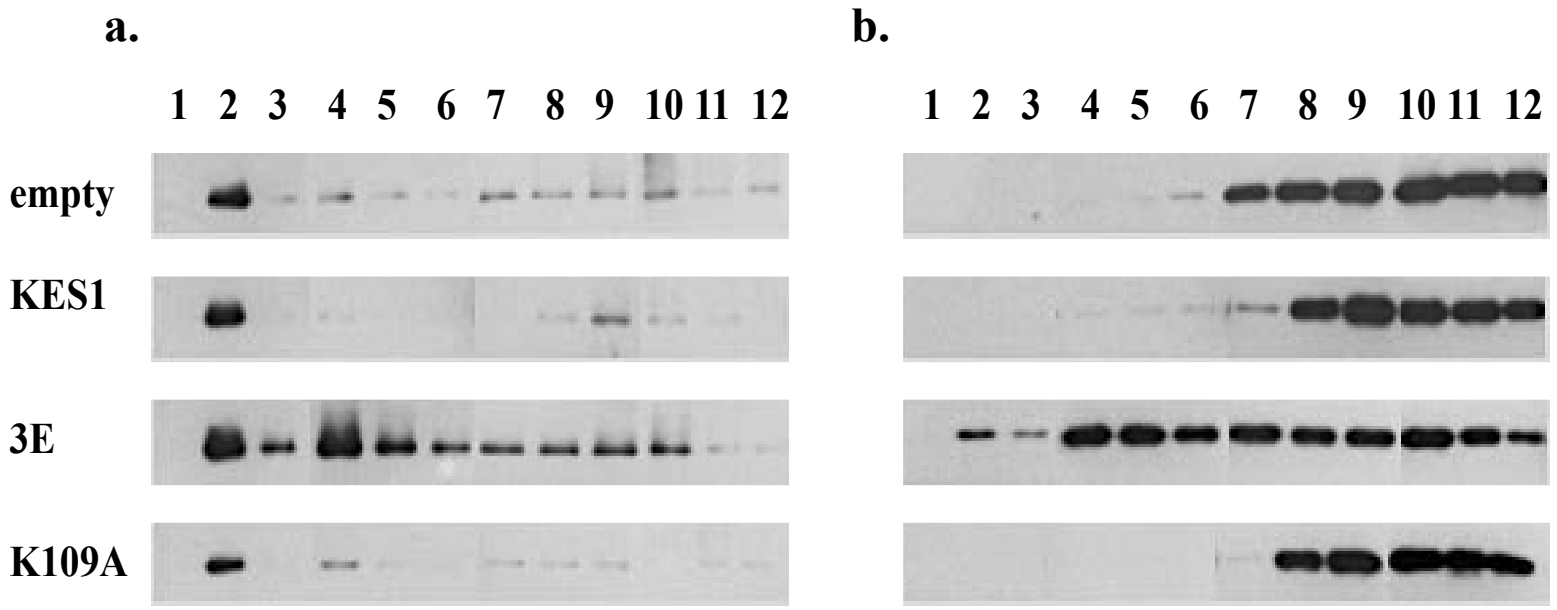

Figure A1.4: Pma1 localization in *kes1Δ* strains were transformed with low copy plasmids, pRS415 (empty), pRS415 expressing Kes1^{WT} (KES1), pRS415 expressing mutant Kes1$^{R236E/K242E/K243E}$ (3E) and pRS415 expressing mutant Kes1^{K109A} (K109A) Cells were grown to mid log phase in defined media for plasmid selection at 30^{o}C, then lysed and equal amounts of protein were subjected to 1% Triton-X 100 incubation followed by Optiprep density gradient centrifugation. Twelve fractions were obtained, and 20ml aliquot of each fraction was analyzed by SDS-PAGE and silver staining **(a)** Western blot against Pma1 **(b)** Same western blot showing loading control Pgk1p.

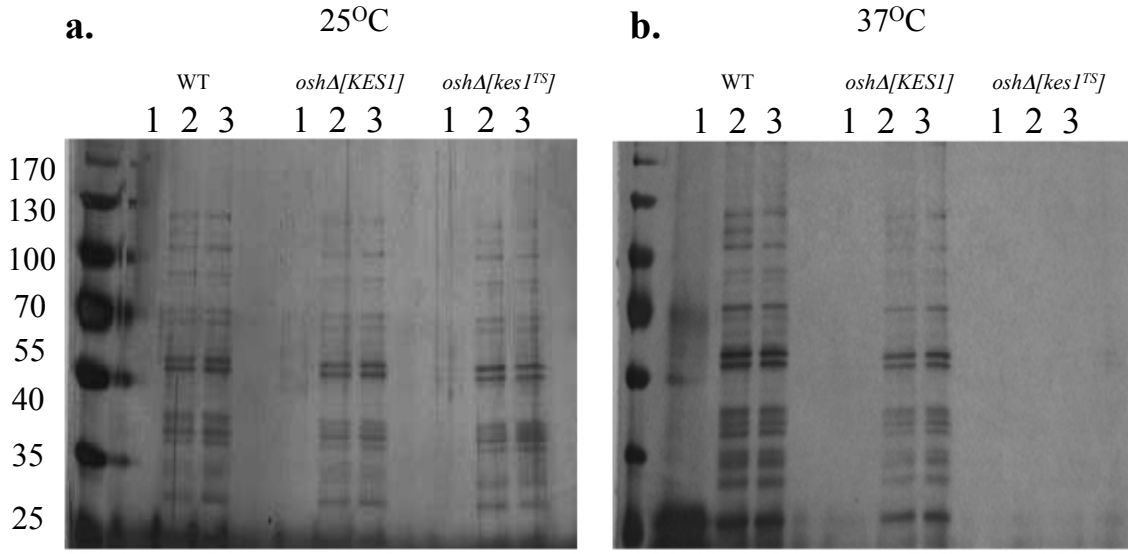

Figure A1.5: Comparing protein expression in WT, hepta-mutant *osh1-7D* expressing KES1 and temperature sensitive kes1^{TS} at different temperatures Cells were grown to early log phase in defined media for plasmid selection at 30^{o}C, and then switched to **(a)** 25^{o}C and **(b)** 37 ^{o}C for 2 hours and collected. Cells were lysed and equal amounts of protein were subjected to 1% Triton-X 100 incubation followed by Optiprep density gradient centrifugation. Twelve fractions were obtained for each temperature, and a 20µl aliquot of each fraction was analyzed by SDS-PAGE and silver staining.

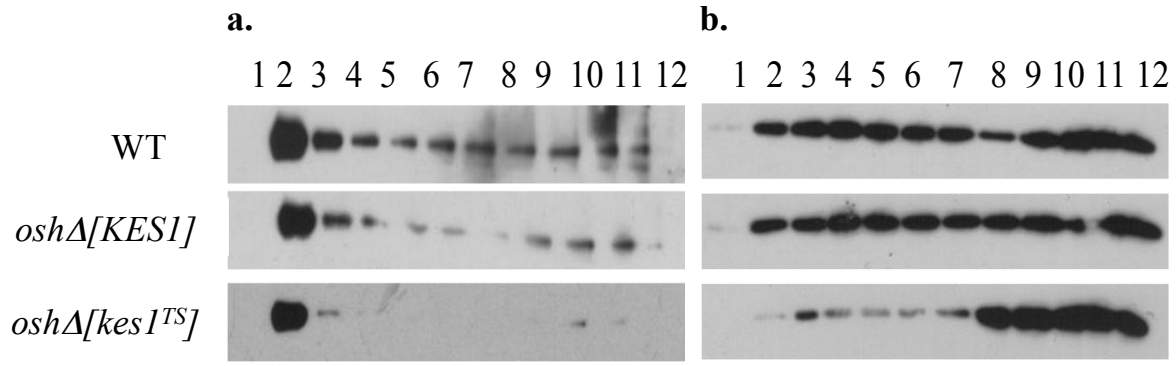

Figure A1.6: Pma1 localization in *osh1-7Δ*[KES1] and *osh1-7Δ*[KES1^{TS}] grown at 37^{o}C Cells were grown to early log phase in defined media for plasmid selection at 30^{o}C and then switched to 37^{o}C for 2 hours. Cell were then lysed and equal amounts of protein were subjected to 1% Triton-X 100 incubation followed by Optiprep density gradient centrifugation. Twelve fractions were obtained, and 20ml aliquot of each fraction was analyzed by SDS-PAGE and silver staining **(a)** Western blot against Pma1 **(b)** Same western blot against Pgk1.

Appendix 2: List of edelfosine-resistant mutants identified in the chemo-genomic screens of the *S. cerevisiae* deletion mutant collection

Table A2.1: Complete list of genes identified in resistance genetic screen

Resistance	Gene	Cellular role	Localization
+++	*RHO4*	Actin cytoskeleton organization, cell polarity	Cytoplasm
+++	*AGP3*	Amino acid transport	Plasma membrane
+++	*AGP2*	Amino acid transport, carnitine, polyamine transport	Plasma membrane, ER, vacuole membrane
+++	*DIA4*	aminoacyl-tRNA synthase, serine	Mitochondrion
+++	*MSR1*	aminoacyl-tRNA synthetase, arginine	Mitochondrion
+++	*CDH1*	Anaphase promoting complex, regulator, Cyclin ubiquitination, cell cycle	Nucleus
+++	*DOC1*	Anaphase promoting complex, Ubiquitin-dependent protein catabolism, cyclin proteolysis	Nucleus
+++	*MCA1*	Apoptosis	Nucleus
+++	*RCN1*	Calcineurin, inhibitor	Cytoplasm
+++	*CAF130*	CCR4-Not complex, Regulation of transcription and mRNA degradation	Cytoplasm
+++	*RLM1*	Cell wall organization and biogenesis, MAPK pathway	Nucleus
+++	*YTA12*	Degradation of misfolded or unassembled proteins	Mitochondrion
+++	*HMI1*	DNA maintenance	Mitochondrion
+++	*RRG9*	DNA maintenance	Mitochondrion
+++	*RAD57*	DNA repair	Nucleus
+++	*RAD18*	DNA repair, ubiquitin-protein ligase activity	Nucleus
+++	*DOA4*	ESCRT complex, complex III, proteasome, protein deubiquitination	Endosome
+++	*GUP2*	Glycerol transport	Plasma membrane
+++	*GPM3*	Glycolysis	Cytoplasm
+++	*EAF6*	Histone regulation, acetylase	Nucleus
+++	*SET3*	Histone regulation, deacetylation	Nucleus
+++	*DJP1*	HSP40 chaperon, Peroxisomal protein import, peroxisome assembly	Cytoplasm
+++	*BSD2*	Metal transport regulation	ER, vacuole
+++	*DIT1*	mid-late spore formation	Unknown
+++	*GEM1*	Mitochondrion organization	Mitochondrion,

Resistance	Gene	Cellular role	Localization
			mitochondrial outer membrane
+++	*GAT1*	Nitrogen catabolite repression, transcription factor, activator	Cytosol, nucleus
+++	*ATP7*	Oxidative phosphorylation, F1-F0 ATP synthase	Mitochondrion
+++	*COX6*	Oxidative phosphorylation, electron transport chain	Mitochondrion
+++	*COX23*	Oxidative phosphorylation, electron transport chain	Mitochondrion, inter-membrane space
+++	*ATP5*	Oxidative phosphorylation, F0F1 ATP synthase	Mitochondrion
+++	*PLB2*	Phospholipid metabolism, lysophospholipase	Cell wall
+++	*LEM3*	Phospholipid translocation across the plasma membrane	Plasma membrane, ER
+++	*SEM1*	Proteasomal ubiquitin-dependent protein catabolic process	Cytosol, proteasome
+++	*RPN14*	Proteasome activity	Cytoplasm
+++	*POC4*	Proteasome assembly	Cytoplasm
+++	*UFD4*	proteasome, ubiquitin-protein ligase	Cytoplasm
+++	*TUF1*	Protein biosynthesis	Mitochondrion
+++	*MLP1*	Protein export from the nucleus	Nuclear envelope
+++	*CPR3*	Protein folding	Mitochondrion
+++	*KTR7*	protein glycosylation	Golgi
+++	*EGD2*	Protein sorting and translocation	Ribosome, cytoplasm
+++	*PKP2*	pyruvate dehydrogenase	Mitochondrion
+++	*DOT5*	Regulation of redox homeostasis, diauxic shift, oxidative stress response	Nucleus
+++	*VPS35*	Retrograde transport	Endosome, retromer complex
+++	*RSM19*	Ribosomal protein	Ribosome, mitochondrion
+++	*MRPS8*	Ribosomal protein	Ribosome, mitochondrion
+++	*MRPL33*	Ribosomal protein	Ribosome, mitochondrion
+++	*MRP7*	Ribosomal protein	Ribosome, mitochondrion
+++	*MRP21*	Ribosomal protein	Ribosome, mitochondrion

Resistance	Gene	Cellular role	Localization
+++	*MRPL38*	Ribosomal protein, protein biosynthesis	Ribosome, mitochondrion
+++	*RPS8A*	Ribosomal protein, protein biosynthesis	Cytosol, ribosome
+++	*RPL42A*	Ribosomal protein, protein biosynthesis	Cytoplasm
+++	*RSM7*	Ribosomal protein, protein biosynthesis	Ribosome, mitochondrion
+++	*RSM25*	Ribosomal protein, protein biosynthesis	Ribosome, mitochondrion
+++	*RPL8B*	Ribosomal protein, protein biosynthesis	Ribosome, cytoplasm
+++	*MRPL35*	Ribosomal protein, protein biosynthesis	Ribosome, mitochondrion
+++	*MRPL10*	Ribosomal protein, protein biosynthesis	Ribosome, mitochondrion
+++	*IMG2*	Ribosomal protein, protein biosynthesis	Ribosome, mitochondrion
+++	*RPL37B*	Ribosomal protein, protein biosynthesis	Ribosome, cytoplasm
+++	*PPT1*	Ser/Thr phosphatase	Cytoplasm, nucleus
+++	*IRC19*	Spore formation	Unknown
+++	*SUT2*	Sterol transport, transcription	Nucleus
+++	*SSA3*	Stress response, protein folding	Cytoplasm
+++	*SUB1*	Transcription	Nucleus
+++	*MTF1*	Transcription	Mitochondrion
+++	*CST6*	Transcription factor, carbon source	Nucleus
+++	*ECM22*	Transcription factor, strerol biosynthesis	Nucleus
+++	*PAT1*	Transcription, chromosome segregation	Ribosome, cytoplasm
+++	*STO1*	Transcription, mRNA transport and degradation	Nucleus
+++	*NRG2*	Transcriptional repressor, pseudohyphal growth	Nucleus
+++	*YRA2*	Translation, mRNA export from nucleus	Nucleus
+++	*YLH47*	Unknown	Mitochondrion
+++	YJL185C	Unknown	Unknown
+++	*YGP1*	Unknown	Cell wall
+++	YDR161W	Unknown	Cytoplasm, nucleus
+++	YDR114C	Unknown	Unknown
+++	YDL118W	Unknown	Unknown
+++	YDL063C	Unknown	Cytoplasm, nucleus
+++	YBR246W/*RRT2*/*ERE1*	Endocytic recycling	Cytoplasm, endosome

Resistance	Gene	Cellular role	Localization
+++	YBR099C	Unknown	Unknown
+++	*AIM25*	Unknown	Mitochondrion
+++	*AIM10*	Unknown	Mitochondrion
+++	YNL228W	Unknown; dubious ORF	Unknown
+++	YNL184C	Unknown; dubious ORF	Unknown
+++	YMR084W	Unknown; dubious ORF	Unknown
+++	YDR417C	Unknown; dubious ORF	Unknown
+++	YDL062W	Unknown; dubious ORF	Unknown
+++	*BUD26*	Unknown; dubious ORF	Unknown
+++	*SWF1*	Vesicle, Retrograde transport, tlg1 palmitoylation, protein palmitoylation, vacuole fusion	Nuclear envelope-ER network
+++	*ATP25*	Vesicle-mediated transport	Mitochondrion
+++	*SVP26*	Vesicle-mediated transport, ER to Golgi	ER, Golgi
++	*MSF1*	Aminoacyl-tRNA synthase, phenylalanine	Mitochondrion
++	*MSY1*	Aminoacyl-tRNA synthetase, tyrosine	Mitochondrion
++	*PDE2*	cAMP-mediated protein kinase signalling	Cytoplasm, nucleus
++	*NOT5*	CCR4-Not complex, Regulation of transcription and mRNA degradation	Cytoplasm
++	*HPC2*	Cell cycle, chromatin remodelling, histone genes repression	Nucleus
++	*YPS7*	Cell wall, yapsin	ER, cytoplasm
++	*MSB1*	Cell wall biogenesis, MAPK signalling	Mitochondrion, bud
++	*SIR4*	Cryptic mating loci silencing, pheromone sensitivity	Nucleus
++	*SIR3*	Cryptic mating loci silencing, pheromone sensitivity	Nucleus, mitochondrion
++	*RAD14*	DNA repair	Nucleus
++	*MGM101*	DNA repair	Mitochondrion
++	*PMS1*	DNA repair, mismatch repair	Nucleus
++	*MSH2*	DNA repair, mismatch repair	Nucleus
++	*MLH1*	DNA repair, mismatch repair	Nucleus
++	*EXO1*	DNA repair, mismatch repair	Nucleus
++	*END3*	Endocytosis, actin cytoskeletal organization	Actin cortical patch
++	*SSM4*	Erad (ER-associated protein degradation), ubiquitin-protein ligase	ER, nuclear envelope
++	*VPS27*	ESCRT complex, complex 0, doa4D suppressor, Recycling Golgi proteins	Endosome
++	*SRN2*/*VPS37*	ESCRT complex, complex I	Endosome

Resistance	Gene	Cellular role	Localization
++	*VPS24*	ESCRT complex, complex III, doa4D suppressor	Endosome
++	*DID4*/*VPS2*	ESCRT complex, complex III, doa4D suppressor	Endosome
++	*VPS4*	ESCRT complex, complex III, Endosome to vacuole transport, sterol metabolism, doa4D suppressor	Endosome
++	*BRO1*	ESCRT complex, complex III, Protein deubiquitination, vacuolar transport	Endosome, cytoplasm
++	*HIS2*	Histidine biosynthesis	Cytoplasm
++	*TOM1*	Histone regulation, degradation, protein ubiquitination	Nucleus
++	*SGF11*	Histone regulation, deubiquitination	Nucleus
++	*RPL23A*	HSP70 chaperone, ribosomal protein, protein biosynthesis	Ribosome, cytoplasm
++	*MDM38*	Mitochondrion organization and biogenesis	Mitochondrion, mitochondrial inner membrane
++	*DNM1*	Mitochondrion organization and biogenesis, endocytosis	Mitochondrion
++	*SPO7*	Nuclear organization and biogenesis, phosphatase activity	Nuclear envelope-ER network
++	*ALO1*	Oxidative stress response	Mitochondrion
++	*YHC3*	pH homeostasis	Vacuole
++	*STE24*	Pheromone maturation, metallo-protease activity	ER
++	*DNF2*	Phospholipid translocation, alkyllysophospholipid uptake	Plasma membrane
++	*DRS2*	Phospholipid translocation, flippase, vesicle	Golgi, trans-Golgi network
++	*RPN4*	Proteasome, transcription factor	Nucleus
++	*RPL1B*	Protein biosynthesis	Ribosome, cytoplasm
++	*UBP8*	Protein deubiquitination	Nucleus, SAGA complex
++	*ULA1*	Protein neddylation	Unknown
++	*CSN9*	Protein neddylation, deneddylation	Cytoplasm, signalosome
++	*YSY6*	Protein secretion	ER
++	*SXM1*	Protein transport between cytoplasm and nucleoplasm	Nucleus
++	*BUL2*	Protein ubiquitination	Cytoplasm
++	*VPS29*	Retrograde transport	Endosome, retromer

Resistance	Gene	Cellular role	Localization
			complex
++	*VPS17*	Retrograde transport	Endosome, retromer complex
++	*PEP8*/*VPS26*	Retrograde transport	Endosome, retromer complex
++	*VPS52*	Retrograde transport, garp complex, cvt pathway	Golgi
++	*RPL6B*	Ribosomal protein, protein biosynthesis	Ribosome, cytoplasm
++	*RPL21A*	Ribosomal protein, protein biosynthesis	Ribosome, cytoplasm
++	*RPL19A*	Ribosomal protein, Protein biosynthesis	Ribosome, cytoplasm
++	*MRPL11*	Ribosomal protein, protein biosynthesis	Ribosome, mitochondrion
++	*MRP20*	Ribosomal protein, protein biosynthesis	Ribosome, mitochondrion
++	*MRT4*	Ribosome biogenesis	Nucleolus
++	*TGS1*	Ribosome synthesis, RNA maturation	Nucleolus
++	*ISC1*	Sphingolipids metabolism, ceramide production, response to salt stress	ER, mitochondrion, mitochondrial outer membrane
++	*TIR2*	Stress response	Cell wall
++	*UAF30*	Transcription	Nucleus
++	*EDC3*	Transcription, mRNA processing	Cytoplasm
++	*SLM3*	Translation, tRNA modification, 2-thiouridylase	Mitochondrion
++	*PET8*	Transporter of S-adenosylmethionine, respiratory function	Mitochondrion
++	YPL080C	Unknown	Unknown
++	YNR004W	Unknown	Nucleolus
++	YDR042C	Unknown	Unknown
++	YCR061W	Unknown	Cytoplasm
++	*TMA22*	Unknown	Ribosome, cytoplasm
++	*RBS1*	Unknown	Cytoplasm
++	*NST1*	Unknown, mediates sensitivity to salt stress	Cytoplasm
++	YNR005C	Unknown; dubious ORF	Unknown
++	YNL171C	Unknown; dubious ORF	Unknown
++	YDR442W	Unknown; dubious ORF	Unknown
++	*VAM10*	Vacuole fusion	Vacuole, vacuolar membrane

Resistance	Gene	Cellular role	Localization
++	*VPS3*	Vesicle corvet complex, Protein targeting to vacuole, vacuolar acidification	Cytoplasm
+	*PPA2*	Aerobic respiration, inorganic pyrophosphatase activity	Mitochondrion
+	*SNX42/ATG20*	Autophagy, cvt pathway, retrograde transport, vacuolar transport	Endosome
+	*SNX4*	Autophagy, cvt pathway, retrograde transport, vacuolar transport	Endosome
+	*BUD17*	Bud site selection	Cytoplasm, nucleus
+	*KNH1*	Cell wall biosynthesis, 1,6-beta-glucan synthesis	Cell wall
+	*BGL2*	Cell wall organization and biogenesis	Cell wall
+	*CNM67*	Chromosome segregation, Spindle orientation and mitotic nuclear migration	Nucleus
+	*SIR1*	Cryptic mating loci silencing, pheromone sensitivity	Nucleus
+	*MSH1*	DNA repair	Mitochondrion
+	*LDB17*	Endocytosis	Actin cortical patch (transient recruitment), Cell periphery and bud
+	*MYO5*	Endocytosis, Actin cytoskeleton organization	Actin cortical patch
+	*STP22/VPS23*	ESCRT complex, complex I	Endosome
+	*VPS20*	ESCRT complex, complex III	Endosome
+	*DID2*	ESCRT complex, complex III	Endosome
+	*UBP2*	ESCRT complex, complex III, Protein deubiquitination	Cytoplasm
+	*ADH3*	Ethanol metabolism	Mitochondrion
+	*HDA2*	Histone regulation, deacetylation	Nucleus
+	*YTA7*	Histone regulation, gene expression	Nucleus
+	*APJ1*	HSP40 putative chaperone	Mitochondrion
+	*DIA1*	Invasive and pseudohyphal growth	Cytoplasm
+	*RPO41*	Mitochondrial transcription	Mitochondrion
+	*PTC6/AUP1*	Mitochondrion number regulation, mitophagy	Mitochondrion
+	*UTH1*	Mitochondrion selective mitophagy	Mitochondrion, mitochondrial outer membrane
+	*MKS1*	Nitrogen catabolite repression, cell signalling, retrograde mitochondria-to-nucleus signalling	Cytoplasm

Resistance	Gene	Cellular role	Localization
+	*AAT2*	Nitrogen metabolism	Cytosol, peroxisome
+	*MOG1*	Nuclear protein import	Nucleus
+	*ATP20*	Oxidative phosphorylation, F1-F0 synthase	Mitochondrion
+	*AEP2*	Oxidative phosphorylation, F0F1 Translation	Mitochondrion
+	*ATP23*	Oxidative phosphorylation, F1-F0 assembly	Mitochondrion, mitochondrial inner membrane
+	*ATP4*	Oxidative phosphorylation, F1-F0 ATP synthase	Mitochondrion
+	*ATP18*	Oxidative phosphorylation, F1F0 ATP synthase	Mitochondrion
+	*ATP14*	Oxidative phosphorylation, F1F0 ATP synthase	Mitochondrion
+	*MSS51*	Oxidative phosphorylation, electron transport chain	Mitochondrion
+	*CYT1*	Oxidative phosphorylation, electron transport chain	Mitochondrion
+	*COX19*	Oxidative phosphorylation, electron transport chain	Mitochondrion, cytosol
+	*COX16*	Oxidative phosphorylation, electron transport chain	Mitochondrion, mitochondrial inner membrane
+	*COQ9*	Oxidative phosphorylation, electron transport chain	Mitochondrion
+	*COQ6*	Oxidative phosphorylation, electron transport chain	Mitochondrion
+	*COQ3*	Oxidative phosphorylation, electron transport chain	Mitochondrion, mitochondrial inner membrane
+	*CAT5*	Oxidative phosphorylation, electron transport chain	Mitochondrion
+	*INH1*	Oxidative phosphorylation, F1F0 ATPase regulation	Mitochondrion
+	*PET122*	Oxidative phosphorylation, mitochondrial translation	Mitochondrion
+	*MFA2*	Pheromone a-factor	Extracellular region
+	*KEX2*	Pheromone maturation, Calcium-dependent serine protease	Golgi
+	*KEX1*	Pheromone maturation, carboxipeptidase	Golgi, trans-Golgi
+	YML082W	Predicted sulfur metabolism	Cytoplasm, nucleus
+	*PBA1*	Proteasome assembly	Cytoplasm
+	*ADD66*	Proteasome assembly	Cytoplasm

Resistance	Gene	Cellular role	Localization
+	*BLM10*	Proteasome assembly and activation	Nucleus, proteasome complex
+	*UBS1*	Protein export from nucleus, protein ubiquitination	Nucleus
+	*PMT2*	Protein glycosylation	ER
+	*ALG8*	Protein glycosylation	ER
+	*ALG6*	Protein glycosylation	ER
+	*RUB1*	Protein neddylation	Cytoplasm
+	*RRI2*/*CSN10*	Protein neddylation, deneddylation	Signalosome
+	*CSI1*	Protein neddylation, deneddylation	Signalosome
+	*GCN2*	Protein phosphorylation, translation	Ribosome, cytoplasm
+	*NUP170*	Protein transport to/from the nucleus	Nuclear pore
+	*ULS1*	Proteolytic control of sumoylated substrates	Mitochondrion, nucleus
+	*RCY1*	Recycling of plasma membrane proteins, endocytosis	Endosome, site of polarized growth
+	*SSF1*	Ribosomal large subunit maturation	Nucleolus
+	*RPL37A*	Ribosomal protein	Ribosome, cytoplasm
+	*MRPL15*	Ribosomal protein	Ribosome, mitochondrion
+	*RPL33B*	Ribosomal protein, protein biosynthesis	Ribosome, cytoplasm
+	*CBS2*	Ribosomal protein, protein synthesis, cytochrome B mRNA activator	Ribosome, mitochondrion
+	*RPL9B*	Ribosomal protein, translation	Ribosome, cytoplasm
+	*TMA23*	Ribosome biogenesis	Nucleolus
+	*ARX1*	Ribosome biogenesis and assembly	Cytoplasm
+	*NOP12*	Ribosome biogenesis, rRNA metabolism	Nucleolus
+	*PTC7*	Ser/Thr phosphatase activity	Mitochondrion
+	*LCB3*	Sphingolipids biosynthesis	ER
+	*MSN2*	Stress response, transcription factor	Cytosol, nucleus
+	*ATG26*	Synthesis of sterol glucoside membrane lipids	Cytoplasm
+	*YAP7*	Transcription factor	Nucleus
+	*ACE2*	Transcription factor, G1-specific transcription in mitotic cell cycle	Nucleus, cytoplasm
+	*LIN1*	Transcription, RNA splicing	Nucleus
+	*IFM1*	Translational initiation	Mitochondrion
+	*POR1*/*VDAC*	Transporter, Voltage-dependent anion channel activity	Mitochondrion

Resistance	Gene	Cellular role	Localization
+	*GIM5*	Tubulin folding, pre-folding complex	Cytoplasm
+	YOR186W	Unknown	Unknown
+	YNL050C	Unknown	Unknown
+	YML108W	Unknown	Cytoplasm, nucleus
+	*SOV1*	Unknown	Mitochondrion
+	*SKG3*	Unknown	Bud
+	*EMI1*	Unknown	Unknown
+	YNL170W	Unknown; dubious ORF	Unknown
+	YLR202C	Unknown; dubious ORF	Unknown
+	YLL044W	Unknown; dubious ORF	Unknown
+	*PML39*	Unknown; dubious ORF. Probable mRNA export from nucleus	Nuclear pore
+	*OPI8*	Unknown; dubious ORF; doa4D suppressor	Unknown
+	YDR065W	Vacuolar acidification	Mitochondrion
+	*VPS1*	Vacuolar transport	Cytoplasm
+	*VPS8*	vesicle corvet complex, Late endosome to vacuole transport	Endosome
+	*TLG2*	vesicle mediated transport, Retrograde transport, vesicle fusion, garp complex tethering, cvt pathway	Golgi, endosome
+	*GLO3*	Vesicle, Retrograde transport, Golgi to ER	Golgi
+	*CCZ1*	Vesicle, vacuole fusion	Endosome
+	*GYP6*	Vesicle-mediated protein transport	Endosome, clathrin-coated vesicles
+	*VPS9*	Vesicle-mediated transport, Protein targeting to vacuole	Cytoplasm
+	*YPT7*	Vesicle-mediated transport, vesicle fusion, retrograde transport	Cytoplasm